UNIVERSIDADE FEDERAL DOS VALES DO JEQUITINHONHA E MUCURI

Programa de Pós-Graduação em Geologia

Lara Carneiro Matos

EVOLUÇÃO ESTRATIGRÁFICA E QUIMOESTRATIGRÁFICA (C, O, Sr) DA BORDA SUL DO AULACÓGENO DE PIRAPORA (CRÁTON DO SÃO FRANCISCO), A PARTIR DE DADOS DE SUBSUPERFÍCIE

Diamantina

2019

Lara Carneiro Matos

EVOLUÇÃO ESTRATIGRÁFICA E QUIMOESTRATIGRÁFICA (C, O, Sr) DA BORDA SUL DO AULACÓGENO DE PIRAPORA (CRÁTON DO SÃO FRANCISCO), A PARTIR DE DADOS DE SUBSUPERFÍCIE

Dissertação apresentada ao programa de Pós-Graduação em Geologia da Universidade Federal dos Vales do Jequitinhonha e Mucuri, como requisito para obtenção do título de Mestre.

Orientador: Prof. Dr. Matheus Henrique Kuchenbecker do Amaral
Coorientador: Prof. Dr. Humberto Luiz Siqueira Reis

Diamantina

2019

Elaborado com os dados fornecidos pelo(a) autor(a).

M433e Matos, Lara Carneiro
Evolução Estratigráfica e Quimoestratigráfica (C, O, Sr) da borda sul do Aulacógeno de Pirapora (Cráton do São Francisco), a partir de dados de subsuperfície / Lara Carneiro Matos, 2019.
91 p. : il.

Orientador: Matheus Kuchenbecker
Coorientador: Humberto Luiz Siqueira Reis

Dissertação (Mestrado – Programa de Pós-Graduação em Geologia) - Universidade Federal dos Vales do Jequitinhonha e Mucuri, Diamantina, 2019.

1. Aulacógeno de Pirapora. 2. Estratigrafia de sequências. 3. Glaciações neoproterozoicas. 4. Sistema petrolífero. 5. Bacia do São Francisco. I. Kuchenbecker, Matheus. II. Reis, Humberto Luiz Siqueira. III. Título. IV. Universidade Federal dos Vales do Jequitinhonha e Mucuri.

CDD 551

Ficha Catalográfica – Serviço de Bibliotecas/UFVJM
Bibliotecária Nádia Santos Barbosa, CRB6 – 3468

Lara Carneiro Matos

EVOLUÇÃO ESTRATIGRÁFICA E QUIMOESTRATIGRÁFICA (C, O, Sr) DA BORDA SUL DO AULACÓGENO DE PIRAPORA (CRÁTON DO SÃO FRANCISCO), A PARTIR DE DADOS DE SUBSUPERFÍCIE

Dissertação apresentada ao programa de Pós-Graduação em Geologia da Universidade Federal dos Vales do Jequitinhonha e Mucuri, como requisito parcial para obtenção do título de Mestre.

Orientador: Prof. Dr. Matheus Henrique Kuchenbecker do Amaral

Data de aprovação 17/09/2019.

Dr. Gustavo Macedo de Paula Santos
Instituto de Geociências - Unicamp

Profª. Dra. Gislaine Amorés Battilani
Instituto de Ciências e Tecnologia - UFVJM

Prof. Dr. Matheus Henrique Kuchenbecker do Amaral
Instituto de Ciências e Tecnologia - UFVJM

Diamantina

RESUMO

Aulacógenos são riftes abortados comumente preservados em domínios cratônicos, que podem ser sucessivamente reativados ao longo do tempo, registrando assim, evidencias sedimentares, climáticas e tectônicas a respeito da evolução de seu continente hospedeiro. No Cráton do São Francisco – umas das peças chave da geologia precambriana da América do Sul – dois aulacógenos registram sucessivos ciclos da Bacia do São Francisco ocorridos entre o Paleoproterozóico e o Neoproterozóico. Um deles, o aulacógeno de Pirapora, está quase inteiramente coberto por rochas sedimentares neoproterozóicas e mesozóicas, e por isso permanece quase sem estudos. Com base em dados de subsuperfície não publicados, recentemente adquiridos, pela primeira vez descrevemos três sequencias de 1ª ordem, Espinhaço-Superior, Macaúbas e Bambuí, limitadas por discordâncias erosivas, depositadas na margem sul da Bacia do São Francisco. A sequência de 1ª ordem basal Espinhaço-Superior registra a reativação Steniana do aulacógeno, e engloba fácies siliciclásticas e carbonáticas arranjadas em tendência progradacional. Um intervalo basal siciliciclástico rico em matéria orgânica foi reconhecido como um forte candidato a rocha fonte no sistema petrolífero precambriano da Bacia do São Francisco, reforçado pela presença de dolomitas em sela/barrocas e betume residual. Pela primeira vez, dois diamictitos sobrepostos foram descritos na mesma seção dentro da Bacia do São Francisco. A Formação Jequitaí, a mais antiga, provavelmente representa um registro da glaciação sturtianacriogeniana, e está correlacionada a sequência de 1ª ordem Macaúbas, enquanto o diamictito mais jovem é atribuído à Formação Carrancas (sequência de 1ª ordem Bambuí). A Formação Jequitaí foi submetida a alteração pós-deposicional pedogênica/freática, anterior a deposição da sequência sobrejacente, indicada por feições petrográficas e valores isotópicos de C e O. A Formação Carrancas, por outro lado, compreende depósitos diamictíticos maciços, cobertos por carbonados de capa da Formação Sete Lagoas, e tem sido considerada um registro da glaciação ediacarana tardia. A sequência de 1ª ordem Bambuí compreende uma plataforma siliciclástica-carbonática, arranjadas em um Trato de Sistema Transgressivo de 2ª ordem, correlata ao Intervalo-Quimioestratigráfico-1 e base do Intervalo-Quimioestratigráfico-2, e uma Trato de Sistema de Mar Alto, que está em acordo com as correlações intrabasinais. Na Formação Sete Lagoas, os estromatólitos associados a valores negativos de $\delta^{13}C$, descritos após o diamictito, podem ser o registro precoce da atividade biológica na bacia. Dois intervalos aragoníticos registram diferentes processos de supersaturação na água do mar, e ambos produzem maiores relações Sr/Ca em relação a seções adjacentes, as quais apresentam as maiores razões Mg/Ca. Processos diagenéticos precoces poderiam estar condicionados pelos parâmetros ambientais predominantes no momento da deposição. Os dados também esclarecem a evolução diagenética do aulacógeno de Pirapora através dos três estágios de reativação, que parecem ter forte influência pelo arcabouço estrutural da bacia. Um estágio hidrotermal tardio, relacionado ao fraturamento tectônico ocorrido durante o seu último ciclo de reativação, causou remobilização da matéria orgânica e percolação de fluido enriquecido em Fe, indicando o potencial de tal unidade para os sistemas petrolíferos e metalogenéticos da Bacia do São Francisco.

Palavras-chave: Aulacógeno de Pirapora, Estratigrafia de sequências, Glaciações neoproterozoicas, Sistema petrolífero, Bacia do São Francisco

ABSTRACT

Aulacogens are failed rift troughs commonly preserved within cratonic domains, which may be successively reactivated through time, thus recording evidence of the sedimentary, climatic and tectonic evolution of their host continent. Within the São Francisco craton - one of the key tectonic pieces of South America Precambrian geology - two aulacogens record successive basin cycles occurred between the Paleoproterozoic and Neoproterozoic. One of them, the Pirapora aulacogen, is almost entirely covered by Neoproterozoic and Mesozoic sedimentary rocks, and because of that it remains almost unstudied. Based on unpublished, recently acquired, subsurface data we describe, for the first time, three unconformity-bounded 1st-order sequences deposited within the southern margin of basin. The basal Upper-Espinhaço 1st order sequence records a Stenian reactivation of the aulacogen, and encompasses siliciclastic and carbonate facies arranged in a progradational trend. A basal organic-rich siliciclastic interval was recognized as a strong candidate to source rock in the Precambrian petroleum system of the São Francisco basin, as reinforced by the presence of baroque/saddle dolomites and residual bitumen. For the first time, two overlapping diamictite units were described in the same section within the São Francisco basin. The older one, the Jequitaí Formation, likely represents a record of the Cryogenian Sturtian glaciation, and is correlated to the Macaúbas 1st order sequence, while the younger one, is assigned to the Carrancas Formation (Bambuí 1st order sequence). The Jequitaí Formation is bounded by an erosive unconformity, and underwent pedogenic/phreatic post-depositional alteration, prior to the deposition of the overlying sequence, indicated by the petrographic features and C and O isotopic values. The Carrancas Formation, on the other hand, comprises massive diamictite deposits, covered by Sete Lagoas Formation cap carbonates, which has been considered as a record of a late Ediacaran glaciation. The Bambuí 1st order sequence comprises a mixed siliciclastic-carbonate platform, arranged in a 2nd order Transgressive System Tract, correlated to Chemostratigraphic Interval-1 and the base of Chemostratigraphic Interval-2, and a High Stand System Tract, which are in good agreement with basinwide correlations. Within the Sete Lagoas Formation, stromatolites described just after the diamictite, associated to negative $\delta^{13}C$ values, could be the early record of biological activity in the basin. Two aragonite intervals record different processes of oversaturation in seawater, and both yield higher Sr/Ca ratios than adjacent dolomitized sections, whose presents the higher Mg/Ca ratios. Early diagenetic processes could be conditioned by the parameters prevailing in the depositional environment. Our data also shed light into the diagenetic evolution of the Pirapora aulacogen through these three stages of reactivation, which seems to be strongly influenced by the structural framework of the basin. A younger hydrothermal stage related to tectonic fracturing occurred during its the last reactivation cycle caused organic matter remobilization and the percolation of Fe-rich fluid, suggesting the potential of such unit to the petroleum and metalogenetic systems of São Francisco basin.

Keywords: Pirapora aulacogen, Sequence stratigraphy, Neoproterozoic glaciations, Petroleum system, São Francisco basin

Sumário

Introdução

Aulacógenos são riftes abortados, comumente reativados por múltiplos eventos tectônicos, que podem hospedar subsequentes ciclos bacinais em regiões cratônicas (e.g. MILANOVSKY, 1992), constituindo importantes registros sedimentares, climáticos, biológicos e tectônicos da evolução da Terra no Precambriano (BURKE, 1977).

O Cráton do São Francisco – um dos principais elementos tectônicos da América do Sul - apresenta dois importantes aulacógenos: o Aulacógeno do Paramirim, a norte, e o Aulacógeno de Pirapora, a sul (CRUZ and ALKMIM, 2017, 2006). O Aulacógeno de Pirapora foi aparentemente formado durante o Paleoproterozoico, sucessivamente reativado durante dois episódios de rifteamentoproterozóicos, e durante o desenvolvimento do sistema foreland Ediacarano, contemporâneo à amalgamação do supercontinente Gondwana ocidental. Em virtude da longa atividade do Aulacógeno de Pirapora enquanto sítio deposicional, seu estudo possibilita o acesso aos registros das mudanças paleoambientais ocorridas na transição do Proterozóico para o Fanerozóico. Além disso, seu registro pode ser essencial para a compreensão dos sistemas petrolífero e metalogenético da Bacia do São Francisco.

Esta dissertação apresenta a análise estratigráfica e quimioestratigráfica detalhada de um testemunho de sondagem obtido na margem sul do Aulacógeno de Pirapora, no setor leste da Bacia do São Francisco (Fig. 1). A seção estudada apresenta o registro de três sequências estratigráficas de primeira ordem: Espinhaço Superior, Macaúbas e Bambuí. As três sequências foram analisadas detalhadamente a partir de descrição macroscópica 1:10, e foram realizadas petrografia microscópica e análises geoquímicas ($\delta^{13}C$, $\delta^{18}O$, $^{87}Sr/^{86}Sr$, [Sr], [Ca] e [Mg]) em amostras selecionadas.

No Capítulo 1 são apresentados os resultados petrográficos e estratigráficos obtidos na seção, que compõem o artigo "A windowintothehistoryof São Francisco craton: the Meso-Neoproterozoicstratigraphicevolutionofthe Pirapora aulacogen, Brazil", submetido a revista SedimentaryGeology, conforme comprovante abaixo.

No Capítulo 2 são apresentados os dados de geoquímica isotópica e elementar obtidos em rochas carbonáticas que ocorrem ao longo da seção, discutidos à luz do arcabouço estratigráfico da bacia. Estes resultados, no futuro, integrarão um segundo artigo científico, que será submetido em revista especializada.

No Capítulo 3 estão integradas as principais conclusões dos resultados discutidos nos capítulos 1 e 2.

20/08/2019 Yahoo Mail - Acknowledgement of receipt of your submitted article

Acknowledgement of receipt of your submitted article

De: Sedimentary Geology (eesserver@eesmail.elsevier.com)

Para: laracmatos@yahoo.com.br; laracarneiromatos@gmail.com

Data: terça-feira, 20 de agosto de 2019 15:05 BRT

*** Automated email sent by the system ***

Dear Mrs. Matos,

Your submission entitled "A window into the history of São Francisco craton: the Meso-Neoproterozoic stratigraphic evolution of the Pirapora aulacogen" has been received by Sedimentary Geology.

Your paper will be considered as belonging to the category Research Paper. Please contact us if this is not correct.

Please note that submission of an article is understood to imply that the article is original and is not being considered for publication elsewhere. Submission also implies that all authors have approved the paper for release and are in agreement with its content.

You will be able to check on the progress of your paper by logging on to https://ees.elsevier.com/sedgeo/ as Author.

Your manuscript will be given a reference number in due course.

Thank you for submitting your work to this journal.

Kind regards,

Elsevier Editorial System
Sedimentary Geology

Capítulo 1: Artigo científico

A window into the history of São Francisco craton: the Meso-Neoproterozoic stratigraphic evolution of the Pirapora aulacogen

Authors: Lara Matos[1] (corresponding author), Matheus Kuchenbecker[1,2,6], Humberto Reis[3], Evelyn Sanchez[2], Sergio Caetano-Filho[4], Marly Babinski[4]and Ricardo Trindade[5]

[1] Programa de Pós-Graduação em Geologia, Universidade Federal dos Vales do Jequitinhonha e Mucuri, Instituto de Ciência e Tecnologia; Rodovia MGT 367, Km 583 – Diamantina, Brazil – ZIP code 39100-000; laracmatos@yahoo.com.br

[2] Universidade Federal dos Vales do Jequitinhonha e Mucuri, Instituto de Ciência e Tecnologia; Rodovia MGT 367, Km 583 – Diamantina, Brazil – ZIP code 39100-000

[3] Laboratório de Modelagem Tectônica (LabMod), Universidade Federal de Ouro Preto, Departamento de Geologia-Escola de Minas; Campus Morro do Cruzeiro – Ouro Preto, Brazil – ZIP code 35400-000

[4] Universidade de São Paulo, Instituto de Geociências; Rua do Lago, 562 – São Paulo, Brazil – ZIP code 05508-080

[5] Universidade de São Paulo, Instituto de Astronomia, Geofísica e Ciências Atmosféricas; Rua do Matão, 1226 – São Paulo, Brazil – ZIP code 05508-090

[6] Centro de Pesquisa Professor Manoel Teixeira da Costa, Universidade Federal de Minas Gerais, Instituto de Geociências; Av. Antônio Carlos, 6627 – Belo Horizonte, Brazil – ZIP code 05508-080

Abstract: Aulacogens are failed rift troughs commonly preserved within cratonic domains, which may be successively reactivated through time, thus recording evidence of the sedimentary, climatic and tectonic evolution of their host continent. Within the São Francisco craton - one of the key tectonic pieces of South America Precambrian geology - two aulacogens record successive basin cycles occurred between the Paleoproterozoic and Neoproterozoic. One of them, the Pirapora aulacogen, is almost entirely covered by Neoproterozoic and Mesozoic sedimentary rocks, and because of that it remains almost unstudied. Based on unpublished, recently acquired, subsurface data we describe, for the first time, three unconformity-bounded 1st-order sequences, Upper-Espinhaço, Macaúbas and Bambuí, deposited within the southern margin of basin. The basal Upper-Espinhaço 1st order sequence records a Stenian reactivation of the aulacogen, and encompasses siliciclastic and carbonate facies arranged in a progradational trend. A basal organic-rich siliciclastic interval was recognized as a strong candidate to source rock in the Precambrian petroleum system of the São Francisco basin, as reinforced by the presence of baroque/saddle dolomites and residual bitumen. For the first time, two overlapping diamictite units were described in the same section within the São Francisco basin. The older one, the Jequitaí Formation, likely represents a record of the Cryogenian Sturtian glaciation, and is correlated to the Macaúbas 1st order sequence, while the younger one, is assigned to the Carrancas Formation (Bambuí 1st order sequence). The Jequitaí Formation is represented by an unconformity bounded layer of diamictite and mudstone, which underwent intense post-depositional alteration prior to the deposition of the overlying sequence, likely in a pedogenic/phreatic environment. The Carrancas Formation, on the other hand, comprises massive diamictite deposits, covered by Sete Lagoas Formation cap carbonates, which has been considered as a record of a late Ediacaran glaciation. The Bambuí 1st order sequence comprises a mixed siliciclastic-carbonate platform, arranged in a 2nd order Transgressive System Tract and a High Stand System Tract, which are in good agreement with basinwide correlations. Within the Sete Lagoas Formation, stromatolites described just after the diamictite could be the early record of biological activity in the basin, and two aragonite intervals record different processes of oversaturation in seawater. Our data also shed light into the diagenetic evolution of the Pirapora aulacogen through these three stages of reactivation, which seems to be strongly influenced by the structural framework of the basin. A younger hydrothermal stage related to tectonic fracturing occurred during its the last reactivation cycle caused organic matter remobilization and the percolation of Fe-rich fluid, indicating the potential of such unit to the petroleum and metalogenetic systems of São Francisco basin.

Keywords: Pirapora aulacogen, Sequence stratigraphy, Neoproterozoic glaciations, Petroleum system, São Francisco basin

1.1. Introduction

Due to plate tectonic processes, the Earth's lithosphere has been repeatedly affected by cycles of continental breakup, ocean spreading, subduction and continental collision, which form the background for most of the natural phenomena that took place in the surface of our planet, such as life and climate evolution. These tectonic cycles – referred as to Wilson's cycles – always begin with the rifting of the lithosphere, a complex mechanical process that is strongly influenced by the tectonic inheritance (e.g. MILANOVSKY, 1992). Rifts that do not evolve into passive marginsare usually referred to as "failed rifts", "aborted rifts" or, simply, aulacogens (e.g.KELLER and STEPHENSON, 2007).

Aulacogens are long-lived and fault-bounded troughs, which are commonly preserved within cratonic lithospheres (e.g. MILANOVSKY, 1992). They are commonly reactivated through multiple tectonic events and may exert a first-order control on the evolution of intracratonic depocenters also preserving the sedimentary record of different basin-cycles developed since the stabilization of its hosting craton. For these reasons, aulacogens might be considered some of the most important depocenters recording evidence on the sedimentary, climatic and tectonic evolution of the Precambrian Earth (BURKE, 1977). Due to their long-lived nature and influence on subsequent basin-cycles, aulacogens might also play an important role on hydrocarbon systems of intracratonic depocenters, as well as on the characteristics of associated sedimentary-hosted mineral deposits (e.g. SHU et al., 2015; REIS, 2016; TROFIMOV et al., 2016).

In South America, the São Francisco craton (together with its African counterpart, the Congo craton) represents the inner and stable portion of one of the various paleocontinents involved in the assembly of West Gondwana (e.g. HEILBRON et al., 2017). This former continent was stabilized along a Rhyacian-Orosirian orogeny (BARBOSA and BARBOSA, 2017; ALKMIM and TEIXEIRA, 2017), experiencing multiple rifting events since then (e.g. PEDROSA-SOARES and ALKMIM, 2011; GUADAGNIN et al., 2015; Kuchenbecker et al., 2015b; Reis et al., 2017a). Within the São Francisco craton, most expressive Proterozoic rifting stages are recorded in two important aulacogens: the Paramirim aulacogen (CRUZ and ALKMIM, 2017, 2006), to the north, and the Pirapora aulacogen, to the south (Fig.1).

The Pirapora aulacogen is a NW-trending trough that hosts the thickest Precambrian succession over the São Francisco craton, exceeding 10 km-thick within its depocenter (REIS, 2016). It has apparently formed during the Paleoproterozoic, being successively reactivated during two Proterozoic rifting episodes and along the development of an Ediacaran foreland system contemporaneous with the West Gondwana assembly (REIS et al., 2017a, 2017b). Exerting a major influence on the sedimentary and deformation partitioning during these basin-cycles, the buried rift accumulated a thick sedimentary succession that preserves some of the most important Paleoproterozoic to early Paleozoic climate and tectonic events known in South America up to date (e.g. ALKMIM and MARTINS-NETO, 2012; CAXITO et al., 2012; REIS et al., 2017a; CAETANO-FILHO et al., 2019). Although much of this sedimentary record has been extensively studied along the last decades, the scarcity of continuous sections and the poorly preserved conditions of exposed strata hampered the complete understanding of their depositional to post-depositional history, as well as important aspects related to the sedimentary evolution of this buried graben (see discussions on section 6). Open questions also include the relationship of the sedimentary strata preserved in the aulacogen and the unconventional hydrocarbon system of the proterozoic successions preserved in the São Francisco craton (e.g. REIS, 2018).

This paper presents, for the first time, a detailed stratigraphicand diagenetic analysis of three different 1st-order sequences preserved within the Pirapora aulacogen. The study is based on the description of a continuous 80-meters-thick section sampled by a well recently drilled during hydrocarbon exploration campaigns. Recording the final stages of a Mesoproterozoic-early Neoproterozoic rift-sag strata, two different late Neoproterozoic glaciations and the distal section of an Ediacaran carbonate ramp, this section provides new insights on tectonic, climatic, chemical and biological changes affecting the São Francisco plate (and elsewhere) during the Proterozoic-Phanerozoic transition. Since the studied section includes the unique record of the contact between different basin-cycle record, it also allow a complete analysis of the post-depositional history of these successions, including the effect of multiple sedimentary gaps e exposure on their meso to microscopic texture.

1.2. Geological context

The São Francisco craton is one of the most important tectonic features in South America, and, together with its african counterpart - the Congo craton -, it represents the inner and stable portion of one of the various paleocontinents that assembled to form the West Gondwana in the late Neoproterozoic (e.g. ALMEIDA, 1977; ALKMIM et al. 2006; HEILBRON et al., 2017). The craton is completely surrounded by orogenic belts evolved during complex and diachronic collisional processes, and most of its area is covered by the thick sedimentary strata of the intracratonic São Francisco basin (Fig.1). Following the craton boundaries, the western and eastern limits of the basin are defined by the Brasília and Araçuaí belts, respectively. Its northeastern limit, on the other hand, is marked by a Neoproterozoic intracratonic deformation corridor, while its southern boundary is erosional (ALKMIM and MARTINS-NETO, 2001).

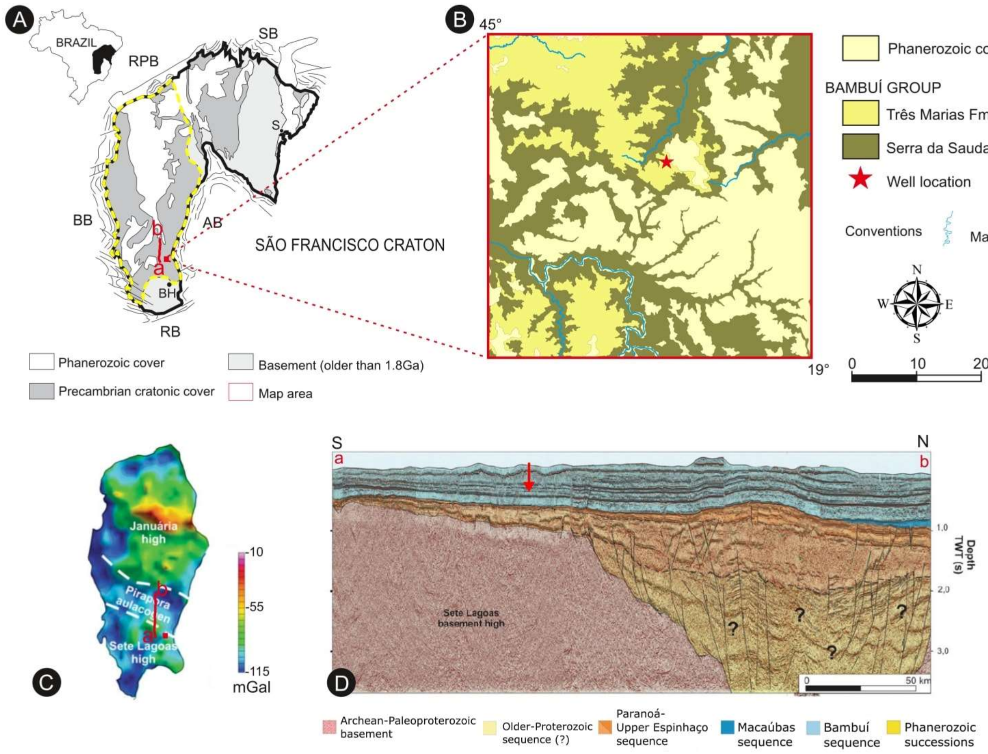

Figure1:(a) The São Francisco basin (yellow dashed line) in the southern São Francisco craton, with the location of the studied area (AB = Araçuaí Belt; RB = Ribeira Belt; BB = Brasília Belt; RPB: Rio Preto and Riacho do Pontal belts; SB: Sergipana Belt) The ab red line marks the location of the seismic section shown on Fig.1-d. (b) Geological map of the area, red star marking the well location. (c) Bouguer anomaly map of the SFC, with the main basement structures. Note the aulacogen through and the basement highs. (d) Seismic profile ab, showing the overall structure of the Pirapora aulacogen. The red arrow illustrates the approximate position of the section in the basin. Modified from Kuchenbecker et al. (2016a), Kuchenbecker et al. (2014) and Reis (2016).

The São Francisco basin records a series of superimposed basin-cycles ranging from Paleoproterozoic to Mesozoic in age, and extends for more than 350000 km² in eastern Brazil (ALKMIM and MARTINS-NETO, 2001). Its oldest units have been interpreted as marking a Statherian rifting event, whose structures modeled the main structural framework of the basin basement (e.g. ALKMIM and MARTINS-NETO 2001; REIS et al., 2017a). This framework comprises two structural highs, namely, the Januária and Sete Lagoas highs, to north and south, respectively, separated by a deep NW trending rift through, named Pirapora aulacogen (ALKMIM and CRUZ, 2005; COELHO et al., 2008; KUCHENBECKER et al., 2015b; REIS et al., 2017a). After its formation, the aulacogen was successively reactivated through the Proterozoic, mostly as a remarkable subsiding domain. It has culminated in the preservation of the thickest sedimentary succession known in the cratonic area (ALKMIM and MARTINS-NETO 2001; REIS and ALKMIM, 2015).

The sedimentary record of the São Francisco basin encompasses multiple 1st-order Proterozoic sequences (Fig.2), reflecting tectonic and climatic events younger than 1,8 Ga (ALKMIM and MARTINS-NETO, 2001; ALKMIM and MARTINS-NETO, 2012; REIS et al., 2017a). Mostly preserved within the Pirapora aulacogen, three of them are especially important for this work: i) the Mesoproterozoic-early Neoproteorozoic Paranoá-Upper-Espinhaço, ii) the Neoproterozoic Macaúbas and iii) the Ediacaran Bambuí.

The Paranoá-Upper-Espinhaço sequence records a Mesoproterozoic to early Neoproterozoic rift-sag basin (REIS et al., 2017a), mostly exposed in the marginal Araçuaí and Brasília belts. In the Araçuaí orogen, this sequence is represented by the middle to upper units of the Espinhaço Supergroup (e.g. SANTOS et al., 2015; GUADAGNIN and CHEMALE, 2015), while in the Brasília belt it is mostly represented by the rocks of the Paranoá Group (e.g. CAMPOS et al., 2013). Within the São Francisco basin, the Paranoá-Upper-Espinhaço sequence shows its thickest section in the Pirapora aulacogen, cropping out in deformed sectors, especially in the zone where the aulacogen is partially inverted at the Araçuaí orogen front (e.g. HERCOS et al., 2008; KUCHENBECKER et al., 2015b; REIS, 2016). The sequence comprises two 2nd-order sequences, identified through seismic and well data: i) a lower rift sequence, composed of fluvial to deltaic sandstones and conglomerates, and ii) a lower sag sequence, made up by aeolian sandstones and an upper marine siliciclastic-carbonatic succession (REIS et al., 2017b). In the eastern São Francisco basin, the upper continental to transitional deposits are exposed within anticlinal cores, where they comprise the Galho do Miguel Formation and the Conselheiro Mata Group of the Espinhaço Supergroup (HERCOS et al., 2008; MARTINS et al. 2011; REIS et al., 2011; LOPES, 2012).

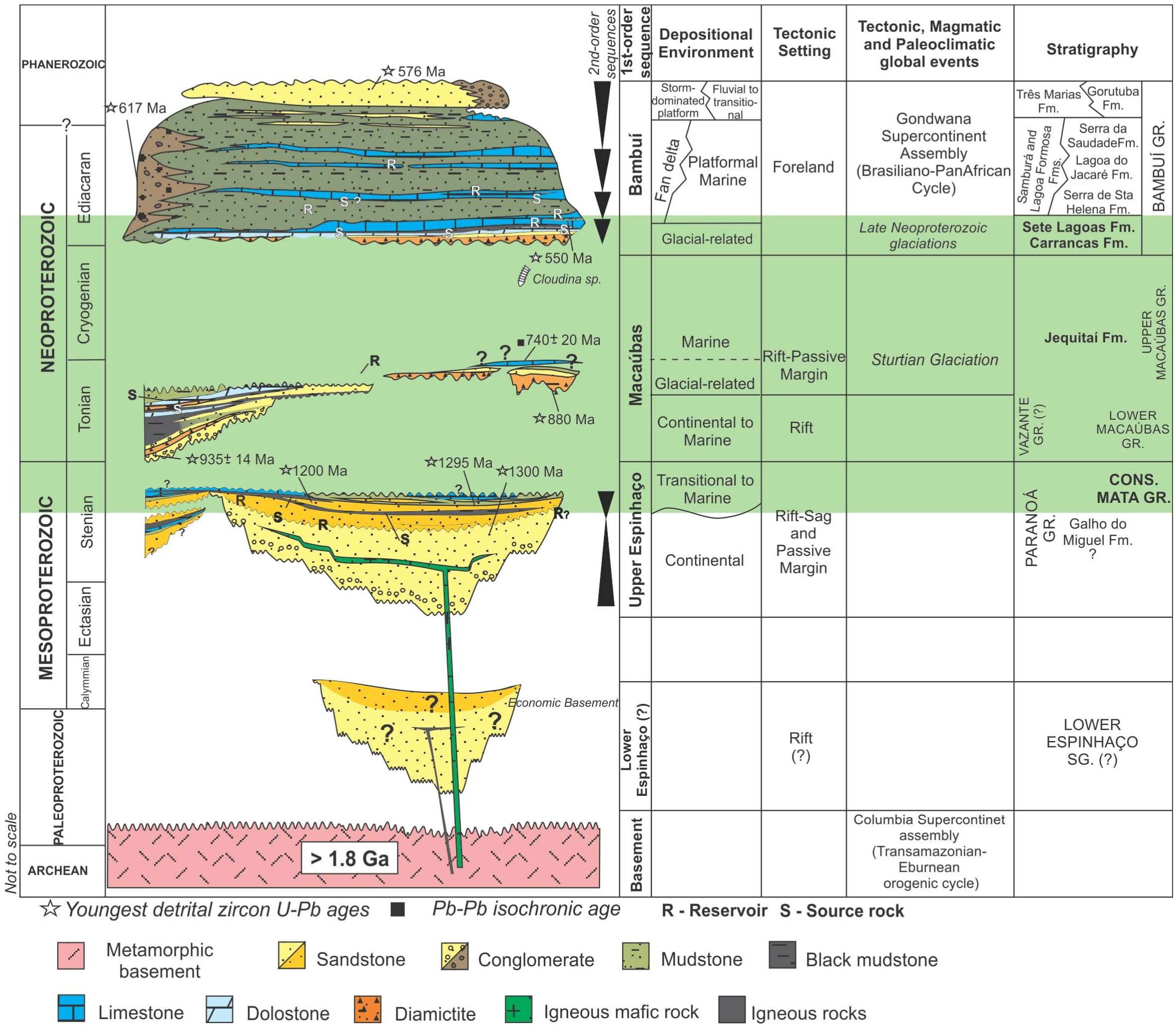

Figure 2:Stratigraphic chart for the Precambrian strata of the São Francisco basin. The light green area marks the studied intervals of the first-order sequences. Modified from Reis and Alkmim, 2015.

The overlying Macaúbas sequence comprises rift to passive margin units that occur within the Araçuaí orogen and, subordinately, in the São Francisco basin. At the orogen, the sequence encompasses a thick Sturtian glacially-related rift sequence, succeeded by post-glacial passive margin deposits and ophiolitic remains (e.g. KUCHENBECKER et al., 2015a;ALKMIM et al., 2017). Within the São Francisco basin, the sequence is represented by the diamictites, sandstones and pelites from the Jequitaí Formation, deposited in continental to marine environments (e.g. KARFUNKEL and HOPPE, 1988; UHLEIN et al., 2004). In the western portion of the basin, these deposits grade into fluvial-deltaic siliciclastic strata recently recognized in subsurface data (REIS et al., 2017a).

The Ediacaran to Cambrian Bambuí 1st-order sequence records an apparently confined foreland basin system that evolved on the São Francisco paleocontinent during the diachronous collisions that lead to the amalgamation of West Gondwana (e.g. ALKMIM and MARTINS-NETO, 2012; MARTINS-NETO, 2009; REIS et al., 2017b). The main subsidence mechanism that controlled the basin dynamics was the lithospheric flexure caused by the uplift of the Brasilia belt, to west, with subordinate contribution of the overbuden caused by the Araçuaí orogen, to east (e.g. MARTINS-NETO et al., 2001; KUCHENBECKER 2014; REIS et al., 2017a, 2017b). This evolution has culminated with the sedimentary partitioning of the basin into two major depocenters: i) a western foredeep filled with deep water siliciclastic-dominated deposits and a ii) eastern flexural ramp, hosting mixed carbonate-siliciclastic shallow water deposits (e.g. ALKMIM and MARTINS-NETO, 2012b; CASTRO and DARDENNE, 1995; REIS and SUSS, 2016; REIS et al., 2017b; UHLEIN et al., 2017). Available subsurface data also indicate the partition of the eastern flexural ramp depocenter due to the reactivation of the Pirapora aulacogen. This reactivation has apparently caused changes on the balance between the sedimentary supply and accommodation rates, accompanied by an overall thickening of the Ediacaran strata and the overall increasing on siliciclastic/carbonate ratios within the failed rift (REIS, 2016).

The Bambui sequence is represented by the homonymous group, which corresponds to the main sedimentary deposit exposed in the São Francisco basin. In the eastern flexural ramp depocenter, it encompasses four 2nd-order transgressive-regressive sequences, whose evolution was influenced by the climate dynamics, tectonic processes occurring at the marginal orogens, and by the preexisting tectonic features (e.g. MARTINS and LEMOS, 2007; REIS et al., 2017a). These sequences comprise six main formations from the base to top (COSTA and BRANCO, 1961; DARDENNE, 1978): the Carrancas (diamictites, pelites), the Sete Lagoas (carbonates, pelites), the Serra de Santa Helena (pelites), the Lagoa do Jacaré (carbonates, pelites), the Serra da Saudade (pelites, sandstones) and the Três Marias (sandstones). Toward the west, these units grade into the pelites, conglomerates, sandstones and subordinate chemical sedimentary rocks of the Samburá (conglomerates and sandstones) and Lagoa Formosa (conglomerates, siltstones, carbonates and jaspilits) formations, which record conglomerate wedges fed by the thrust fronts of Brasilia belt (CASTRO; DARDENNE, 1995; UHLEIN et al., 2017). A few expositions of continental to transitional coarse-grained siliciclastics in the eastern São Francisco basin mark the final stages of the Bambuí basin-cycle and the emerging influence of the Araçuaí orogen overburden (KUCHENBECKER et al., 2016b).

Being the most studied section of the Bambuí sequence, the basal Sete Lagoas carbonate ramp and the underlying Carrancas coarse-grained siliciclastics have been interpreted as recording one of the Neoproterozoic glaciations. They were firstly considered as a Cryogenian Sturtian glacial stratum with basis on Pb-Pb direct dating of cap carbonates (BABINSKI et al., 2007; MARTINS-NETO, 2009; VIEIRA et al., 2007a). Afterwards, sedimentological and isotopic features of the Sete Lagoas Formation carbonates were used to correlate them with the Ediacaran Marinoan glaciation (e.g. ALVARENGA et al., 2014; CAXITO et al., 2012; UHLEIN, 2014; KUCHENBECKER, 2011). Nevertheless, the i) discovery of *Cloudina*sp. index-fossil (WARREN *et al.*, 2014) and the U-Pb dating of c.550 Ma detrital zircons (PAULA-SANTOS et al., 2015) and ii) the lack of any uncorformity within the basal Sete Lagoas formation strata have suggested a late Ediacaran age for the glaciation (e.g. PAULA-SANTOS et al., 2015; KUCHENBECKER et al., 2016a; PAULA-SANTOS and BABINSKI, 2018; REIS et al., 2017a; CAETANO-FILHO et al., 2019).

According to Reis and Suss (2016), most of the Carrancas and Sete Lagoas deposits define an unconformity-bounded and mixed carbonate-siliciclastic 2nd-order sequence, including subaqueous glaciogenic strata and cap carbonates at the base that grade upwards into carbonate ramp successions. This sequence has evolved after an Ediacaran glacial episode and under forebulge low subsidence rates. Available seismic and well data reveal that the post-glacial regressive strata comprises carbonate ramps whose shallower portions are located at the crest of the Sete Lagoas and Januária highs, in the southern and northern sectors of the São Francisco basin (REIS et al., 2017a). Overall, these ramps prograde outward, showing trackable distal sectors within the Pirapora aulacogen. Their stratigraphic characteristics within this failed rift is, however, poorly known so far.

Along the last decades, several C, O and Sr isotopic studies focused in basal units of Bambuí Group and allowed to assess the environmental and tectonic evolution of the basin (e.g. IYER et al., 1995; SANTOS et al., 2000, 2004; VIEIRA et al., 2007a; MARTINS and LEMOS, 2007; KUCHENBECKER, 2011; KUCHENBECKER et al., 2016a; CAXITO et al., 2018, 2012; ALVARENGA et al., 2014; PAULA-SANTOS et al., 2017, 2015; GUACANEME et al., 2017; PERRELLA JÚNIOR et al., 2017; UHLEIN et al., 2016, 2019; CAETANO-FILHO et al., 2019). Using the robust $\delta^{13}C$ and $^{87}Sr/^{86}Sr$ dataset available for the Bambuí Group, Paula-Santos et al. (2017) identified three major Chemostratigraphic Intervals

(CI) in its basal units, which would record major paleoenvironmental changes in the basin. The basal CI-1 is represented by the Sete Lagoas Formation cap carbonates, which present $\delta^{13}C$ between −3 and −5‰ in the base, transitioning to values around 0‰ to the top, and present $^{87}Sr/^{86}Sr$ ratios from 0.7074 to 0.7082. CI-2 is recorded in the middle Sete Lagoas Formation and is characterized by $\delta^{13}C$ values around 0‰ and $^{87}Sr/86^{Sr}$ ratios ~ 0.7084. The following CI-3, in turn, comprises the upper Sete Lagoas, Serra de Santa Helena and Lagoa do Jacaré formations, and shows remarkably high $\delta^{13}C$ values (+8 to +16‰) and $^{87}Sr/^{86}Sr$ ratios ~0.7075. CI-1 would record the initial transgression of the sea over the continental area while the CI-2 is envisaged as a stage of connection between the basin and the global ocean (as attests the presence of *Cloudina*sp., Warren et al., 2014). CI-3, on the other hand, was interpreted as a stage of basin restriction, in which the isolation from the global ocean would prevent isotope homogenization. In this context, the high values of $\delta^{13}C$ would result from enhanced burial of organic carbon and/or from methanogenesis in anoxic conditions (IYER et al., 1995; PAULA-SANTOS et al., 2017).

By analysing multiple stratigraphic sections in the eastern São Francisco basin, Caetano-Filho et al. (2019) reported an overall coupling between chemostratigraphic patterns and the basal Bambuí 2nd-order (and lower-rank) stacking patterns. These authors also show a sudden and basinwide increase in Sr content and Sr/Ca ratios within the first 2nd-order highstand system tract, which has been interpreted as a result of the progressive and enhanced restriction of the foreland basin system. The data presented by Caetano-Filho et al. (2019) addresses exclusively the proximal sections of the basal and post-glacial carbonate ramp occuring in the southern and northern Sete Lagoas and Januária basement highs, respectively. Chemostratigraphic data on these successions at the Pirapora aulacogen axis are still scarce.

1.3. Materials and methods

This study was performed through the detailed analysis of new well data recently acquired during hydrocarbon exploration campaigns in the São Francisco basin. The studied well sampled a continuous sedimentary succession preserved in the southeastern São Francisco basin, within the southern margin of the Pirapora aulacogen (Fig. 1).

In this work, we describe (1:10 scale) an 80 meters-thick section including rocks from three different unconformity-bounded 1st-order sequences: (i) mudstones and limestones of the Paranoá-Upper-Espinhaço sequence; (ii) diamictites, assigned to the Macaúbas sequence; and (iii) a mixed carbonate-siliciclastic deposit of the Bambuí sequence. For these purposes, the hierarchy of the Bambuí subordinated sequences followed the overall stratigraphic framework resented in previous studies (e.g. REIS and SUSS 2016, REIS et al., 2017a, CAETANO-FILHO et al. 2019). Erosional surfaces mark the contact between these sequences.

Rock descriptions were based on the depositional texture, composition, sedimentary structures, grain size and diagenetic features. Siliciclastic rocks were described and classified following the textural classification from Folk (1968), while carbonate rocks were classified according to Terra et al., (2010). This carbonate classification is an adaptation of other classic schemes presented by Dunham (1962), Riding (2000), Embry and Klovan (1971). In cases where depositional textures were completely obliterated by diagenesis, the classification considered the predominant mineral composition. The sedimentary facies were grouped according to the studied 1st-order sequences and the facies codes followed their major compositional characteristics. The overall stratigraphic analysis was also supported by gamma-ray log (GRL) data provided by Petra Energia S.A.

Thin sections from 31 samples were made in the Center of Geoscience Studies of the Federal University of Jequitinhonha and Mucuri Valleys (CeGeo/UFVJM). For the microscopic description, an acid solution of alizarin red-s and potassium ferricyanide (DICKSON, 1965; FRIEDMAN, 1959) was used to distinguish carbonate mineral phases according to stain color: (i) red tones for calcite; (ii) purple tones for ferroan-calcite; (iii) blue tones for ferroan-dolomite and ankerite; (v) dolomite unstained. The diagenetic analysis was conducted considering the paragenetic sequence, mineralogical and textural aspects, allowing the identification of the stages summarized in Figure 7.

1.4. The sedimentary succession within the southern margin of the Pirapora aulacogen

1.4.1. Sedimentary facies

Although some of the studied carbonate successions are intensely recrystallized, much of the original fabric elements remain preserved within the neoformed textures, allowing their classification following Terra et al. (2010). Carbonate facies were coded (C), while siliciclastic and hybrid ones were coded (S) and (H) respectively. The facies poorly preserved due dolomitization received the code (D).

Twenty-four sedimentary facies were identified along the section, and their description and characteristics are shown in Table 1, alongside the observed facies associations. In the following sections are presented the interpretations and discussions regarding the sedimentary processes, depositional systems and stacking patterns.

1.4.2. Facies associations and sedimentary processes

The basal Upper-Espinhaço sequence present fine-grained siliciclastic-dominated deposits grading upward to carbonate layers, bounded on top by an unconformity. The overlying Macaúbas sequence comprises exclusively diamictites, and is also bounded by unconformities, and the topmost Bambuí sequence presents a basal diamictite unit overlain by carbonates deposits, overlied by pelitic beds (Fig. 3).

Sequence stratigraphy nomenclature followed the review papers from Catuneanu, 2006 andCatuneanuet al., 2011. The carbonate facies associations were classified following Burchette and Wright (1992) concept of carbonate ramps. They suggest subdivisions of carbonate ramps in different zones using wave-influence limits: fair-weather wave base (FWWB) and storm wave base (SWB). In this sense, inner, mid and outer ramps are limited as above FWWB, between FWWB and SWB and below SWB, respectively. The boundary of outer-ramp and deeper zones is not clearly defined, but commonly basinal deep water environments will lack coarse tempestites and be dominated by fine-grained siliciclastic deposits (e.g. TUCKER and WRIGHT, 1990).

1.4.2.1. Upper-Espinhaço basin cycle

The basal Upper-Espinhaço sequence is 28.5 meter-thick, and present seven sedimentary facies between carbonate and siliciclastic ones, which are gathered in three facies associations (Table 1). A tectonic *breccia* was also identified breaking through carbonate deposits.

Table 1: Sedimentary facies described within Pirapora aulacogen. Discussions on the facies associations, and the interpreted sedimentary processes and settings are found in Section 1.4.2.

Facies	Type	Code	Main features	Main sedimentary processes	Facies association	Sequence
Graded sandstone	Siliciclastic	S6	Greenish gray sandstone with sparse tabular pebbles (made up by massive and greenish siliciclastic mudstone) in the base and grading upwards into fine- to very fine-grained sandstone. It occurs as decimeters-thick layers (at least 60 cm) along the upper portion of the studied section.	Subaqueous gravity flows	Basinal/outer ramp - Deep water	Bambuí
Rippled sandstone	Siliciclastic	S5	Fine- to very fine-grained greenish gray sandstone, comprising centimetric beds. These beds commonly define a thickening upward pattern and contain in their upper portions asymmetric ripple marks (Fig. 5-j).	Subaqueous gravity flows		
Siliciclastic mudstone	Siliciclastic	S4	Greenish gray and massive to fine laminated siliciclastic mudstone. The facies may show a low carbonate content and occurs as centimetric to metric layers. The lamination is marked by the interbedding of muddy and silty layers.	Suspension/mud plumes		
Marl	Hybrid	H1	Bluish gray marl, which occurs as centimetric layers often showing slump folds. This facies occurs mostly within the gradual transition from carbonate to siliciclastic mudstones.	Suspension/mud plumes	Outer ramp	

Facies	Type	Code	Main features	Main sedimentary processes	Facies association	Sequence
Laminite	Carbonate	C14	Gray laminite with lumpy to peloidal texture and incipient lamination that result from the millimetric intercalation of recrystallized and micritic levels. Spherical grains with darker micritic texture and clearly defined boundaries generally occur aggregated in globular and elongated or grape-like shapes (Fig. 6-e and 6-h). Microphytolites display thin micritic envelopment, diversified shapes (usually lenticular) and small sub-spherical/ellipsoidal peloids within their cores (Fig. 6-g). The microbial mats occur as centimetric beds, often associated with carbonate mudstone layers displaying discrete aragonite pseudomorphs fans.	Biologically induced/ influenced precipitation	Mid to outer ramp	
Wackestone/ mudstone	Carbonate	C13	Light gray medium-grained intraclasticwackestone with peloids. It comprises centimetric to millimetric beds, interbedded with millimetric to centimetric layers of gray siliciclastic mudstones. This facies frequentlly shows dissolution features (stylolites) concentrating residual organic matter.	Eventually reworked by storm-influence and suspension/mud plumes	Outer ramp	
Rippled packstone/ wackestone	Carbonate	C12	Gray packstone to wackestone showing ripples with internal centimeter-scale low angle cross-laminations and locally capped by dark gray lime mudstone (Fig. 5-f). The coarse- to medium- grained packstones/wackestones are made up by peloids and micritic intraclasts surrounded by a micritic matrix.	Hydrodynamic unidirectional dominated flow	Mid ramp	

Facies	Type	Code	Main features	Main sedimentary processes	Facies association	Sequence
Columnar stromatolite	Carbonate	C11	Light gray recrystalized stromatolites showing incipient internal laminations (Fig. 6-d). Morphotypes include commonly branched columns comprising divergent to parallel ramifications (Fig. 5-e and 5-l), with total lenghts varying from 10 to 30 cm. The synoptic relief is predominently high, but low to medium relief is also observed.The branched stromatolites usually show the highest angles. The intercolumnar spaces are filled with gray micritic matrix (Fig.6-c), often showing peloidal layers.	Biologically induced/ influenced, suspension	Mid to outer ramp	
Laminated grainstone/ packstone with syn-sedimentary deformation	Carbonate	C10	Medium- to fine-grained grayish grainstone/packstone. The rock shows cm-thick beds that thicken upwards, often presenting syn-sedimentary deformation features such as overoad-triggered pinch-and-swell structures and slumps.	Storm-influenced oscillatory flow (?)	Mid ramp	
Massive carbonate mudstone	Carbonate	C9	Grayish massive carbonate mudstone made up by sparse fine- to very fine-grained peloids immersed in a mud matrix. This facies occurs often recrystallized and/or dolomitized, in beds ranging from centimeters- to a few decimeters-thick.	Suspension/ mud plumes	Mid to outer ramp (?)	
Massive dolomite	Carbonate	D3	Massive cm-thick beds of dolomite, where the depositional texture was completely obliterated by diagenesis. In thin sections, black amorphous organic matter might be observed filling the intercrystalline space.	-		

Facies	Type	Code	Main features	Main sedimentary processes	Facies association	Sequence
Mudstone with aragonite pseudomorph fans	Carbonate	C8	Grayish massive mudstone with fine-grained peloids and aragonite pseudomorphs, in mm- to cm-thick beds. The pseudomorphs occur in the form of fans or crusts with submillimetric to centimetric crystals.	Chemical precipitation	$CaCO_3$ supersaturated mid ramp	
Intraclasticrudstone	Carbonate	C7	Dark gray and grain-supported intraclasticrudstone comprising cm-thick beds bounded at the base by erosional surfaces. The intraclasts are generally elongated and composed of gray carbonate mudstones, may containing aragonite pseudomorphs needles (often showing broken top) and, locally, embricated clasts of Facies C6.	Storm-influenced oscillatory flow (?)	Mid ramp	
Mudstone/ packstone with hummockys cross-lamination	Carbonate	C6	Light gray peloidal packstone with hummocky cross-lamination and interbedded with cm- to mm-thick layers of peloidal carbonate mudstone (Fig. 5-c).	Storm-influenced oscilltory flow		

Facies	Type	Code	Main features	Main sedimentary processes	Facies association	Sequence
Siliciclastic diamictite	Siliciclastic	S3	Dark gray diamictite supported by a siliciclastic muddy to sandy matrix (Fig. 5-a). The clasts vary from granule to boulder in size and are predominantly angular (some apparently faceted), lacking any orientation. They comprise mainly lithic fragments of metamorphic (quartzite, schist, gneiss and granitoid) and igneous (plutonic and rare vulcanic) rocks, as well as sandstone, mudstone and carbonate rocks(micritic, peloidal, ooidal and/or crystalline). The muddy to sandy matrix contains clay minerals and monomineralic grains of quartz (metamorphic or not), feldspar, micas and rare zircons. This facies comprises a 5,5 m-thick and fining-upward succession, showing increasing contents of diagenetic carbonate toward the top, where it also becomes light gray colored (Fig. 5-h).	Glacially influenced debris flows (?)	Glacial related (?)	
Muddy dolomite	Carbonate	D2	Grayish fine-grained and massive carbonate rock comprising cm- to dm-thick beds and completely replaced by dolomite. In thin sections, it shows dark very fine- to medium-grained peloidal grains scattered through a massive dolomite matrix. The hypidiotopic fabric presents suhbedral medium to anhedral fine crystals. The topmost muddy deposit display tabular pebbles of Facies D1 supported by muddy matrix (Fig. 4-j).	–	Glacial related (?)	Macaúbas

Facies	Type	Code	Main features	Main sedimentary processes	Facies association	Sequence
Carbonate diamictite	Siliciclastic	D1	Light gray diamictite with clasts suported by a dolomitic microcristalline matrix containing subordinate siliciclastic siltly grains (quartz and feldspar). The facies is poorly-sorted and shows rounded to angular clasts (Fig. 4-g, 4-h, 4-i), which range from granule to pebble (cobble) and are predominantly composed of carbonate with subordinate metamorphic rocks (quarzites, schists) and rare sandstone. The diamictite facies comprises a decimeter-thick succession bounded by an erosional surface at the base (Fig. 4-g). This succession defines a fining-upward stacking pattern that grades into the muddy dolomite facies (D2).	Glacially influenced gravity flow (?)		
Microbial laminite	Carbonate	C5	Mm- to cm-thick beds of gray laminite. The microbial lamination is characterized by thin micritic layers alternating with peloidal muddy layers (Fig. 4-f). The facies occur restrictly and the microbial lamination may locally trap and bind peloids.	Biologically induced/ influenced precipitation	Mid ramp (?)	Upper-Espinhaço
Intraclasticwackestone	Carbonate	C4	Medium to coarse-grained and poorly-sorted grayish intraclasticwackestone, arranged into mm- to cm-thick beds. The facies show tabular micritic intraclasts, usually horizontally-oriented and composed of peloidsimersed in a micritic matrix.	Storm-influenced oscillatory flow (?)		

Facies	Type	Code	Main features	Main sedimentary processes	Facies association	Sequence
Coarse-grained packstone/ grainstone	Carbonate	C3	Poorly-sorted and coarse- to very coarse-grained packstone/grainstone, composed of circular to elliptical grains, locally tabular, mainly comprising micritic intraclasts, peloids and coated grains (Fig. 4-d).	Storm-influenced oscillatory flow (?)		
Massive to laminated mudstone	Carbonate	C2	Grayish massive to laminated mudstones comprising cm- to dm-thick beds. The lamination is marked by thin dark layers, often showing remarkable organic content. The facies may contain fine- to very fine-grained peloidsembebed in a micritic matrix and rare siliciclastic siltly grains (quartz, micas).	Suspension/mud plumes	Mid to outer ramp	
Packstone/ wackestone	Carbonate	C1	Intercalation of thin milimetric to centimetric layers of packstone and wackestone composed of ooids, oncoids, peloids and rare intraclasts, within a micritic matrix. A common feature is the occurrence of grapestones by agglutination of grains and matrix.	Eventually reworked of shallow sediments by storm-influence (?)	Outer ramp	
Matrix-supported *breccia*	Siliciclastic	S2	Centimetric beds of gray *breccia* composed of tabular intraclasts of dark gray siliciclastic mudstone supported by a muddy dark-colored matrix (Fig. 4-c).	Subaqueous gravity flow	Basinal/Deep water	
Black siliciclastic mudstone	Siliciclastic	S1	Black to dark gray and massive to fine laminated (locally rippled) siliciclastic mudstone. The lamination is marked by silt grains (quartz, mica, feldspar) and the rock is often carbonate- and organic matter-rich. These facies comprises cm to dm-thick beds.	Suspension/mud plumes		

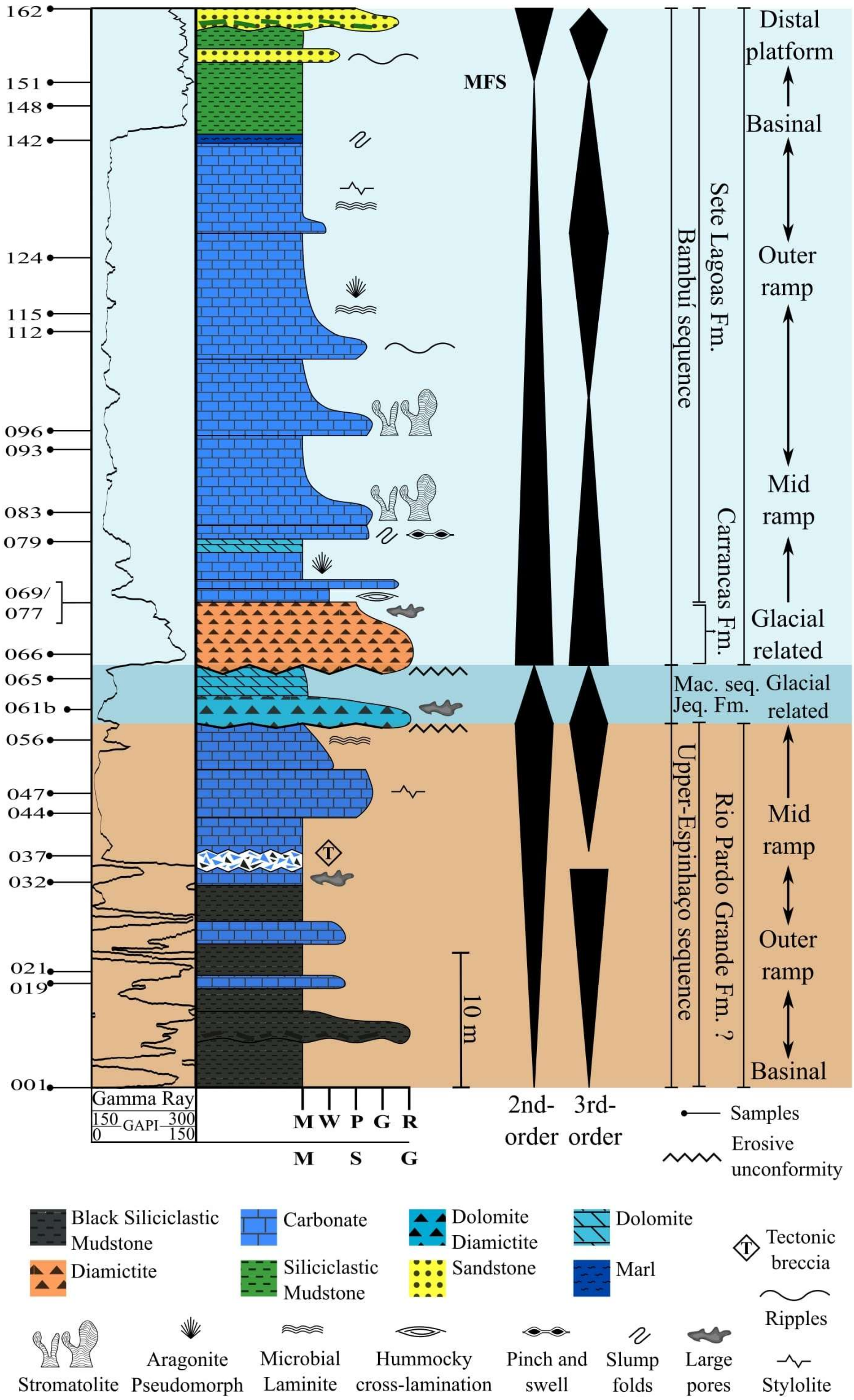
162
151
148
142
124
115
112
096
093
083
079
069/
077
066
065
061b
056
047
044
037
032
021
019
001
MFS
10 m
Sete Lagoas Fm.
Bambuí sequence
Carrancas Fm.
Mac. seq.
Jeq. Fm.
Upper-Espinhaço sequence
Rio Pardo Grande Fm. ?
Distal platform
Basinal
Outer ramp
Mid ramp
Glacial related
Glacial related
Mid ramp
Outer ramp
Basinal
Gamma Ray
150 GAPI 300
0 150
M W P G R
M S G
2nd-order
3rd-order
Samples
Erosive unconformity
Black Siliciclastic Mudstone
Diamictite
Carbonate
Siliciclastic Mudstone
Dolomite Diamictite
Sandstone
Dolomite
Marl
Tectonic breccia
Ripples
Stromatolite
Aragonite Pseudomorph
Microbial Laminite
Hummocky cross-lamination
Pinch and swell
Slump folds
Large pores
Stylolite

Figure 3: Stratigraphic column and gamma-ray log showing the main trend patterns and lithoestratigraphic correlation of the described section. Samples are plotted on the left side. The normal/inverted black triangles represent, respectively, deepening/shallowing-upward trends or fining/coarsening-upward trends. MFS – Maximum flooding surface. Carbonate depositional texture scale: M – mudstone, W – wackestone, P – packstone, G – grainstone and R – rudstone. Siliciclastic granulometry scale: M – mud, S – sand and G – gravel.

Deep water/basinal facies association: intercalation of cm to dm-thick layers of facies S1 and S2 record deep water depositional environments in the basal portion of sequence. The massive deposits of facies S1 (Fig. 4-a) are clearly dominant, usually presenting pyrite crystals concentrated at fine levels, hosted in fractures or nodules (Fig.4-a and 4-c). In thin sections framboidal pyrite crystals occur mainly as rounded aggregates. Matrix-supported *breccia* from facies S2 occur as fining-upward cycles, usually with erosive base (Fig. 4-c).

This facies association is envisage as a product of suspension mud plumes, with rare influence of subaqueous gravity flows driven by giant storm waves or seismic events, typical of distal and deeper basinal environments (BURCHETTE and WRIGHT, 1992; TUCKER and WRIGHT, 1990). Additionally, framboidal pyrite scattered on black muddy layers requires sedimentation with low energy and poorly oxygenated waters, favoring the preservation and early sulfate-reduction degrading organic matter (MORSE and MACKENZIE, 1990; FLÜGEL, 2004). In fact, this interval presents the highest values on gamma-ray log (greater than 150 GAPI), probably reflecting the uranium adsorbed to organic content and potassium associated to primary terrigenous components.

Outer-ramp facies association: Outer ramp settings are recorded by the association of the facies S1, C1 and C2. Facies S1 predominates, frequently displaying dm-thick fining-upward cycles defined by the transition from beds with plane-parallel or rippled lamination (Fig. 4-b) to massive ones. Microscopically, the laminated portions of Facies S1 show fine-grained siliciclastic content, preferably replaced by carbonate crystals. In the packstones and wackestones of Facies C1, grains and carbonate mud are generally aggregated, forming grapestones and lumpy textures. These deposits are often overlain by S1 facies, also defining fining-upward cycles. The Facies C2 deposits occurs on the top of the interval, marking a progressive increase in the carbonate content along the interval.

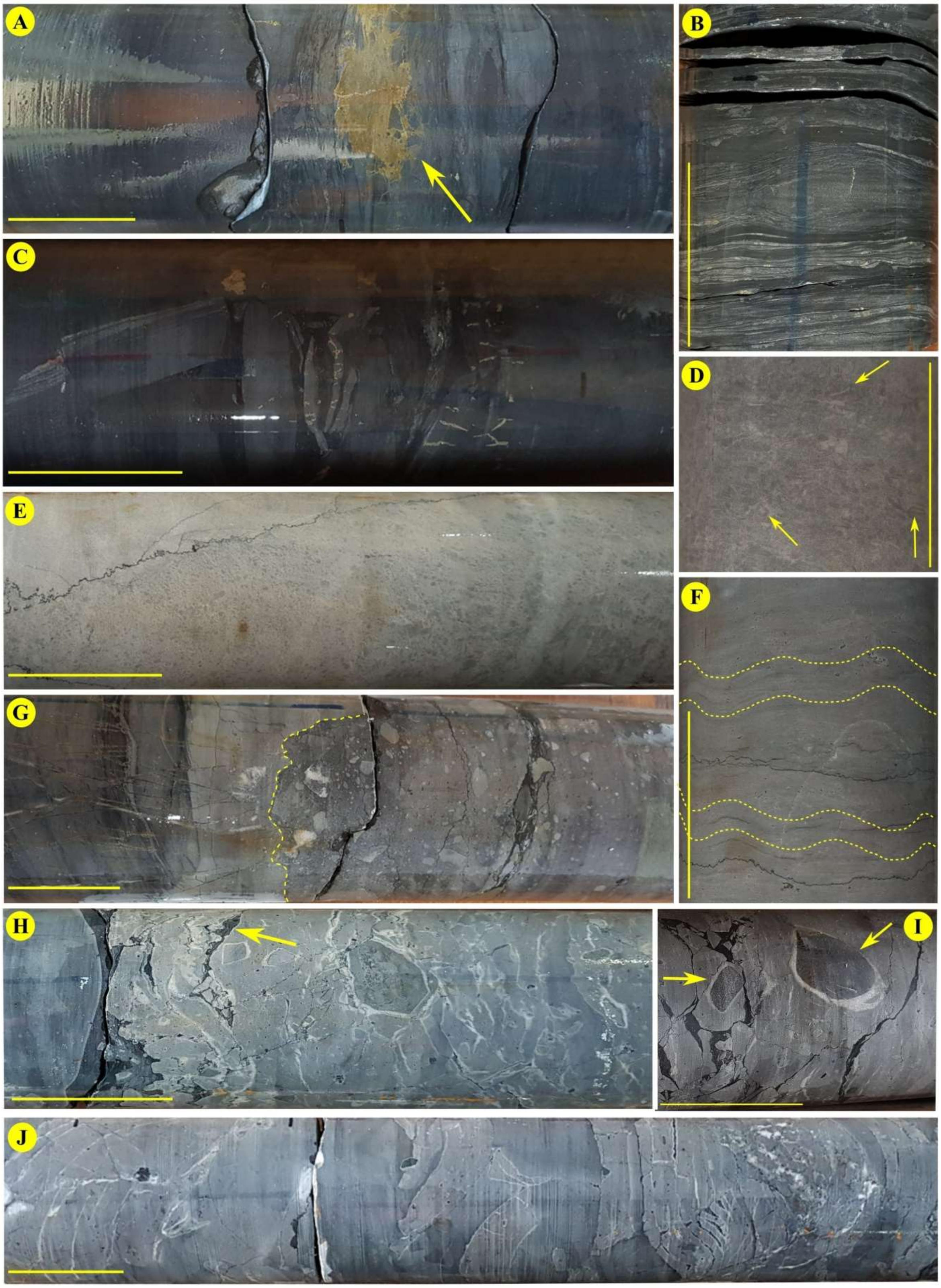

Figure 4: Sedimentary facies from Upper-Espinhaço and Macaúbas 1st order sequences (yellow scale-bar measures 5 cm; top-orientation always to right or up). (a) Black massive siliciclastic mudstone (Facies S1) with large pyrite cluster (arrow). (b) Small asymmetric ripples observed on silt-mud couples of Facies S1. (c) Matrix-supported *breccia* composed of tabular intraclasts of dark gray siliciclastic mudstone. Pyrite fills vertical

fractures hosted on tabular clasts. (d) Carbonate Facies C3 with grain-supported framework. Note the coated carbonate grains (arrows) (e) Subvertical tectonic stylolite marking contact from mud facies to coarse-grained facies. (f) Microbial laminite showing incipient undulated lamination (dashed lines). (g) Erosive unconformity between facies C2 and D1 (dashed lines). (h) (i) Poorly sorted diamicite D1 dolomitizated and dissolved. Detail for *breccia* texture, black muddy (arrow-h) and white coronas (arrow-i). (j) Tabular clasts D1 supported by muddy dolomite D2.

Outer-ramp facies association represent the transition in depositional conditions of siliciclastic to carbonate sediments, clearly observed on gamma-ray log by falling on radioactive values on the top (around 15 GAPI). These deposits show low energy features, indicating deposition within the photic zone below SWB, but eventually affected by reworking of strong storm waves (BURCHETTE and WRIGHT, 1992). Both terrigenous and organic matter contents become less expressive upwards, followed by color changing from black to medium gray, also suggesting a transition of deep suboxic/anoxic conditions to oxygenated ones (BURCHETTEandWRIGHT, 1992; PROUST et al., 1998). Another relevant factor is the presence of ooidal grains with considerable micritic content within the sicliciclastic mud, pointing to occasional resedimentation of oscillatory flow deposits of the adjoining proximal and higher energy environments (TUCKER and WRIGHT, 1990). The agglutination of these grains with carbonate mud by thin micritic coats is a result of syn-depositional process (FLÜGEL, 2004). According to O'Reilly et al. (2016), grapestones and lump grains in modern environments are generated at outer-ramps, with absent or low influence of storm waves, thus preserving the fragile micritic coatings.

Mid-ramp (?) facies association: the mid-ramp set is represented by Facies C2, C3, C4 and C5, which often show intense recrystallization and replacement processes. Pressure solution commonly observed on horizontal and vertical stylolites can be associated to tectonic event that formed *breccia* texture on the interval. The original depositional texture of Facies C3 are masked, despite this, identifies itself a coarse grained-supported carbonate with circular to elliptical shapes (Fig.4-d), even if the vertical stylolite abruptly separate rock with framework supported by carbonate matrix (Fig.4-e). The granular deposits are usually covered by Facies C2 muddy, setting decimetric cycles with deepening-up trend. The intraclasticwackestones of Facies C4 graduate to Facies C2 massive layers, stacked in centimetric cycles of deepening-up trend. The C5 laminite deposits (Fig.4-f) can occur overlapping the muddy layers in these deepening-upward cycles. The mid-ramp facies association is interrupted, to the top, by 1st order erosive unconformity that bounds the Upper-Espinhaço sequence. The gamma-ray log associated to the mid-ramp deposits exhibits a boxcar shape (7-15 GAPI), typical of carbonate system without or with low terrigenous content (EMERY and MYERS, 1996; NAZEER et al., 2016).

The poorly sorted grain-supported carbonate deposits point to a high energy environment, constantly affected by storm waves, below FWWB (BURCHETTE and WRIGHT, 1992), where unidirectional flows could often rework rounded grains to relative deeper zones. On the other hand, the wackestones record a more distal dynamic, with tabular intraclastic layer deposited near or right above SWB (TUCKER and WRIGHT, 1990). In this sense, the associated muddy layers can record calm periods, when suspension processes become dominant. Calm periods with low sedimentation rates would also favor the development of thin distal microbial mats (TUCKER and WRIGHT, 1990).

1.4.2.2. Macaúbas basin cycle

The Macaúbas 1st-order sequence is represented by c. 2.5 meter-thick layer of diamictite and muddy dolomite associated to the Jequitaí Formation, which is bounded on the base (Fig. 4-g) and on the top (Fig. 5-a) by pronounced erosive surfaces. The rocks of this sequence underwent an intense diagenetic dolomitization, which affected both matrix and clasts, and the two described facies were identified based on grain size and remaining sedimentary textures (Table 1). These two facies occur in a single facies association, characterized by meter-scale cycles of D1 diamictites (Fig. 4-h and 4-i) grading upward to D2 muddy deposits. The D2 layer presents its upper boundary marked by an erosive surface (Fig. 5-a), and present tabular pebbles (Facies D1) within muddy matrix (Fig. 4-j).

Although the nature of the studied material (drill core, 1D) hampers the identification of diagnostic glacial features, such as striated pavements or striated clasts, we interpret this facies association as a glaciogenic succession. This interpretation is based on (i) the variety and geometry of the extra-basinal clasts, associated with the fine matrix; (ii) nearby occurrence of this facies association (diamictite-pelite) in sites with diagnostic glacial features (see, for example, ISOTTA et al. 1969; KARFUNKEL and HOPE 1988). In this context, the successive D1-D2 cycles might represent episodic subaquous mass flows associated with deglaciation periods (e.g. PIPER, 1976; READING, 1986; EYLESandEYLES, 2000), followed by stagnant periods of clay decantation. A subglacial (lodgement) origin was discarded based on the lack of preferential orientation of the clast and absence of shear surfaces within the diamictite.

1.4.2.3. Bambuí basin cycle

The topmost 49 meters of the described section are assigned to the Bambuí basin cycle. It presents fifteen different sedimentary facies, which occur in four different facies associations and one glacial-related environment. In an overview, the basal glaciogenic deposits of the Carrancas Formation are overlain by the carbonates and pelites of Sete Lagoas Formation, which record different environments of mixed carbonate–siliciclastic sedimentation.

Glacial related facies: the very base of the Bambuí basin cycle is represented by a 5.5 m-thick layer of a massive diamictite (Facies S3, Table 1), assigned to Carrancas Formation. The rock lacks sedimentary structures or clast orientation and is characterized by an upward decrease in the clast/matrix ratio, followed by a progressive increase in the carbonate content, which marks a meter-scale finning-up cycle. Just as in the previous unit, direct glacial evidence was difficult to find in the 1D analysis, but in this case, there are some apparently faceted clasts (Fig. 5-b) that we interpret as products of glacial abrasion. Moreover, the interpretation of glacial influence in this facies is also based on (i) the great variety and geometry of the extra-basinal clasts; (ii) the fining-upward stacking pattern defined by the transition of S3 to the overlying carbonates (Fig. 5-i), which present post glacial sedimentological features; (iii) regional occurrence of this facies throughout the basin, which in other places presents diagnostic glacial features (e.g. ROMANO and KNAUER 2003; KUCHENBECKER et al., 2013; REIS et al., 2017a). We therefore consider that Facies S3 might record episodic mass flows reworking glacier deposits (e.g. PIPER, 1976; READING, 1986; EYLES and EYLES, 2000).


A
B
C
D
E
F
G
H
I
J
L

Figure 5: Sedimentary facies of Bambuí 1st order sequence (yellow scale-bar measures 5 cm; top-orientation always to right or up). (a) Basal erosive contact on diamictite of Carrancas Formation. (b) Very poorly sorted Facies S3, supported by matrix. The arrow indicates apparently faceted clasts. Vertical fault/fracture system are filled by white calcite. (c) Hummocky cross-lamination of Facies C6. Detail of small subvertical fractures filled by dark organic matter (arrow). (d) and (h) White crusts of aragonite pseudomorphs intercalated to carbonate mud matrix. (e) and (f) Branched columnar stromatolites, clearly divergent on E. Detail in L of dark gray and light gray beds showing deepening-up trend on intercolumnar space. (g) Low-angle cross-laminations of rippled packstone/wackestone (Facies C12). Detail for pyrite cluster (yellow arrow) and dark organic matter on subvertical fractures (red arrow). (i) Contact between Carrancas and Sete Lagoas formations (dashed line). Note diamictite top with large porosity closed by concentric cementation zones and younger fractures filled for abundant pyrite. (j) White aragonite pseudomorph crystal fans with flat top, and thinner levels of micritic and dark needle-shaped aragonite pseudomorph (arrow). Dashed line marks the contact between intraclasticrudstone (C7) and C8. (l) Sandstone layer with ripple marks of Facies S5, fining-upward to siliciclastic mudstone of Facies S4.

Mid-ramp facies association: right over the diamictites of Facies S3, interlayered packstones and mudstones with hummocky cross-lamination (Facies C6, Fig. 5-c) associated to rudstones with intrabasinal clasts (Facies C7) record sedimentation processes under higher energy conditions, affected by storm-waves. In the studied section, mid ramp deposits are the first preserved records of the establishment of Sete Lagoas Formation carbonate ramp, representing drastic climate changes.

Other mid-ramp deposits appear to have been strongly influenced by the $CaCO_3$ saturation of seawater during deposition. They are mainly represented by mudstones hosting a plethora of aragonite pseudomorph fans (Facies C8, Fig. 5-d, 5-h and 5-j), whose needle-shaped crystals reach up to 10 cm in length. It was recognized in two different stratigraphic levels within the described section, in each associated with different deposits: at the most basal occurrence (Fig. 5-j , Fig. 6-a and 6-b), C8 is associated with aragonite-free mudstones (Facies C9) and packstones and grainstones with slump folds and overload pinch-and-swell structures (Facies C10), which are dolomitized in different grades. Furthermore, it is noteworthy the occurrence of massive dolomite beds where the depositional texture is no longer recognizable (Facies D3), presenting black amorphous organic matter preserved between dolomite euhedral crystals (Fig. 10-g and 10-h). In the uppermost occurrence of aragonite fans (Fig. 5-d and 5-h), on the other hand, C8 layers are interbedded with rippled packstone/wackestone, defining decimeter-scale deepening-up cycles. On the top of these cycles, aragonite fans are closely related to thin microbial mats (Fig. 6-e and 6-f).

The mid-ramp deposits record frequent energy variations, attributed to mid-ramp dynamics (BURCHETTEandWRIGHT, 1992), where intense wave action during storm events alternates with periods of calm water-column. During the latter, a $CaCO_3$

supersaturated seawater must have been associated with evaporation rates over 20%, favoring aragonite precipitation (VIEIRA et al., 2015). Even in mid-ramp context, high sedimentary supply in low accommodation areas can generate ramps inclined enough to produce slump structures (VIEIRA et al., 2007a), which can also contribute to the overload recorded by pinch-and-swell structures (KNAUST, 2002).

Mid- to outer-ramp facies association: the analyzed section includes a 12 m-thick interval of carbonate with impressive columnar stromatolites (Facies C11, Fig. 5-e and 5-f), whose branched columnar shape and high synoptic relief indicate a paleobathymetry related to mid- to outer-ramp environments (GROTZINGER, 1989). They occur associated with intracolumnar carbonate muddy sediments (Fig. 6-c), which along with the unusual presence of reworked stromatolites is also coherent with predominantly calm water environment, below FWWB. Rare calcispheres-like microfossils occurs within the muddy intracolumnar material. The stromatolitic interval encompasses two meter-scale deepening-upward cycles marked by the gradual transition between facies C11 and C9.

Outer-ramp facies association: the outer-ramp deposits, composed of Facies C9, C13, C14 and H1 (Table 1), are related to lower energy and deeper environments, allowing deposition of carbonate and siliciclastic muddy in transitional settings. Carbonate mudstones (Facies C9) are more expressive, forming multiples deepening-up cycles interbedded to wackestone layers (Facies C13). These centimeter to millimeter-scale cycles can present microbial mats (Facies C14), developed in periods of low sedimentary input, as well as thin terrigenous layers deposited in relatively deeper conditions. These deposits were affected by pressure-solution processes recorded by abundant stylolites. Facies H1 marl record the gradative transition to basinal environments, often displaying lamination deformed by syn-sedimentary processes, such as slump folds and fluidization structures.

Microfossils were also identified within the outer-ramp setting. Associated with the microbial mats (Facies C14) there are lenticular or irregular shaped microphytolites, with micritic coats and small peloids within their cores (Fig. 6-g). There are also fine-grained, lump and dark micritic peloids, generally displaying spherical, grape-like or irregular forms (Fig. 6-e, h), rarely fragmented.

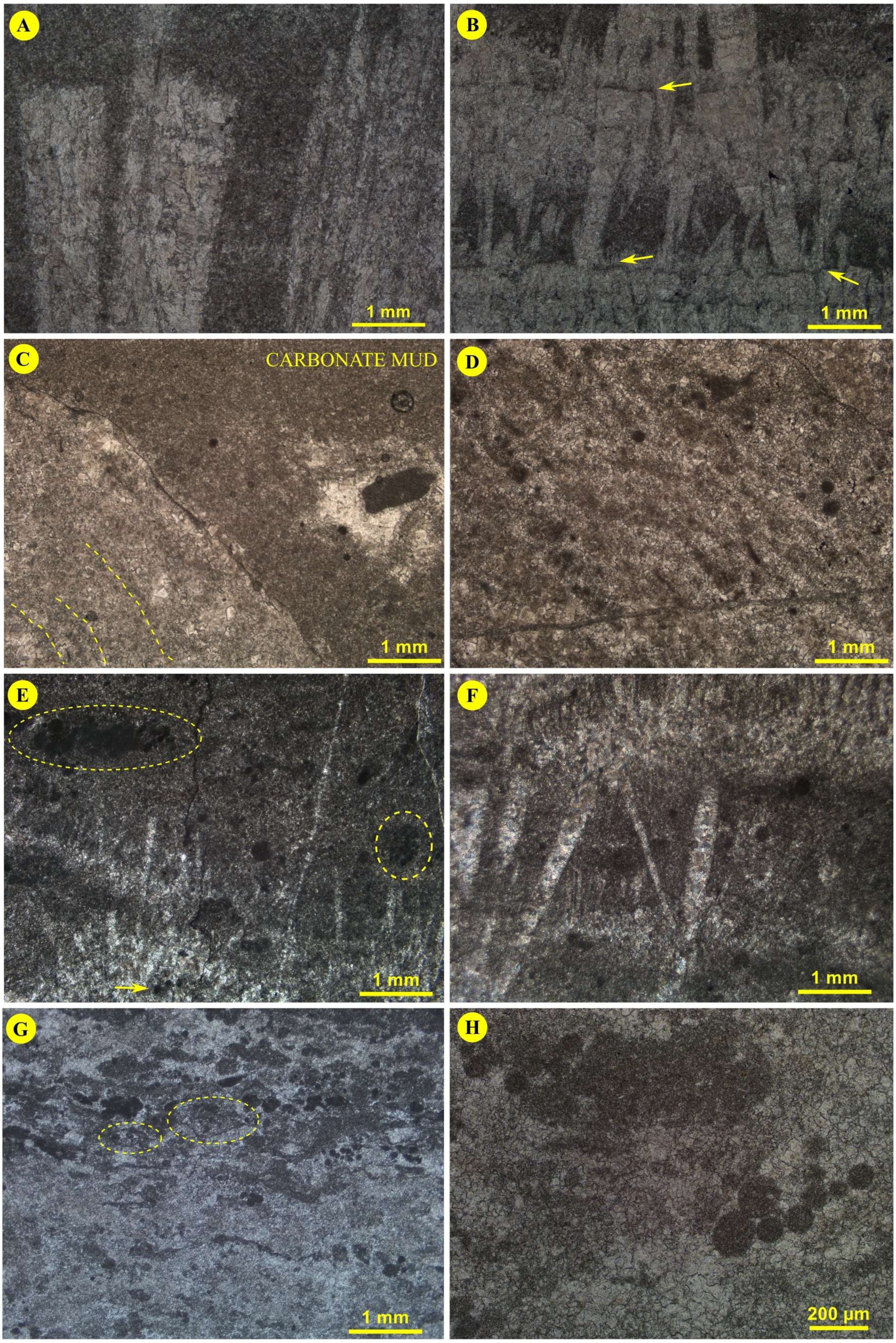

A
1 mm
B
1 mm
C
CARBONATE MUD
1 mm
D
1 mm
E
1 mm
F
1 mm
G
1 mm
H
200 µm

Figure 6: Main microscopic features on carbonate facies of Bambuí 1st order sequence. All thin section photos show plane polarized light and top up. (a) and (b) Needle-like aragonite pseudomorph crystals. Detail of recrystallization on white crystal showing flat-top (a) and micritic thin levels (arrows) marking stages of aragonite precipitation (b). (c) Contact between recrystallized stromatolite and carbonate mud (locally dissolved and cemented). Dashed lines mark incipient internal lamination on stromatolite. (d) Internal micritic lamination and peloidal texture present on recrystallized stromatolite. (e) and (f) Needle-like aragonite pseudomorph crystals precipitated with microbial mat. Detail of the rounded peloids forming agglomerates (dashed circle/ellipse) and trapped into aragonite crystal (arrow). (g) Laminite composed of incipient and discontinuous lamination. Dashed line highlight microphytolites displaying elliptic micritic coats and discrete internal peloids. (h) Spherical peloids lumped like grape-shape. Note clearly boundary between dark micritic and recrystallized carbonate mass.

Basinal/Deep water facies association: the completely drowning of carbonate-ramp is marked by the establishment of a siliciclastic dominated platform, which comprises mainly fine-grained deposits. Facies S4 (Table 1) comprises massive to laminated mudstones, composed by thin couplets of clay minerals and silty grains (quartz and mica), deposited in low energy environment by suspension and action of mud plumes, below SWB (TUCKER and WRIGHT, 1990; BURCHETTE and WRIGHT, 1992). Massive deposits are frequent in the base, and laminated deposits increase to the top, following a transition from plane-parallel lamination to a discrete rippled lamination. This coarsening upward trend is accompanied by the appearance of sandy rippled layers (Facies S5, Fig. 5-l), which become more frequent to the top.

The topward alternation between facies S5 and S4 indicate a shallowing trend, that resulted in influence of stronger storm-waves and unidirectional currents, in a rising rate of sediment supply.

Distal platform facies association: Changes in energy or in sediment input are supported through the establishment of Facies S6 on the top of the studied section. On the basal portion of Facies S6, tabular pebbles of Facies S4 occurs disperse in mid-grained sand, above the local erosive surface, overlain by normal-grading for fine/very fine-grained sand.

1.4.3. Sequence stratigraphy and stacking patterns

The facies associations previously described for each basin cycle can be arranged into subordinated cycles of different orders and natures, whose stacking patterns are described below.

The Upper-Espinhaço deposits are arranged in an overall shallowing-upward trend (Fig. 3), where basinal deep water deposits are overlain by a carbonate ramp, bounded on top by an erosive surface. This decameter-scale progradational stacking pattern is envisaged as part of a 2nd-order cycle and present a coherent gamma-ray log, with the highest values on the base (reflecting organic matter rich facies), decreasing upward at siliciclastic muddy facies, and getting a characteristic box shape at the carbonate deposits. As this 2nd-order progradational cycle is the only record of the Upper-Espinhaço sequence in the section, and no stratigraphic surfaces were characterized, it was not possible to determine if the deposits correspond to a highstand or a lowstand systems tract.

The 2nd-order progradational cycle encompasses several meter-scale cycles that may show shallowing- or deepening-upward trends, marked by alternating carbonate and siliciclastic facies, depending on the sedimentary setting in which they were developed (basinal, outer- or mid-ramp). Shallowing-up cycles usually are marked by the transition of S1 to C1 facies, while deepening-up cycles can occur by the transitions C1-S1, C3-C2 or C4-C5.

In the Macaúbas basin cycle, the JequitaíFm deposits present a general retrogradational pattern, characterized by the stacking of decimeter-scale fining-upward cycles where gravel-grained diamictites (D1) transition to muddy dolomite. The sequence present low values in the GRL (15-30 GAPI), likely due to the extreme diagenetic dolomitization (see section 5.2) and the abundance of carbonate clasts.

Finally, in the Bambuí basin cycle, the stacking pattern of the described facies associations define two main system tracts, both related to the basal 2nd-order sequence of the basin. The basal Transgressive System Tract (TST) encompasses the Carrancas and the basal Sete Lagoas formations, recording the transition from a glacial-related environment to a marine carbonate-ramp, progressively drowned and replaced by pelagic environments to the top. The massive deposits of terrigenous mud on deep water environment (Facies S4) marks the maximum flooding surface (MFS) that bounds the TST. Above the MFS, the pelites are gradually replaced by sandy layers that get thicker towards the top, in a progradational stacking pattern that marks the beginning of a Highstand System Tract (HST).

Within the basal TST, 3rd-order cycles are marked by the alternance of different carbonate ramp settings (from mid- to outer-ramp), which configure retrogradational and progradational trends (Fig. 3).

The GRL is coherent with the above mentioned stratigraphic framework. It shows a sudden decrease of values after the diamictite (135 to 30 GAPI), assuming a boxcard shape in the carbonate section (30-15 GAPI). The gradual change to exclusively terrigenous deposits is followed by the increase in gamma ray values (135-150 GAPI), mainly due to the potassium content of clay minerals. To the top, the GRL present a slight decrease (150 to 120 GAPI) related to sand content.

1.5. Diagenesis

The post-depositional processes were mainly defined according to Tucker and Wright (1990) and Choquette and Pray (1970) concepts for carbonate diagenesis. Different processes occur within the carbonates throughout the burial history of the basin, since early diagenesis on the depositional environment (eodiagenesis), to effective burial settings (mesodiagenesis) and late superficial conditions (telodiagenesis) caused by tectonic uplift (MORAD et al., 2000; CHOQUETTE and PRAY, 1970; MOORE, 1989). Although many authors (FOLK, 1965; TUCKER and WRIGHT, 1990; FLÜGEL, 2004; SCHOLLE and ULMER-SCHOLLE, 2003) may distinguish neomorphism to recrystallization (strict sense), this terminology was generically applied for processes that resulted on crystallinity changes (increase/decrease) at minerals with the same chemical composition with different phases of stability (ie. aragonite to calcite).

The main diagenetic processes identified throughout the section were recrystallization, dolomite, calcite and silica cementation, replacement by dolomite and quartz, mechanical compaction, chemical compaction (pressure solution), dissolution and generation of secondary porosity and pyritization (related to both organic matter reduction and hydrothermalism). These diagenetic features record interaction with fluids from superficial (marine or mixed) to buried settings, later affected by ascending hydrothermal fluids, which often obliterates previous crystalline textures. Petrographic porosity is absent.

The observed features were classified and organized according to their temporal relations, in order to reveal the post depositional history of each 1st order sequence described in the section. In an overview, we recognize processes of eo- and mesodiagenesis, partially obliterated by a younger hydrothermal stage, related to a tectonic event. The post depositional evolution of the studied section is summarized in Figure 7 and described in the following sections.

1.5.1. Upper-Espinhaço sequence

In the Upper-Espinhaço sequence, the eodigenesis is recorded by early marine fibrous/acicular calcite/aragonite (in Facies C1), followed by dolomitization (replacement and cementation). The dolomitization is also observed at rhombohedral crystals with cloudy cores and clear out zone (Fig.8-a and 8-b). In cases of pervasive dolomitization, the fabric was generally hypidiotopic to idiotopic, inequigranular to equigranular (from very fine to medium grained). Another eodiagenetic feature is pyritization of organic matter in suboxic/anoxic bottom conditions (mainly S1 facies), which generated framboidal pyrite crystals occurs disseminated (Fig. 8-c) or in larger rounded clusters/agglomerates (Fig. 4-a).

During mesodiagenesis, micaceous grains and dolomitic coats were deformed by mechanical compaction. Pressure solution formed stylolites and dissolution seams parallel/sub parallel to bedding, within which pyritization of organic matter also generated framboidal crystals. In this stage, silicification included cementation by quartz overgrowing on silty grains or formation of poikilotopic blocks.

The next diagenetic process caused localized dissolution (unsaturated fluid percolate through tectonic fractures), which formed cave and vugular secondary porosity. These vugs were partially cemented by fine to medium-grained euhedral dolomite crystals and also by calcite in both botryoidal and rhombic/scalenohedral crystals, commonly zonate (Fig. 8-b and 8-d). Subordinately, some of them were filled by saddle/baroque dolomite (Fig. 8-a and 8-h). Later silicification locally replaced the depositional carbonate fabric and also siliciclastic mudstones clasts within the tectonic *breccia*, also causing cementation by euhedral hexagonal quartz prisms (Fig. 8-a, 8-f and 8-g). The silica also formed microcrystalline masses (Fig. 8-d) and, punctually, chalcedony.

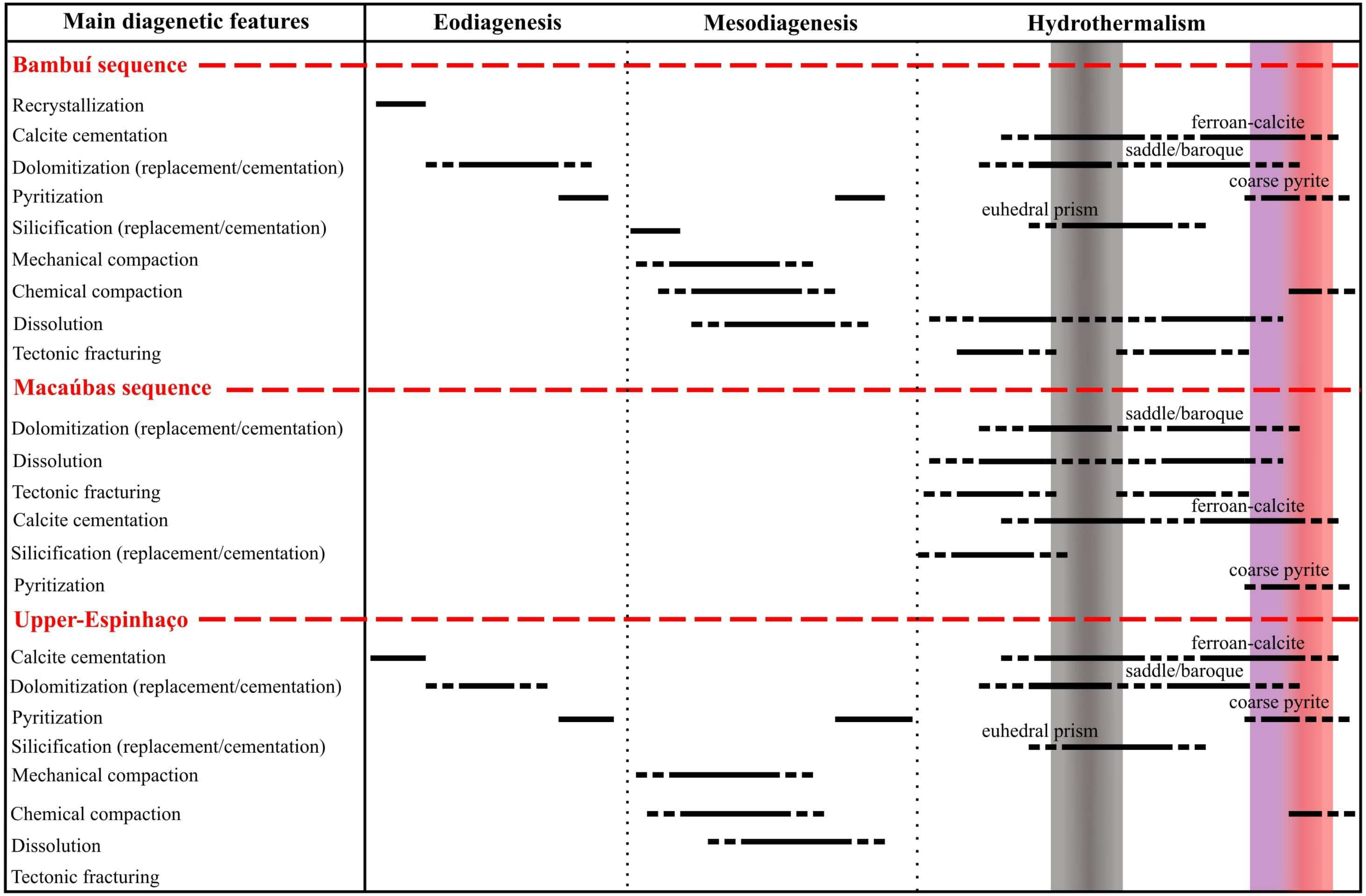
Main diagenetic features
Eodiagenesis
Mesodiagenesis
Hydrothermalism
Bambuí sequence
Recrystallization
Calcite cementation
Dolomitization (replacement/cementation)
Pyritization
Silicification (replacement/cementation)
Mechanical compaction
Chemical compaction
Dissolution
Tectonic fracturing
ferroan-calcite
saddle/baroque
coarse pyrite
euhedral prism
Macaúbas sequence
Dolomitization (replacement/cementation)
Dissolution
Tectonic fracturing
Calcite cementation
Silicification (replacement/cementation)
Pyritization
saddle/baroque
ferroan-calcite
coarse pyrite
Upper-Espinhaço
Calcite cementation
Dolomitization (replacement/cementation)
Pyritization
Silicification (replacement/cementation)
Mechanical compaction
Chemical compaction
Dissolution
Tectonic fracturing
ferroan-calcite
saddle/baroque
coarse pyrite
euhedral prism

Figure 7: Schematic diagenetic evolution of the 1st-order sequences based on petrography. The gray column mark organic matter emplacement, while the colored column represent Fe content depleted on hydrothermal fluid, changing carbonate-stain color from purple (ferroan-calcite) to red (non-ferroan calcite). Pyritization includes framboidal and euhedral (cubic/hexagonal) crystals.

After this stage, vertical fractures cut the vugular pores (Fig. 8-d), and are cemented by mosaic block of quartz, calcite and cubic/hexagonal pyrite, often related to sphalerite masses. Dolomite cores may be dissolved by silica rich fluid and filled by late calcite. The calcite cement of this stage present large crystals in poikilotopic blocks (Fig. 8-e), replacing some terrigenous grains. Some of these large crystals stained by acid solution of alizarin and potassium-ferrocyanide indicate Fe depleted on fluid by pyrite precipitation, triggering color change from purple border (ferroan-calcite) to red nuclei (non-ferroan calcite). Also worth mention the occurrence of vertical stylolites, likely related to compressional tectonics.

1.5.2. Macaúbas sequence (Jequitaí Formation)

Macaúbas sequence represents the most extremely altered interval in the described section. The two facies within the sequence were extensively dissolved and dolomitized, which obliterated almost all the original sedimentary texture and also the records of early diagenetic stages. The process generated a microcrystalline fabric made of very fine to medium grained crystals of dolomite, with heterogeneously distributed coarse well-formed ones (Fig. 9-a). The pervasive dolomitization also resulted on cryptocrystalline dark clusters, dispersed on a cloudy fabric (Fig. 9-f).

After dolomitization, there was a dissolution and fill of secondary porosity. On coarser facies, centimetric elongated pores occurs oriented according to the bedding (Fig. 9-d), pebbles and granules commonly present rims similar to circum-granular fracture (Fig. 9-b). This pore type is often connected to vugs, and both were filled by two dolomitic phases. Euhedral to subhedral medium rhombs precipitated preferentially on pores surfaces, followed by saddle/baroque dolomitic cements (Fig. 9-c and 9-d). These medium to coarse crystals shows undulating extinction on polarized light. The dolomitic cements association may close the porosity forming drusy textures. Dark muddy sediments, often with organic content, were injected between larger crystals on pores (Fig. 9-b, 9-c, 9-d and 9-e). This ductile mechanical process concentrates on *brecciated* levels, with sediment between the angular clasts and filling channels/fractures (Fig. 4-h and 4-i). The dissolution on fine-graded sediments above coarse layers generated submilimetricvugs, cemented by well-formed clear rhombs (Fig. 9-

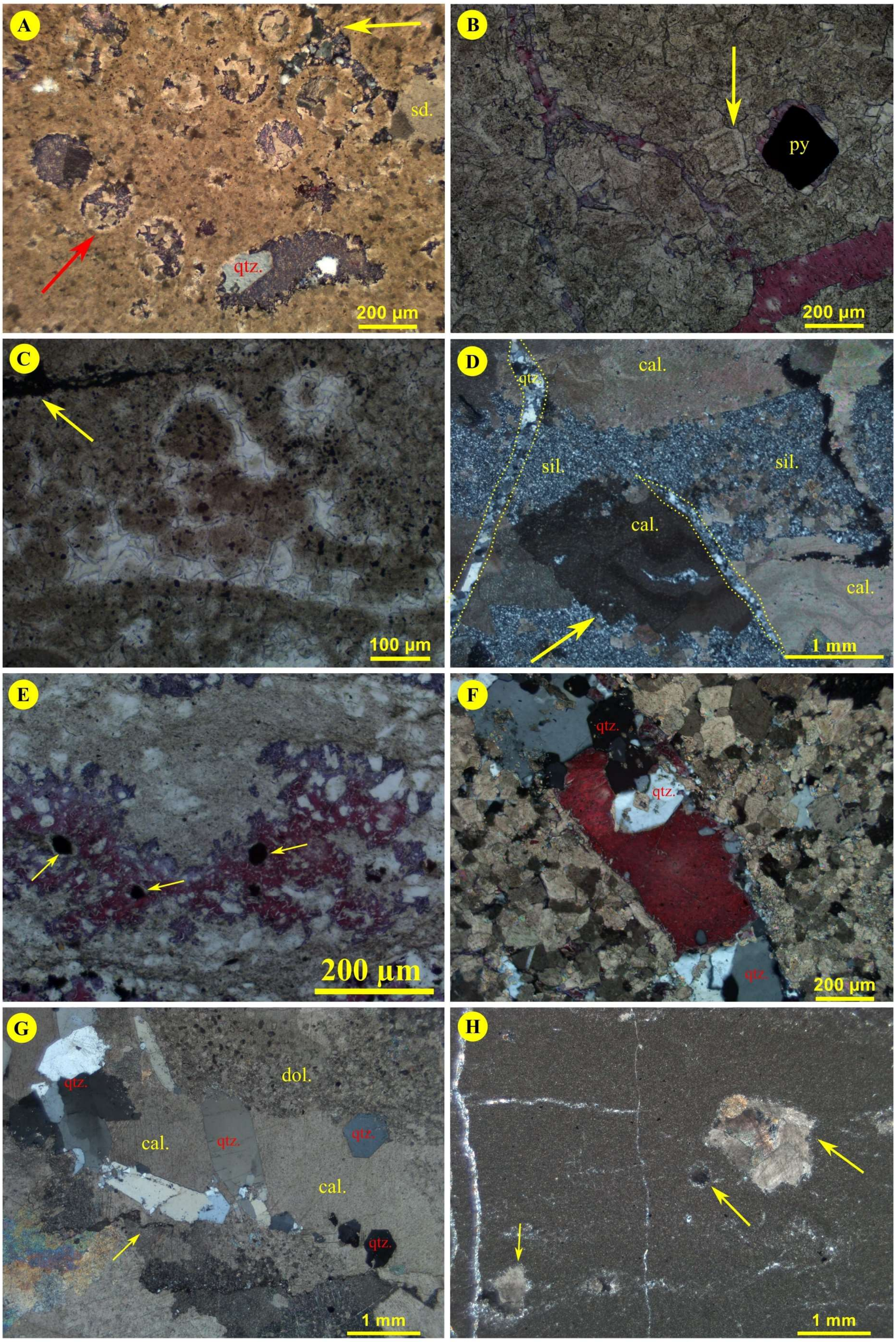

Figure 8: Main diagenetic features of Upper-Espinhaço 1st order sequence. (a) Facies C1 hosting moldic/inter-intragranular porosity cemented by dolomite (red arrow), saddle dolomite, quartz and ferroan-calcite (purple

stain). Detail for rounded oolites (yellow arrow). (b) Dolomite crystals showing darker cloudy nuclei contrasting to clear edges (arrow). Ferroan/non-ferroan calcite filling in enlarged fractures. Note coarse-pyrite related to Fe-enriched fluid. (c) Framboidal pyrite crystals disseminated on Facies C1 and locally concentrated (arrow). (d) Silicification recorded by microcrystalline fabric and late quartz cement at fractures (dashed line). Detail of vugular porous filled by botryoidal calcite (arrow). (e) Poiquilotopic calcite encompassing silt grains (white molds) of Facies S1. Ferroan calcite edges, non-ferroan cores and euhedral coarse pyrite (arrow) are associated to hydrothermalism. (f) and (g) Second porosity cemented by prismatic quartz and block calcite. The arrow points to stylolite surface. (h) Baroque dolomite (arrows) filling in vug porosity. Cal:calcite; dol:dolomite; qtz:quartz; sil:silica; sd:saddle dolomite; py:pyrite. Thin section photos are top up and taken under plane polarized light (c,d,e,f) and crossed polarized light (a,b).

e). The same brownish mud fills secondary porosity and intercrystalline space (Fig. 9-e and 9-f). The vertical/subvertical fractures cuts the dolomitic mass, cemented by quartz, calcite (ferroan or non-ferroan) and pyrite.

1.5.3. Bambuí sequence

Recrystallization in the early eodiagenetic stages is recorded in different facies of Bambuí sequence. Due to this process, the aragonite pseudomorphs (Facies C8) got a mosaic fabric (Fig. 6-a, 6-b and 6-f), with non-equidimensional to equidimensional medium-grained crystals often showing non-planar boundaries. A discrete increase in the crystallinity of the stromatolite columns and associated carbonate mud (Facies C11) are also attributed to early recrystallization (Fig. 6-c and 6-d). Other eodiagenetic processes include: (i) widespread dolomitization, which in some places obliterates depositional textures (Fig. 10-h); (ii) Pyritization of organic matter in microbial mats, which generated disperse of agglomerated framboidal crystals.

Mesodiagenetic mechanical compaction is recorded by deformed mica grains, muddy films molded to clasts and clast fracturing. Quartz overgrowth occurs in some clasts of the diamictite (Facies S3). Stylolites parallel to the bedding as well as sutured contacts resulted from pressure solution caused by sedimentary load. In this stage there was also pyritization of organic matter.

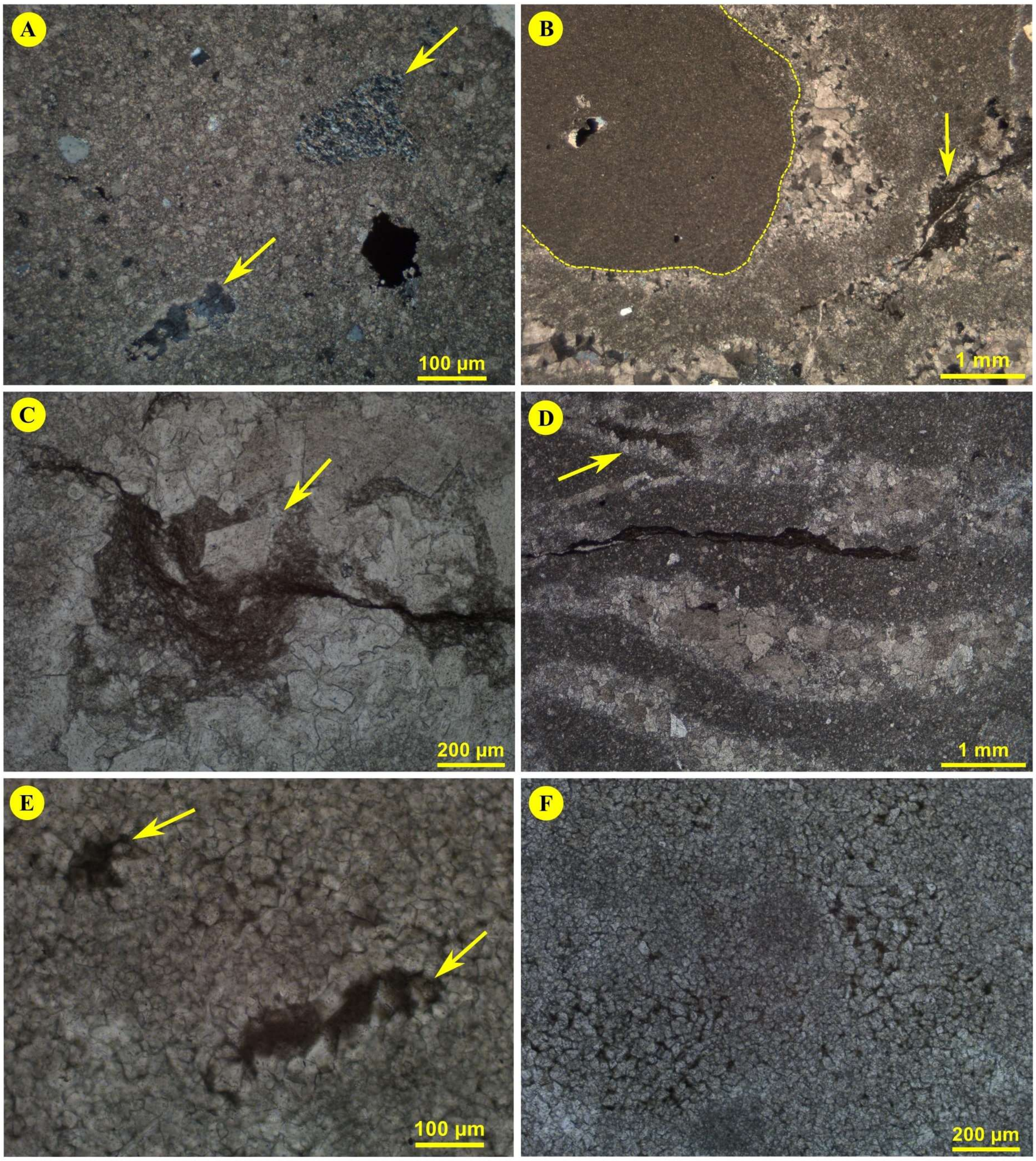

Figure 9: Main diagenetic features of Macaúbas 1st order sequence. Thin section photos are top up and taken under plane polarized light (c,d,e,f) and crossed polarized light (a,b). (a) Dolomite groundmass showing relict clasts (arrows) and late pyritization. (b) and (d) Dolomite crystals precipitated at pore wall, posteriorly filled by dark clay with organic content (arrow). Note on B that cementation occurs along contact between clast and dolomitic replaced matrix (dashed line) and fenestral porosity closed by dolomite and baroque dolomite on D. (c) Saddle dolomite partially corroded (arrow) and dark content filling intercrystalline space. (e) and (f) Muddy dolomite (Facies D2) with dark organic content in small pore (arrows) and between rhombohedral crystals.

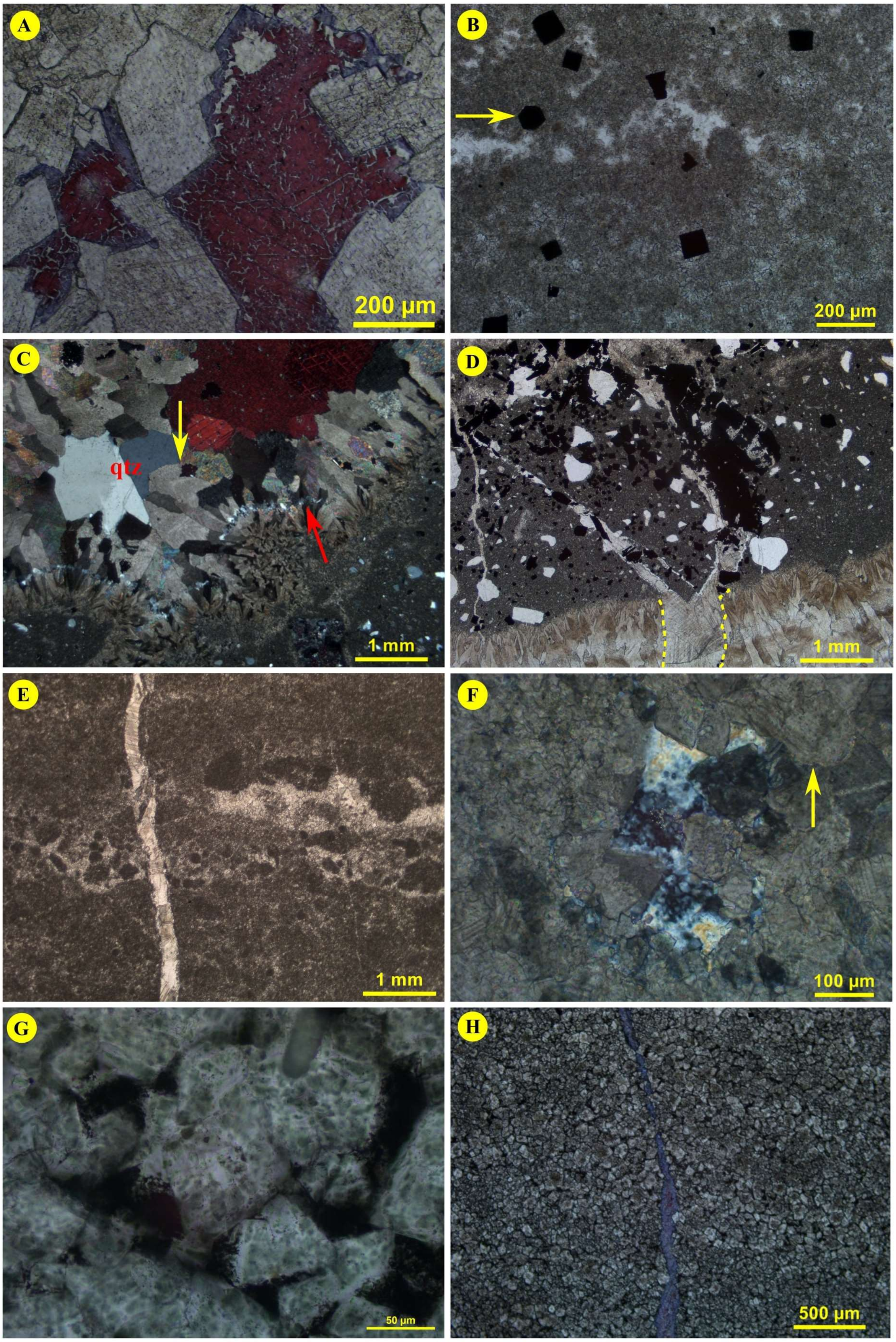

Figure 10:Main diagenetic features of Bambuí 1st order sequence. Thin section photos are top up and taken under plane polarized light (a,b,d,e,g,h) and crossed polarized light (c,f); qtz:quartz. (a) Saddle dolomites and

calcite cement with purple edges and red core stained by acid solution of alizarin and potassium-ferrocyanide. (b) Coarse euhedral pyrite cubic and hexagonal (arrow). (c) and (d) Centimeter-sized cavities cemented by euhedral zonate dolomites (yellow arrow), quartz and calcite (red stained). Note (c) silica replacing internal zone on dolomite (red arrow), and (d) late fracture (dashed line) related to hydrothermal ferrous fluid (calcite and abundant coarse pyrite). (e) secondary porosity formed on first hydrothermal stage and subvertical late fracture, both filled by calcite. (f) Microcrystalline silica post dolomitic phase. Note silica corroding dolomite edges and zonate crystals (arrow). (g) and (h) Organic matter (bitumen?) hosted on Facies D3. Detail of organic matter on dolomite nuclei and intercrystalline pores (g). Late subvertical tectonic fracture filled by ferroan-calcite (h).

The opening of secondary porosity in the contact between the diamictite and the cap carbonate (Facies S3 and C6) record a late hydrothermal process, which generated centimeter-sized cavities. These pores were then filled by cloudy bladed dolomite, covered by broad crystals of pyramidal (radiaxial fibrous) terminations, well zoned and with optical continuity (Fig. 10-c and 10-d). Saddle/baroque dolomite (Fig. 10-a) shows undulating extinction. It is worth mentioning the presence of amorphous organic material (bitumen?) hosted on Facies C9, within rhombohedron nuclei, between crystals and, locally, in thin fractures (Fig. 10-g).

This late hydrothermal stage is followed by localized silicification, which closed or reduced the vug porosity throughout the succession. Between the dolomite rhombohedral crystals, quartz occur in microcrystalline texture (Fig. 10-f), while in bigger pores it precipitates as large euhedral/subhedral crystals (Fig. 10-c).

Just like in the other sequences, the last observed diagenetic processes include the calcite filling of vertical fractures (Fig. 10-h), which cut the secondary porosity (Fig. 10-d and 10-e). The wider crystals commonly exhibit ferrous content evidenced by the purple color stain on the edges (ferroan calcite) and reddish (non-ferroan calcite) on the nuclei (Fig. 10-a). In this stage also occurred the precipitation of euhedral pyrite crystals (Fig. 10-b and 10-d).

1.6. Discussions

1.6.1. Regional correlations

The seismic, well and field data available in the literature, indicate that the described 1st order sequences are widely distributed in the São Francisco craton and their adjoining orogenic belts.

Within the São Francisco craton, the Upper-Espinhaço sequence present its maximum thickness in the Pirapora aulacogen, but also occur on the Januária basement high. It crops out in the easternmost portion of the aulacogen in regional-sized antiformal culminations (Cabral, Água Fria and Bicudo ridges) caused by the partial inversion of the basin’s basement during the uplift of the Araçuaí orogen. In these structures, the units of the Upper-Espinhaçosequence are comprised in the Conselheiro Mata Group, which also occur in the eastern border of the Araçuaí orogen, in the Southern Espinhaço range (e.g. HERCOS et al. 2008; REIS, 2016).

The Conselheiro Mata Group is represented by sag marine shallow-water platform, whose deposits configure three major regressive-transgressive cycles. In the topmost one (Rio Pardo Grande Fm.), lower shoreface fine grained siliciclastic deposits are succeeded by a carbonate-siliciclastic shelf, in a regressive trend (e.g. SANTOS et al. 2015). Based on the stratigraphic pattern of the Upper-Espinhaço sequence in the described section, a correlation with the topmost progradational tract of Rio Pardo Grande Formation would be possible. If compared to the fine grained units of the Conselheiro Mata Group, the deposits of facies S1 have a larger amount of clay and organic matter, which could indicate the presence of deeper environments within the aulacogen. The correlation with the Conselheiro Mata Group is also corroborated by the analysis of seismic sections (e.g. HERCOS et al. 2008; REIS, 2011; REIS et al. 2017a), that demonstrates the subsurface continuity of the outcropping strata of the unit to the aulacogen region. The deposition of the Conselheiro Mata Group is constrained between c. 1280 Ma and 930 Ma, based on the age of detrital zircons and the age of intrusive basic rocks (e.g. KUCHENBECKER, et al., 2015b). Thus, considering the proposed correlation, the described Upper-Espinhaço 1st order sequence would record a Stenian reactivation cycle of the Pirapora aulacogen.

The nature and thickness of the unconformity bounded diamictite strata described in our section support its correlation with Macaúbas 1st order sequence. In the Pirapora aulacogen domain, Macaúbas 1st order sequence is represented by the Jequitaí Formation glaciogenic deposits, which also crops out at the rims of Cabral, Bicudo and Água Fria antiformal culminations (e.g. KARFUNKEL and HOPE 1988; MARTINS et al., 2011). According to seismic and field data, the sequence is up to 300m thick near the northern edge of the aulacogen, becoming thinner toward its southern edge, where the described section is located (REIS et al., 2017a).

The Jequitaí Formation presents subsurface continuity with the diamictite bearing units of the Macaúbas Group that crops out extensively in the Araçuaí orogen, and these units has long been considered as correlatives (e.g. UHLEIN et al., 2004). These units also have glacial correlatives in the West Congo belt (the african counterpart the Araçuaí orogen), which are interbedded to volcanic rocks dated in c. 700 Ma (STRAATHOF, 2011; THIÉBLEMONT et al., 2011). For this reason, they have been considered as recording the

Cryogenian Sturtian glaciation, one of the greatest climatic events in Earth's history (BABINSKI et al., 2012; KUCHENBECKER et al., 2016a, 2015a; REIS et al., 2017a).

From a tectonic point of view, the Macaúbas 1st order sequence is the sedimentary record of a Cryogenian rifting event, which is also marked by plutonic and volcanic magmatism both in Brazil and Africa (e.g. ROSA et al., 2007; KUCHENBECKER et a. 2015b). The pericratonic branches of such rifting system evolved to a passive margin stage (e.g. ALKMIM et al., 2006, 2017; PEDROSA-SOARES et al. 2011), while in the cratonic domain it caused fault reactivation in the Pirapora aulacogen (REIS et al. 2017a), which generated accommodation space to the described succession.

Finally, the stratigraphic data of the Bambuí sequence presented in this paper allow us to establish basinward correlations. The Bambuí 1st order sequence comprise a basal 2nd-order TST, usually interpreted as a consequence of post-glacial eustatic rise (VIEIRA et al., 2007; MARTINS and LEMOS, 2007; ALKMIM and MARTINS-NETO, 2012; KUCHENBECKER et al., 2016; PERRELLA JÚNIOR et al., 2017; REISandSUSS, 2016; REIS et al., 2017a; CAETANO-FILHO et al., 2019). As demonstrated by Caetano-Filho et al. (2019), this stratigraphic array is recognizable in sections on both Januária and Sete Lagoas highs, including in those deposited within forebulge grabens (REIS and SUSS, 2016). In a conservative interpretation of the stacking patterns and cycles hierarchy, our data are in good agreement with this stratigraphic framework and demonstrates that it is also valid for the Pirapora aulacogen domain (Fig. 11).

It is worth mentioning that the analysis of previously published seismic sections images (REIS, 2016) suggests that the whole carbonatic succession presented by this study could represent the condensed section of the entire basal 2nd-order sequence of the Bambuí basin cycle. In that case, the described maximum flooding surface would be related to the second 2nd-order sequence of the basin, usually represented by Serra de Santa Helena Formation deposits. Further discussion of this matter, however, would require detailed seismic analysis, which is beyond the scope of this paper.

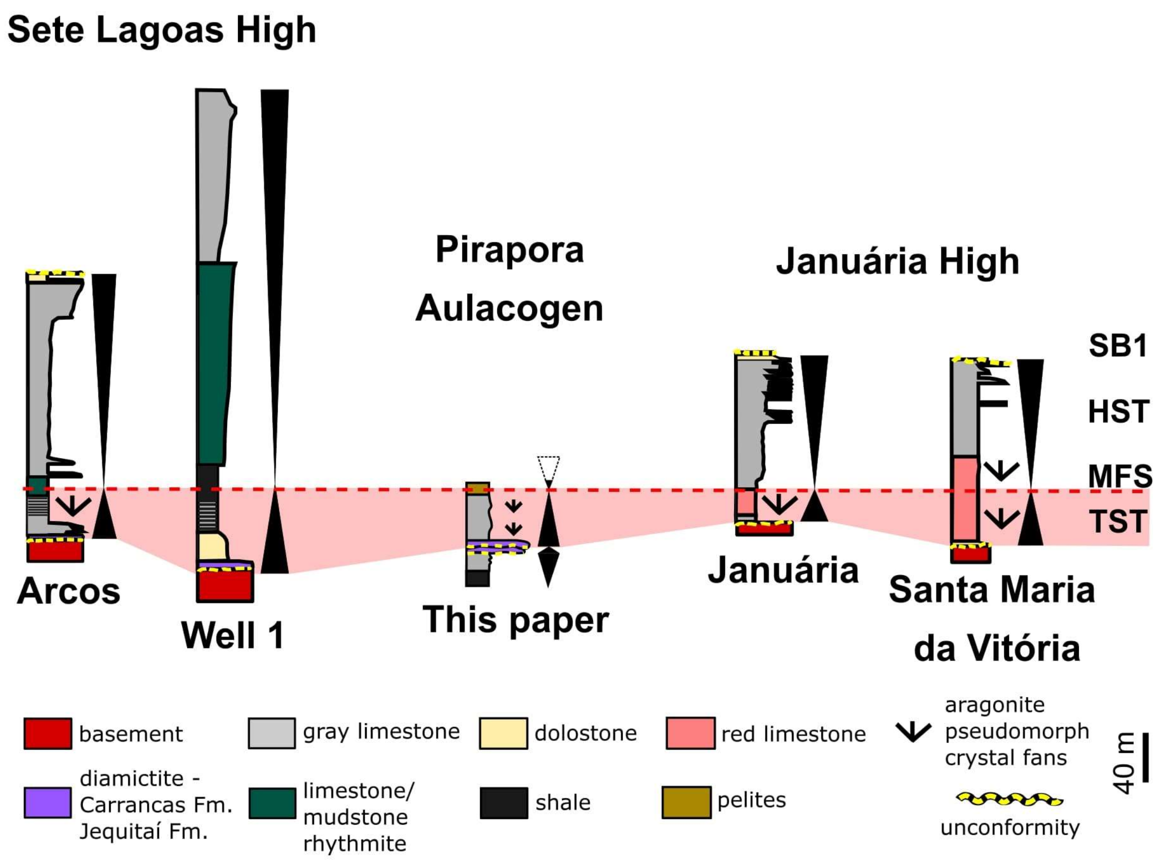

Figure 11: Schematic stratigraphic correlation for Transgressive System Tract (TST) of basal Bambuí sequence (light pink area), according to Caetano-Filho et al. (2019). Maximum flooding surface (MSF) establish the datum between sections located at Sete Lagoas High, Pirapora aulacogen and Januária High, (HST) Highstand System Tract and (SB1) Sequence Boundary. Modified from Caetano-Filho et al. (2019).

1.6.2. Structural reactivation of the Pirapora aulacogen during the Bambuí basin cycle

The three 1st order sequences describes in this paper are in good agreement with those described in the seismic sections that crosscut the Pirapora aulacogen and confirms that this through was successively reactivated along the Proterozoic, in a remarkable example of tectonic inheritance (REIS et al., 2017a). As revealed by seismic sections, the lower Bambuí sequence presents a slight thickening over the preexisting structures of the Pirapora aulacogen, suggesting reactivation of older fabric elements induced by the orogenic overburden along the craton margins (REIS, 2016), which is also indicated by provenance data (KUCHENBECKER et al., 2015b). In this sense, the stratigraphic patterns observed in the basal 2nd-order sequence of the Bambuí basin cycle at the aulacogen area should provide information on the timing and mechanics of such reactivation. Two sections located along the northern border of the aulacogen present a lithological pattern distinct from that described in the section studied. In both the Jequitaí (SANTOS et al., 2004) and 1-RF-1-MG (MARTINS and LEMOS, 2007) sections, the basal TST encompasses the direct passage of diamictites to pelites, without intermediate carbonate units. Thus, when considering the data presented here, in the initial stages of the basin filling at the Pirapora aulacogen domain, there would be carbonate platforms in its southern portion (likely connected to those recorded at the Sete Lagoas high) and a depocenter to north, marked by deep water pelagic sedimentation. This might suggest that the faults in the northern border of the aulacogen may have been reactivated before those of its southern edge.

1.6.3. Microbialites and microfossils

The Sete Lagoas Formation encompasses several stromatolite occurrences at the Sete Lagoas and Januária highs, and also at Brasília Belt (e.g. VIEIRA et al., 2007b; ALVARENGA et al., 2014; SANCHEZ, 2014; FANTINEL et al. 2015, BITTENCOURT et al., 2015; KUCHENBECKER et al., 2016a; PERRELLA JÚNIOR et al., 2017; CAETANO-FILHO et al., 2019). The microbialites occur within shallow carbonate facies (inner ramp) in the two basal 2nd order sequences, more frequently in the upper one (REIS et al., 2017a). The stromatolites described in this paper are the first reported in the Pirapora aulacogen domain, and can be correlated with other basinwide occurrences. They were formed in mid- to outer-ramp settings during the TST, and the most basal stromatolite beds are about 5 meters above the Carrancas Formation diamictite, likely one of the earliest biological records of the entire basin. Perrella Júnior et al. (2017) reported early microbialite deposits at Januária High domain also in an outer ramp setting within the TST. The hybrid and stratiform microbialites described by the authors are in the basal 15 meters of the Sete Lagoas Formation are associated with aragonite pseudomorphs, and display the negative $\delta^{13}C$ pattern that characterizes the lowermost deposits throughout the basin (CI-1, PAULA-SANTOS et al., 2017; CAETANO-FILHO et al. 2019). Sanchez (2014) also described four stromatolitic deposits within the lower Sete Lagoas Formation at Cabeceiras (GO), Unaí, Piumhí and Pains (MG), but only the Unaí occurrence displays such negative $\delta^{13}C$.

The microfossils described in the mid- to outer-ramp associations were already reported on carbonate from Sete Lagoas Formation in other parts of the basin (e.g. NOBREandCOIMBRA, 2000;SANCHEZ, 2014), and also in another Neoproterozoic basins worldwide (e.g. Draken Formation, Spitsbergen-Norway, Swett and Knoll, 1985). In all these cases, however, such microfossils were found in facies recording moderate energy environments, like grainstone and packstones. In the described section, on the other hand, the microfossil assemblage occur within lower energy facies, and the association with the microbial mats suggest a lower sediment supply, allowing the full development of microbial laminites.

1.6.4. Oversaturation and aragonite precipitation

At least two events of carbonate oversaturation in seawater are recorded within the Bambuí 1st order sequence in the described section. The older one is recorded by aragonitic layers less than 1m above the Carrancas Formation diamictite, which present aragonite pseudomorphs fans with crystals up to 10cm-high, surrounded by alternated couples of aragonite crusts and micrite laminae. The second supersaturated moment is recorded by the aragonitic layers above the stromatolite interval, where up to 2cm-high aragonite fans and aragonitic crusts are associated with microbial mats in anoxic/suboxic conditions.

The petrogenesis of aragonite crystal fans has been explained by two not mutually exclusive models, both assuming a supersaturated setting as a premise: (i) the abiotic model, which envisage the formation of aragonite fans as resulting from high frequency environmental changes promoted by ocean degassing (FABRE et al., 2013) or seasonal high frequency variation in evaporation rates (VIEIRA et al, 2015); and (ii) the biotic model, which associates the high alkalinity to bacterial sulfate-reduction in anoxic/suboxic conditions (e.g. LORENTZ et al., 2004; BERGMANN et al., 2013; OKUBO et al., 2018).

The first episode of carbonate oversaturation recorded within the described section is most likely related to the abiogenic model, since it occurs right after the glacial deposits, with no microbial influence. The upper aragonite fan deposits, on the other hand, seems to be related to a biogenic trigger, since they are interbedded to microbial mats and present abundant eodiagenetic framboidal pyrite. A biogenic model was already claimed to explain the formation of aragonite fans at Januária High (OKUBO et al., 2018). It is also worth mentioning that the flooding recorded by the TST would favor anoxic/suboxic bottom conditions, and consequently, the bacterial sulfate reduction, as recorded in the Late Ediacaran Johnnie Formation (United States), in which precipitation of aragonite fans occurred at the maximum flooding interval (PRUSS et al, 2008).

1.6.5. Diagenetic events

The three 1st order sequences described within the Pirapora aulacogen present distinct diagenetic histories, although sharing records of a late hydrothermal event. Both diagenetic and hydrothermal processes described within the section seem to have been influenced by the structural framework of the basin.

In the siliciclastic-dominated succession of the Upper-Espinhaço sequence, ooids in the intercalated grapestone layers (C1-Table 1) indicate the presence of coastal environments nearby in the basin. These marine ooids/peloids were cemented by calcite/aragonite, and subsequently, the rock was totally dolomitized, yet in early diagenetic stages. Several mechanisms have been proposed in the literature to explain the early dolomitization of sedimentary deposits. In general, the principal ones involve (i) interaction with freshwater saturated in calcium carbonate due to evaporation; or (ii) interaction with marine water mixed with other fluids such as meteoric water (TUCKER and WRIGHT, 1990; FLÜGEL, 2004). Since the rocks in question were formed in deeper environments, it seems incompatible with the first model, being more likely related to fluid mixing processes. Taking into account the association with coastal settings, it can be related to mixing with meteoric fluids, because phreatic percolation or in deep confined aquifers could have reached the basin and promoted early dolomitization (TUCKER and WRIGHT, 1990; SCHOLLE and ULMER-SCHOLLE, 2003;FLÜGEL, 2004). In any case, the expressive normal faults that bound the Pirapora aulacogen may have acted as routes to the migration of fluids involved in the dolomitization.

The Kohout convection model offers another possibility for the early dolomitization process, based on fluid migration driven by geothermal heat (KOHOUT, 1967; KOHOUT et al., 1977; TUCKER and WRIGHT, 1990; FLÜGEL, 2004). Nevertheless, since there is no record of magmatic activity in the Pirapora aulacogen during the Upper-Espinhaço basin cycle, this possibility seems remote. It is worth mentioning, however, that Chaves (2013) reported volcanic *breccia*s with c. 1200 Ma in the southern Espinhaço ridge, probably coeval to the Upper-Espinhaço sequence in that adjoining rift through.

The pervasive dolomitization of the Jequitaí Formation diamictites seems to have been influenced by meteoric process, such as pedogenesis or phreatic alteration, and later by a hydrothermal event. The coarse-grained facies commonly show white dolomite coronas around the clasts (Fig.4-h, 4-i), often connected to fenestral porosity. These structures are very similar to circum granular desiccation cracks followed by dolomitic crack-filling related displacement, both typical features of abiogenic dolocretes (Alpha-type, Wright 1990, 2007), related to seasonal variation of the phreatic level (WRIGHT and TUCKER, 1991).

Furthermore, dolocretes with phreatic genesis occurs mostly on non-carbonate hosts (ALONSO-ZARZA and WRIGHT; 2010), which is the case of the described rocks. Additionally, the fenestral porosity architecture is less compatible for vadose zones. The dirty and cloudy aspect of microcrystalline dolomite fabric possibly points to secondary genesis by clay replacement. It is worth mentioning that late hydrothermal saddle/baroque dolomites occur filling large pores. Oxidized paleosoil-like mudstones affected by periodic exposures was also reported on the Macaúbas sequence elsewhere (Reis et al., 2017a).

It is important to emphasize that these post-depositional processes that affected the Jequitaí Formation clearly occurred before the deposition of the overlying diamictite (Carrancas Fm.), since the later was not affected by them. This is an important finding, since the stratigraphic position and geologic significance of the glacial deposits in the São Francisco basin have been extensively discussed (e.g. REIS and SUSS 2014, KUCHENBECKER et al. 2016a, UHLEIN et al., 2017; CAETANO-FILHO et al. 2019).

A late hydrothermal event affected the three 1st order sequences of the section, and was strongly influenced by the tectonic activity in the aulacogen. In all the cases, it was a two-step process, as follows: after tectonic fracturing, the percolation of unsaturated fluids occured with greater potential of corrosion. The three 1st-order sequences presents zones of preferential dissolution, such as the tectonic *breccia* that cuts the Upper-Espinhaço sequence, the enlarged fenestral porosity in the diamictite (Facies D1) from Macaúbas sequence and the stratiform cavities hosted on the Carrancas Formation diamictites. The high permeability may be related to both the primary porous system, the inherited secondary porosity, and/or discrete discontinuities (tectonic structures, lithological or permo-porous contrast, sequence boundary). The fluids that percolated in this stage drived the precipitation of silica (prismatic quartz, microcrystalline quartz and chalcedony), calcite (non-ferroan) and dolomite.

The last hydrothermal stage begin with reactivation and enlargement of fractures systems. It is characterized by dolomite and saddle/baroque dolomite, ferroan to non-ferroan calcite, amorphous organic matter, large cubic to hexagonal pyrites and sphalerite. Saddle dolomites are commonly associated with epigenetic sulphide mineralization (TUCKER and WRIGHT, 1990; FLÜGEL, 2004), which is discreetly present in the section. Furthermore, this dolomitic phase is closely associated to organic content inside inter/intracrystalline porosity (Facies D3) and rare thin fractures (Fig. 6-c and 6-f). Baroque/saddle dolomite is also related to hydrocarbon systems, which suggest temperature formation in oil/gas window, between 60-150 °C (RADKE and MATHIS, 1980). In this sense, the basal deposits of organic rich siliciclastic mudstones in the Upper-Espinhaço sequence would represent a potential source rock on the petroleum system of São Francisco Basin, whose gas occurrences have long been studied (e.g. OLIVEIRA, 1998; PINTO et al., 2001; FUGITA and CLARK, 2001; REIS, 2011). Similar diagenetic models with saddle dolomites and bitumen emplacement have already been reported for Sete Lagoas Formation (TONIETTO, 2011).

1.7. Conclusions

Based on the detailed analysis of subsurface data, we describe for the first time a complete sedimentary section of the Pirapora aulacogen, an important multicyclic rift basin buried in the middle of the São Francisco craton. The sedimentary succession preserved within the southern margin of the Pirapora aulacogen encompasses three 1s-order basin cycles, related to three major tectonic processes of the São Francisco craton evolution. According to seismic data, a fourth and older sequence is also preserved in the aulacogen, but exclusively within its main depocenter and out of the range of the described section.

The basal Upper-Espinhaço record a Stenianreactivation of the aulacogen, and encompasses a basal organic-rich siliciclastic interval that is a strong candidate to source rock in the Precambrian petroleum system of the São Francisco basin. Diagenetic features described within this succession, such as baroque/saddle dolomites and residual bitumen reinforces such potential, suggesting an evolution within the gas and oil P-T window.

For the first time, a section containing two overlapping diamictite units was described within the São Francisco basin. The older one, the Jequitaí Formation, likely represents a record of the Cryogenian Sturtian glaciation, and is correlated to the Macaúbas basin cycle, which crops out extensively in the Araçuai orogen (e.g. BABINSKI et al. 2012; KUCHENBECKER et al. 2015a, 2016a; REIS et al. 2017a; CAETANO-FILHO et al. 2019). This unconformity bounded unit underwent intense post-depositional alteration prior to the deposition of the overlying sequence, likely in a pedogenic/phreatic environment. The younger diamictite unit is the first record of the Bambuí basin cycle in the section, and is assigned to the Carrancas Formation. It transition to the top to the Sete Lagoas Formation cap carbonates, which has been considered as a record of a Late Ediacaran glaciation (e.g. KUCHENBECKER et al. 2016a; PAULA-SANTOS and BABINSKI, 2018; CAETANO-FILHO et al., 2019).

The stratigraphy of the Bambuí sequence includes a TST and a HST which correspond to the basal 2nd-order sequence of the basin. This stratigraphic array is in good agreement with recent basinwide correlations involving sections from both Januaria and Sete Lagoas highs (CAETANO-FILHO et al. 2019), and demonstrates that such evolution is also valid for the Pirapora aulacogen domain. A few meters above the diamictite, a columnar stromatolite interval could record the early record of biological activity in the basin, in the glacial aftermath. Two aragonite intervals were recognized in the carbonates from basal Sete Lagoas Formation, which seems to record different processes of oversaturation in seawater driven by the climate and biological evolution of the basin. Finally, based on comparison with data from the literature, the stratigraphic array of the Bambuí sequence suggest that, during the Ediacaran reactivation of the aulacogen, the faults in its northern boundary were reactivated prior to the southern ones.

A late hydrothermal event affected the three major sequences of the aulacogen and was influenced by tectonic fracturing likely occurred during its the last reactivation cycle, in the late Ediacaran. It caused organic matter remobilization and the percolation of Fe-rich fluids, which is recorded by bitumen and coarse sulfides on pores and fractures of the carbonates from the Sete Lagoas Formation. These features indicates the potential of such unit both to the petroleum and metalogenetic systems of São Francisco basin.

Finally, this research demonstrated that the Pirapora aulacogen is an important and, so far, almost not studied basin, whose records can certainly contribute to the understanding of the several processes involved in the evolution of the São Francisco craton - a key piece in the Precambrian tectonic history of South America.

Acknowledgments

The authors are grateful to Petra Energia S.A. for providing the well data, and to FAPESP (#2016/06114-6) and FAPEMIG (#APQ-02459-16) for financial support. Thisstudywasfinanced in partbythe Coordenação de Aperfeiçoamento de Pessoal de Nível Superior – Brasil (CAPES) – FinanceCode 001. Lara Matos holds a CAPES scholarship (Financial Code 001). Sergio Caetano-Filho holds a FAPESP scholarship grant (#2016/11496-5). Marly Babinski, Ricardo Trindade and Matheus Kuchenbecker are fellows of the Brazilian Research Council (#309447/2006-2, #206997/2014-0 and #309106/2017-6, respectively).

References

ALKMIM, Fernando F. and CRUZ, Simone C.P. Crátogenos, aulacógenos, orógenos e sua interação: O caso do Cráton do São Francisco-Congo e sistemas brasilianos/ pan-africanos adjacentes. *Anais III Simpósio sobre o Cráton do São Francisco*, SBG, Núcleo BA/SE, 2005. p. 185–187.

ALKMIM, Fernando F. *et al.* The Araçuaí Belt. In: HEILBRON, MONICA; ALKMIM, FERNANDO F.; CORDANI, UMBERTO G. (Org.). *São Francisco Craton,Eastern Brazil. Tectonic Genealogy of a Miniature Continent.*[S.l: s.n.], 2017. p. 255–276. Disponível em: <http://link.springer.com/10.1007/978-3-319-01715-0_14>.

ALKMIM, Fernando F. *et al.* Kinematic evolution of the Araçuaí-West Congo orogen in Brazil and Africa: Nutcracker tectonics during the Neoproterozoic assembly of Gondwana. *Precambrian Research*, 149, 43–64, 2006.

ALKMIM, Fernando F.; MARTINS-NETO, Marcelo A. Bacia intracratonica do São Francisco: Arcabouço estrutural e cenários evolutivos. In: PINTO C.P.; MARTINS-NETO M.A. (eds) *Bacia do São Francisco: Geologia e Recursos Naturais*, p. 9-30 SBG/MG, Belo Horizonte, 2001.

ALKMIM, Fernando F.; MARTINS-NETO, Marcelo A. Proterozoic first-order sedimentary sequences of the São Francisco craton, eastern Brazil. *Marine and Petroleum Geology*, v. 33, n. 1, p. 127–139, 2012.

ALKMIM, Fernando F; TEIXEIRA, Wilson. The Paleoproterozoic Mineiro Belt and the Quadrilátero Ferrífero. In: HEILBRON, MONICA; ALKMIM, FERNANDO F.; CORDANI, UMBERTO G. (Org.). . *São Francisco Craton,Eastern Brazil. Tectonic Genealogy of a Miniature Continent.* [S.l.]: Regional Geology Reviews, Springer International Publishing, 2017. p. 71–94. Disponível em: <http://link.springer.com/10.1007/978-3-319-01715-0_5>.

ALMEIDA, Fernando Flávio Marques. O Craton do São Francisco. *Revista Barsileira de Geociências*, v. 7, p. 349–364, 1977.

ALONSO-ZARZA, A.M., WRIGHT, V.P. Calcretes. In ALONSO-ZARZA, A.M.; TANNER, L.H. (Eds), Carbonate in Continental Settings: Facies, Environments and Processes, Vol 61, Elsevier, Amsterdam, pp. 225-267, 2010.

ALVARENGA, Carlos J.S. *et al.* Meso-Neoproterozoic isotope stratigraphy on carbonates platforms in the Brasilia Belt of Brazil. *Precambrian Research*, v. 251, p. 164–180, set. 2014. Disponível em: <http://dx.doi.org/10.1016/j.precamres.2014.06.011>.

BABINSKI, Marly. *et al.* Neoproterozoic glacial deposits from the Araçuaí orogen, Brazil: Age, provenance and correlations with the São Francisco craton and West Congo belt. *Gondwana Research*, v. 21, n. 2–3, p. 451–465, 2012. Disponível em: <http://dx.doi.org/10.1016/j.gr.2011.04.008>.

BABINSKI, Marly; VIEIRA, Lucieth Cruz; TRINDADE, Ricardo I F. Direct dating of the Sete Lagoas cap carbonate (Bambuí Group, Brazil) and implications for the Neoproterozoic glacial events. *Terra Nova*, v. 19, n. 6, p. 401–406, 2007.

BARBOSA, Johildo S. F.; BARBOSA, Rafael G. The Paleoproterozoic Eastern Bahia Orogenic Domain. In: HEILBRON, Monica; ALKMIM, Fernando F.; CORDANI, Umberto G. (Org.). *São Francisco Craton,Eastern Brazil. Tectonic Genealogy of a Miniature Continent.* [S.l.]: Regional Geology Reviews, Springer International Publishing, 2017. p. 57–69. Disponível em: <http://link.springer.com/10.1007/978-3-319-01715-0_4>.

BERGMANN, Kristin D.; GROTZINGER, John P.; FISCHER, Woodward W. Biological

Influences on seafloor carbonate precipitation. *PALAIOS*, v. 28, n. 2, p. 99–115, 21 fev. 2013. Disponível em: <https://pubs.geoscienceworld.org/palaios/article/28/2/99-115/146310>.

BITTENCOURT, Jonathas S. *et al.*O registro fóssil das coberturas cedimentares do cráton do São Francisco em Minas Gerais. *Geonomos*, v. 23, n. 2, p. 39–62, 31 dez. 2015. Disponível em: <https://periodicos.ufmg.br/index.php/revistageonomos/article/view/11692>.

BURCHETTE, T.P.; WRIGHT, V.P. Carbonate ramp depositional systems. *Sedimentary Geology*, v. 79, n. 1–4, p. 3–57, ago. 1992. Disponível em: <https://linkinghub.elsevier.com/retrieve/pii/003707389290003A>.

BURKE, Kevin. Aulacogens and Continental Breakup. *Annual Review of Earth and Planetary Sciences*, v. 5, n. 1, p. 371–396, maio 1977. Disponível em: <http://www.annualreviews.org/doi/10.1146/annurev.ea.05.050177.002103>.

CAETANO-FILHO, Sergio *et al.*Sequence stratigraphy and chemostratigraphy of an Ediacaran-Cambrian foreland-related carbonate ramp (Bambuí Group, Brazil). *Precambrian Research*, v. 331, n. June, p. 105365, set. 2019. Disponível em: <https://doi.org/10.1016/j.precamres.2019.105365>.

CAMPOS, José E. G. *et al.*Geologia do Grupo Paranoá na porção externa da Faixa Brasília. *Brazilian Journal of Geology*, v. 43, n. 3, p. 461–476, 1 set. 2013. Disponível em: <http://ppegeo.igc.usp.br/scielo.php?script=sci_arttextandpid=S2317-48892013000300004andlng=ptandnrm=isoandtlng=pt>.

CASTRO, Paulo de T. A.; DARDENNE, Marcel A. O Conglomerado Samburá (Grupo Bambuí, Neoproterozóico) E Rochas Sedimentares Associadas No Flanco Leste Da Serra Da Pimenta, Sw De Minas Gerais: Um Sistema De Fan Delta. *Geonomos*. [S.l: s.n.]. , 1995

CATUNEANU, Octavian. *Principles of Sequence Stratigraphy*. [S.l.]: Elsevier, 2006.

CATUNEANU, Octavian *et al.* Sequence Stratigraphy: Methodology and Nomenclature. *Newsletters on Stratigraphy*, v. 44, n. 3, p. 173–245, 1 nov. 2011. Disponível em: <http://openurl.ingenta.com/content/xref?genre=articleandissn=0078-0421andvolume=44andissue=3andspage=173>.

CAXITO, Fabrício A. *et al.* Multiproxy geochemical and isotope stratigraphy records of a Neoproterozoic Oxygenation Event in the Ediacaran Sete Lagoas cap carbonate, Bambuí Group, Brazil. *Chemical Geology*, v. 481, n. February, p. 119–132, mar. 2018. Disponível em: <https://doi.org/10.1016/j.chemgeo.2018.02.007>.

CAXITO, Fabrício A. *et al.* Marinoan glaciation in east central Brazil. *Precambrian Research*, v. 200–203, p. 38–58, abr. 2012. Disponível em: <https://linkinghub.elsevier.com/retrieve/pii/S0301926812000101>.

CHAVES, Mario L. de S. C. *et al.*Grenvillian age magmatism in the Southern Espinhaço Range (Minas Gerais): evidence from U-Pb zircon ages. *Brazilian Journal of Geology*, v. 43, n. 3, p. 477–486, 1 set. 2013. Disponível em: <http://ppegeo.igc.usp.br/scielo.php?script=sci_arttextandpid=S2317-48892013000300005andlng=ptandnrm=isoandtlng=pt>.

CHOQUETTE, P. W. and PRAY, L. C. Geologic nomenclature and classification of porosity in sedimentary carbonates: *AAPG Bulletin*, v. 54, no. 2, p. 207– 250, 1970.

COELHO, J. C. C.; MARTINS-NETO, M.A; MARINHO, M. S. Estilos estruturais e evolução tectônica da porção mineira da bacia proterozóica do São Francisco. *Revista*

Brasileira de Geociências, v. 38, p. 149–165, 2008.

COSTA, M. T.; BRANCO, J. J. R. Roteiro para excursão Belo Horizonte-Brasília. 1961, [S.l: s.n.], 1961. p. 25.

CRUZ, Simone C. P.; ALKMIM, Fernando F. The Paramirim Aulacogen. In: HEILBRON, Monica; ALKMIM, Fernando F; CORDANI, Umberto G (Org.). . *São Francisco Craton,Eastern Brazil. Tectonic Genealogy of a Miniature Continent.*[S.l.]: Regional Geology Reviews, Springer International Publishing, 2017. p. 97–115. Disponível em: <http://link.springer.com/10.1007/978-3-319-01715-0_6>.

CRUZ, Simone C. P.; ALKMIM, Fernando F. The tectonic interaction between the Paramirim aulacogen and the Araçuaí belt, São Francisco craton region, Eastern Brazil. *Anais da Academia Brasileira de Ciências*, v. 78, n. 1, p. 151–173, 2006.

DARDENNE, Marcel. A. *Síntese sobre a estratigrafia do Grupo Bambuí no Brasil Central. Congresso Brasileiro de Geologia*. [S.l: s.n.]. , 1978

DICKSON, J. A. D. A modified staining technique for carbonates in thin sections. *Nature Publishing Group*, p. 587, 1965.

DUNHAM, Robert J. Classification of carbonate rocks according to depositional texture. In: HAM,W.E. (Ed.), *Classification of carbonate rocks. American Association of Petroleum Geologists Memoir*, pp. 108–121, 1962

EMBRY, A.F., KLOVAN, J.E. A late Devonian reef tract on northeastern Banks Island. N.W.T. – Bull. *Canadian Petrol. Geol*., 19, 730-781, 1971.

EMERY, D.; MYERS, K.J. Sequence Stratigraphy. *Blackwell Science*, Oxford, 297, 1996.

EYLES; EYLES. Subaqueous mass flow origin for Lower Permian diamictites and associated facies of the Grant Group, Barbwire Terrace, Canning Basin, Western Australia. *Sedimentology*, v. 47, n. 2, p. 343–356, 25 dez. 2000. Disponível em: <http://doi.wiley.com/10.1046/j.1365-3091.2000.00295.x>.

FABRE, Sébastien *et al.* Origin of cap carbonates: An experimental approach. *Palaeogeography, Palaeoclimatology, Palaeoecology*, v. 392, p. 524–533, dez. 2013. Disponível em: <https://linkinghub.elsevier.com/retrieve/pii/S0031018213004628>.

FANTINEL, L. M., *et al*. Microbialitos da Formação Sete Lagoas (Grupo Bambuí), Neoproterozoico, estados de Minas Gerais e Goiás. In Microbialitos do Brasil do Pré-Cambriano ao Recente: um atlas (p. 168-193). Rio Claro, SP: IGCE/UNESP, 2015.

FLÜGEL, Erik. *Microfacies of Carbonate Rocks*. Berlin, Heidelberg: Springer Berlin Heidelberg, 2004. Disponível em: <http://link.springer.com/10.1007/978-3-662-08726-8>.

FOLK, Robert L. Petrology of the sedimentary rocks. *Geomorphology*, p. 190, 1968. Disponível em: <https://www.lib.utexas.edu/geo/folkready/folkprefrev.html>.

FOLK, Robert. L. Some aspects of recrystallization in ancient limestones. In: PRAY, L. C., MURRAY, R.C. (Eds), *Dolomitization and Limestones Diagenesis*. Society of Economic Paleontologists and Mineralogists, Special Publication 13, pp. 13-48, 1965.

FRIEDMAN, Gerald M.. Identification of Carbonate Minerals by Staining Methods. *SEPM Journal of Sedimentary Research*, v. Vol. 29, n. 1, p. 87–97, 1959. Disponível em: <https://pubs.geoscienceworld.org/jsedres/article/29/1/87-97/95441>.

FUGITA A.M. and CLARK-FILHO J.G. Recursos Energéticos da Bacia do São Francisco: Hidrocarbonetos líquidos e gasosos. In: PINTO C.P., MARTINS-NETO M.A. (eds.) *Bacia do São Francisco: Geologia e Recursos Naturais*. Belo Horizonte, Sociedade Brasileira de Geologia (SBG), pp.265-284, 2001.

GROTZINGER, J.P. Facies and evolution of Precambrian carbonate depositional systems: Emergence of the modern platform archetype. In: CREVELO, P.D.; WILSON, J.L.; SARG, J.F.; READ, J.F. (eds.). *Controls on Carbonate Platforms and Basin Development*, Special Publication of Society of Economic Paleontologists and Mineralogists, Tulsa, 44: 79-106, 1989.

GUACANEME, Cristian *et al.* C, O, and Sr isotopic variations in Neoproterozoic-Cambrian carbonate rocks from Sete Lagoas Formation (Bambuí Group), in the Southern São Francisco Basin, Brazil. *Brazilian Journal of Geology*, v. 47, n. 3, p. 521–543, 2017. Disponível em: <https://www.ars.usda.gov/ARSUserFiles/80400525/Articles/JN_FoodNutrDB.pdf%0Ahttp://www.sjmms.net/text.asp?2015/3/2/141/156425%0Ahttp://web.b.ebscohost.com.ezproxy.lib.utexas.edu/ehost/resultsadvanced?sid=7f6126c9-b053-47c1-89f6-49a395934040@sessionmgr113and>.

GUADAGNIN, Felipe *et al.* Age constraints on crystal-tuff from the Espinhaço Supergroup — Insight into the Paleoproterozoic to Mesoproterozoic intracratonic basin cycles of the Congo–São Francisco Craton. *Gondwana Research*, v. 27, n. 1, p. 363–376, jan. 2015. Disponível em: <http://dx.doi.org/10.1016/j.gr.2013.10.009>.

GUADAGNIN, Felipe; CHEMALE, Farid. Detrital zircon record of the Paleoproterozoic to Mesoproterozoic cratonic basins in the São Francisco Craton. *Journal of South American Earth Sciences*, v. 60, n. July, p. 104–116, jul. 2015. Disponível em: <https://linkinghub.elsevier.com/retrieve/pii/S0895981115000334>.

HEILBRON, Monica; CORDANI, Umberto G.; ALKMIM, Fernando F. *São Francisco Craton, Eastern Brazil*. Cham: Springer International Publishing, 2017. Disponível em: <http://link.springer.com/10.1007/978-3-319-01715-0>. (Regional Geology Reviews).

HERCOS, Cízia Mara. Arcabouço Tectono-Estratigráfico Da Bacia do São Francisco Nos Arredores Das Serras Da Água Fria E Da Onça, Porção Centro-Norte Do Estado De Minas Gerais. p. 207, 2008.

HERCOS, Cízia Mara; MARTINS-NETO, Marcelo Augusto; DANDERFER FILHO, André. Arcabouço estrutural da Bacia do São Francisco nos arredores da Serra da Água Fria (MG), a partir da integração de dados de superfície e subsuperfície. *Revista Brasileira de Geociências*, v. 38, n. 2, p. 197–212, 1 jun. 2008. Disponível em: <http://ppegeo.igc.usp.br/index.php/rbg/article/view/8172/7452>.

ISOTTA, C.A.L.; ROCHA-CAMPOS, A.C.; YOSHIDA, R. Striated pavement of the upper Precambrian glaciation in Brazil. Nature, 222:466-468, 1969.

IYER, S; BABINSKI, M; KROUSE, H; CHEMALEJR, F. Highly 13C-enriched carbonate and organic matter in the Neoproterozoic sediments of the BambuíGroup, Brazil. *Precambrian Research*, v. 73, n. 1–4, p. 271–282, maio 1995. Disponível em: <https://linkinghub.elsevier.com/retrieve/pii/0301926894000823>.

KARFUNKEL, Joachim; HOPPE, Andreas. Late Proterozoic glaciation in central-eastern Brazil: Synthesis and model. *Palaeogeography, Palaeoclimatology, Palaeoecology*, v. 65, n. 1–2, p. 1–21, maio 1988. Disponível em:

<https://linkinghub.elsevier.com/retrieve/pii/0031018288901083>.

KELLER, G. Randy; STEPHENSON, Randell A. The Southern Oklahoma and Dniepr-Donets aulacogens: A comparative analysis. *Memoir of the Geological Society of America*. [S.l: s.n.], 2007. v. 200. p. 127–143. Disponível em: <https://pubs.geoscienceworld.org/books/book/443/chapter/3799094/>.

KNAUST, D. Pinch-and-swell structures at the Middle/Upper Muschelkalk boundary (Triassic): evidence of earthquake effects (seismites) in the Germanic Basin. *International Journal of Earth Sciences*, v. 91, n. 2, p. 291–303, 1 mar. 2002. Disponível em: <http://link.springer.com/10.1007/s005310100225>.

KOHOUT, F.A.; HENRY, H.R.; BANKS, J.E. Hydrogeology related to geothermal conditions of the Floridan Plateau. In: SMITH, DOUGLAS L.; GRIFFIN, GEORGE M. (Org.). . *The Geothermal Nature of the Floridan Plateau*. Special pu ed. [S.l.]: Bureau of Geology, 1977. p. 1–41.

KOHOUT, F.A. Groundwater flow and the geothermal regime of the Floridan plateau. Trans. Gulf-Cst. Aa. *Geol. Socs*. 17, 339-354,1967.

KUCHENBECKER M. Relações entre as coberturas do Cráton do São Francisco e bacias situadas em orógenos marginais: o registro de datações U-Pb de grãos detríticos de zircão e suas implicações geotectônicas. PhD thesis, Instituto de Geociências, Universidade Federal de Minas Gerais, Belo Horizonte, 173 p, 2014.

KUCHENBECKER, M. *Quimioestratigrafia e proveniência sedimentar da porção basal do Grupo Bambuí em Arcos (MG)*. 2011a. 91 f. Universidade Federal de Minas Gerais, 2011.

KUCHENBECKER, Matheus *et al.* Proveniência e análise sedimentar da porção basal do Grupo Bambuí em Arcos (MG). *Geologia USP. Série Científica*, v. 13, n. 4, p. 49–61, 1 dez. 2013. Disponível em: <http://www.revistas.usp.br/guspsc/article/view/78914>.

KUCHENBECKER, Matheus *et al.* Age constraints for deposition and sedimentary provenance of Espinhaço Supergroup and Bambuí Group in Eastern São Francisco craton. *Geonomos*, v. 23, n. 2, p. 14–28, 31 dez. 2015a. Disponível em: <http://www.igc.ufmg.br/portaldeperiodicos/index.php/geonomos/article/view/708>.

KUCHENBECKER, Matheus *et al.* Detrital zircon age patterns and provenance assessment for pre-glacial to post-glacial successions of the Neoproterozoic Macaúbas Group, Araçuaí orogen, Brazil. *Precambrian Research*, v. 266, p. 12–26, set. 2015b. Disponível em: <http://dx.doi.org/10.1016/j.precamres.2015.04.016>.

KUCHENBECKER, Matheus *et al.* Chemostratigraphy of the lower Bambuí Group, southwestern São Francisco Craton, Brazil: insights on Gondwana paleoenvironments. *Brazilian Journal of Geology*, v. 46, n. X, p. 145–162, 2016a. Disponível em: <http://www.scielo.br/scielo.php?script=sci_arttextandpid=S2317-48892016000700145andlng=enandnrm=isoandtlng=en>.

KUCHENBECKER, Matheus *et al.* The Gorutuba Formation: Coastal to continental sedimentation on the eastern margin of Bambuí Basin (MG). *Geologia USP - Serie Cientifica*, 2016b.

LOPES, T.C. O Supergrupo Espinhaço na Serra do Cabral, Minas Gerais: contribuição ao estudo de proveniência sedimentar. Masters Dissertation, Universidade Federal de Minas Gerais, 136p, 2012.

LORENTZ, Nathaniel J.; CORSETTI, Frank A.; LINK, Paul Karl. Seafloor precipitates and C-isotope stratigraphy from the Neoproterozoic Scout Mountain Member of the Pocatello Formation, southeast Idaho: implications for Neoproterozoic earth system behavior. *Precambrian Research*, v. 130, n. 1–4, p. 57–70, abr. 2004. Disponível em: <https://linkinghub.elsevier.com/retrieve/pii/S0301926803003061>.

MARTINS, M.S. et al. Mapa geológico 1:100.000 da Folha Serra do Cabral (SE.23-X-C-V). UFMG/CPRM, 2011.

MARTINS-NETO, M. A.; PEDROSA-SOARES, A. C.; LIMA, S. A A. Tectono-sedimentary evolution of sedimentary basins from Late Paleoproterozoic to Late Neoproterozoic in the S??o Francisco craton and Ara??ua?? fold belt, Eastern Brazil. *Sedimentary Geology*, 2001.

MARTINS-NETO, Marcelo A. Sequence stratigraphic framework of Proterozoic successions in eastern Brazil. *Marine and Petroleum Geology*, v. 26, n. 2, p. 163–176, 2009.

MARTINS, Mariela and LEMOS, Valesca Brasil. Análise estratigráfica das seqüências neoproterozóicas da Bacia do São Francisco. *Revista Brasileira de Geociências*, v. 37, n. 4S, p. 156–167, 1 dez. 2007. Disponível em: <http://ppegeo.igc.usp.br/index.php/rbg/article/view/9231/8710>.

MILANOVSKY, E.E. Aulacogens and aulacogeosynclines: Regularities in setting and evolution. *Tectonophysics*, v. 215, n. 1–2, p. 55–68, dez. 1992. Disponível em: <https://linkinghub.elsevier.com/retrieve/pii/004019519290074G>.

MOORE, C. H. *Carbonate diagenesis and porosity*. [S.l.]: Elsevier, 1989.

MORAD, S.; KETZER, J. M.; DE ROS, L. F. Spatial and temporal distribution of diagenetic alterations in siliciclastic rocks: implications for mass transfer in sedimentary basins. *Sedimentology*, v. 47, n. SUPPL. 1, p. 95–120, fev. 2000. Disponível em: <http://doi.wiley.com/10.1046/j.1365-3091.2000.00007.x>.

MORSE, J.W. and MACKENZIE, F.T. Geochemistry of sedimentary carbonates. Developments in Sedimentology 48, Elsevier 708 p, 1990.

NAZEER, Adeel; ABBASI, Shabeer Ahmed; SOLANGI, Sarfraz Hussain. Sedimentary facies interpretation of Gamma Ray (GR) log as basic well logs in Central and Lower Indus Basin of Pakistan. *Geodesy and Geodynamics*, v. 7, n. 6, p. 432–443, 2016. Disponível em: <http://dx.doi.org/10.1016/j.geog.2016.06.006>.

NOBRE, Jane; COIMBRA, Armando Márcio. Microfitólitos associados a construções estromatolíticas go Grupo Bambuí, Proterozóico Superior, na região de Arcos - MG. *Revista Brasileira de Geociências*, v. 30, n. 4, p. 589–592, 1 dez. 2000. Disponível em: <http://ppegeo.igc.usp.br/index.php/rbg/article/view/10876/10336>.

OLIVEIRA, W. J. de. Caracterização das emanações gasosas de hidrocarbonetos na região do Remanso do Fogo (MG), através do uso integrado de Sensoriamento Remoto, Geoquímica, Geofísica, Geologia Estrutural e Espectrometria de Reflectância. Instituto de Geociências, Universidade Estadual de Campinas, Campinas, Tese de Doutoramento, 239 p., 1998.

O'REILLY, S. S. *et al.* Molecular biosignatures reveal common benthic microbial sources of organic matter in ooids and grapestones from Pigeon Cay, The Bahamas. *Geobiology*, v. 15, n. 1, p. 112–130, jan. 2016. Disponível em: <http://doi.wiley.com/10.1111/gbi.12196>.

OKUBO, J. *et al.* Phosphogenesis, aragonite fan formation and seafloor environments following the Marinoan glaciation. *Precambrian Research*, v. 311, n. February, p. 24–36, jul.

2018. Disponível em: <https://linkinghub.elsevier.com/retrieve/pii/S0301926817302991>.

PAULA-SANTOS, Gustavo Macedo De; BABINSKI, Marly. Sedimentary provenance in the southern sector of the São Francisco Basin, SE Brazil. *Brazilian Journal of Geology*, v. 48, n. 1, p. 51–74, jan. 2018. Disponível em: <http://www.scielo.br/scielo.php?script=sci_arttextandpid=S2317-48892018000100051andlng=enandtlng=en>.

PAULA-SANTOS, Gustavo M. *et al.*Tracking connection and restriction of West Gondwana São Francisco Basin through isotope chemostratigraphy. *Gondwana Research*, v. 42, p. 280–305, fev. 2017. Disponível em: <http://dx.doi.org/10.1016/j.gr.2016.10.012>.

PAULA-SANTOS, Gustavo Macedo *et al.*New evidence of an Ediacaran age for the Bambuí Group in southern São Francisco craton (eastern Brazil) from zircon U-Pb data and isotope chemostratigraphy. *Gondwana Research*, v. 28, n. 2, p. 702–720, 2015. Disponível em: <http://dx.doi.org/10.1016/j.gr.2014.07.012>.

PEDROSA-SOARES, Antônio Carlos; ALKMIM, Fernando Flecha De. How many rifting events preceded the development of the Araçuaí-West Congo orogen? *Geonomos*, v. 19, n. 2, p. 244–251, 13 fev. 2011. Disponível em: <https://periodicos.ufmg.br/index.php/revistageonomos/article/view/11775>.

PEDROSA-SOARES A.C. et al. The Neoproterozoic Macaúbas Group (Araçuaí orogen, SE Brazil) with emphasis on the diamictite formations. In: Arnaud, E., Halverson, G.P., Shields-Zhou, G. (orgs.) *The Geological Record of Neoproterozoic Glaciations*. Memoir of the Geological Society of London, 36, London, Geological Society, p. 523-534, 2011.

PERRELLA JÚNIOR, Pascoal *et al.* Facies analysis, sequence stratigraphy and chemostratigraphy of the Sete Lagoas Formation (Bambui Group), northern Minas Gerais State, Brazil: evidence of a cap carbonate deposited on the Januária basement high. *Brazilian Journal of Geology*, v. 47, n. 1, p. 59–77, jan. 2017. Disponível em: <https://www.ars.usda.gov/ARSUserFiles/80400525/Articles/JN_FoodNutrDB.pdf%0Ahttp://www.sjmms.net/text.asp?2015/3/2/141/156425%0Ahttp://web.b.ebscohost.com.ezproxy.lib.utexas.edu/ehost/resultsadvanced?sid=7f6126c9-b053-47c1-89f6-49a395934040@sessionmgr113and>.

PINTO, C. P., PINHO, J.M.M., SOUSA, H. A. de. Recursos minerais e energéticos da Bacia do São Francisco emMinas Gerais: Uma abordagem regional. In: Pinto, C. P. & Martins-Neto, M. A. (eds.) *Bacia do São Francisco: Geologia e Recursos Naturais.* Belo Horizonte, SBG/MG, 139-160, 2001.

PIPER, J. D. A. Palaeomagnetic evidence for a Proterozoic Super-Continent. *Philosophical Transactions of the Royal Society A: Mathematical, Physical and Engineering Sciences*, v. 280, n. 1298, p. 469–490, 22 jan. 1976. Disponível em: <http://rsta.royalsocietypublishing.org/cgi/doi/10.1098/rsta.1976.0007>.

PROUST, J. N. *et al.*Carbonate platform drowning in a foreland setting; the Mid-Carboniferous platform in western Urals (Russia). *Journal of Sedimentary Research*, v. 68, n. 6, p. 1175–1188, 1 nov. 1998. Disponível em: <https://pubs.geoscienceworld.org/jsedres/article/68/6/1175-1188/114017>.

PRUSS, Sara Brady; CORSETTI, Frank A.; FISCHER, Woodward W. Seafloor-precipitated carbonate fans in the Neoproterozoic Rainstorm Member, Johnnie Formation, Death Valley Region, USA. *Sedimentary Geology*, v. 207, n. 1–4, p. 34–40, jun. 2008. Disponível em:

<https://linkinghub.elsevier.com/retrieve/pii/S0037073808000663>.

RADKE, Bruce M.; MATHIS, Robert L. On the Formation and Occurrence of Saddle Dolomite: REPLY. *SEPM Journal of Sedimentary Research*, v. Vol. 51, n. 4, p. 1149–1168, 1980. Disponível em: <http://search.datapages.com/data/doi/10.1306/212F7EB9-2B24-11D7-8648000102C1865D>.

READING H.G. Sedimentary environments and facies, 2nd ed. Oxford, Blackwell Scientific Publications, 615p., 1986.

REIS, Humberto L. S. *Estratigrafia e tectônica da bacia do Francisco na zona de emanações de gás natural di baixo rio Indaiá (MG)*. 2011. Universidade Federal de Ouro Preto, 2011.

REIS, Humberto Luis Siqueira. *Neoproterozoic evolution of the São Francisco Basin, Se Brazil: effects of tectonic inheritance on foreland sedimentation*. 2016. 190 f. Universidade Federal de Ouro Preto, 2016.

REIS, Humberto L S. Gás natural. In: PEDROSA-SOARES, ANTONIO CARLOS; VOLL, ELIANE; CUNHA, EDSON CAMPOS (Org.). . *Recursos Minerais de Minas Gerais on Line: síntese do conhecimento sobre as riquezas minerais, história geológica, e meio ambiente e mineração de Minas Gerais*. [S.l.]: Companhia de Desenvolvimento de Minas Gerais (CODEMGE), 2018. p. 1–39. Disponível em: <http://recursomineralmg.codemge.com.br/substancias-minerais/gas-natural/>.

REIS, Humberto L.S. *et al.*Ediacaran forebulge grabens of the southern São Francisco basin, SE Brazil: Craton interior dynamics during West Gondwana assembly. *Precambrian Research*, v. 302, n. September, p. 150–170, nov. 2017a. Disponível em: <https://linkinghub.elsevier.com/retrieve/pii/S0301926817301687>.

REIS, Humberto L S *et al.The São Francisco Basin*. Cham: Springer International Publishing, 2017b. Disponível em: <http://link.springer.com/10.1007/978-3-319-01715-0>. (Regional Geology Reviews).

REIS, Humberto L.S. et al. Mapa geológico 1:100.000 da Folha Andrequicé (SE.23-Z-A-I). UFMG/CPRM, 2011.

REIS, Humberto L.S.; ALKMIM, Fernando F. Anatomy of a basin-controlled foreland fold-thrust belt curve: The Três Marias salient, São Francisco basin, Brazil. *Marine and Petroleum Geology*, v. 66, p. 711–731, 2015.

REIS, Humberto L.S.; SUSS, João F. Mixed carbonate-siliciclastic sedimentation in forebulge grabens: An example from the Ediacaran Bambuí Group, São Francisco Basin, Brazil. *Sedimentary Geology*, v. 339, p. 83–103, 2016. Disponível em: <http://dx.doi.org/10.1016/j.sedgeo.2016.04.004>.

REIS, Humberto L.S., Suss, João. Os depósitos glaciogênicos da Bacia do São Francisco (MG): registro de um ou dois episódios glaciais? Anais do 47º Congresso Brasileiro de Geologia. Salvador, 2014.

RIDING, Robert. Microbial carbonates: the geological record of calcified bacterial algal mats and bioerms. *Sedimentology*, v. 47, n. 1, p. 179–214, 2000.

ROMANO A.W. and KNAUER L.G. Evidências da glaciação neoproterozoica na base do Grupo Bambuí - região de Onça do Pitangui - Minas Gerais. In: Simpósio de Gelogia de Minas Gerais, 12, Anais, v. 1, 2003.

ROSA, M *et al.* Neoproterozoic anorogenic magmatism in the Southern Bahia Alkaline Province of NE Brazil: U–Pb and Pb–Pb ages of the blue sodalite syenites. *Lithos*, v. 97, n. 1–2, p. 88–97, ago. 2007. Disponível em: <https://linkinghub.elsevier.com/retrieve/pii/S0024493706003288>.

SANCHEZ, Evelyn Aparecida Mecenero. Microbialitos e microfósseis da Formação Sete Lagoas, Neoproterozoico, Brasil: implicações geomicrobiológicas em um contexto de mudanças climáticas e evolutivas. p. 298, 2014.

SANTOS, M. N. *et al.*Provenance and paleogeographic reconstruction of a mesoproterozoic intracratonic sag basin (Upper-Espinhaço Basin, Brazil). *Sedimentary Geology*, v. 318, p. 40–57, 2015. Disponível em: <http://dx.doi.org/10.1016/j.sedgeo.2014.12.006>.

SANTOS, R.V. *et al.*Carbon and oxygen isotope profiles across Meso-Neoproterozoic limestones from central Brazil: Bambuí and Paranoá groups. *Precambrian Research*, v. 104, n. 3–4, p. 107–122, nov. 2000. Disponível em: <https://linkinghub.elsevier.com/retrieve/pii/S0301926800000826>.

SANTOS, Roberto Ventura *et al.*Carbon isotopes of Mesoproterozoic–Neoproterozoic sequences from Southern São Francisco craton and Araçuaí Belt, Brazil: Paleographic implications. *Journal of South American Earth Sciences*, v. 18, n. 1, p. 27–39, dez. 2004. Disponível em: <https://linkinghub.elsevier.com/retrieve/pii/S0895981104000744>.

SCHOLLE, Peter A.; ULMER-SCHOLLE, Dana S. *A color guide to the petrography of carbonate rocks: grains,textures,porosity,diagenesis. AAPG Memoir 77*. [S.l.]: The American Association of Petroleum Geologists, 2003.

SHU, Liu; MENG, Ning; GANGPING, Xie. Geological significance of paleo-aulacogen and exploration potential of reef flat gas reservoirs in the Western Sichuan Depression. *Natural Gas Industry B*, v. 2, n. 5, p. 406–414, nov. 2015. Disponível em: <http://dx.doi.org/10.1016/j.ngib.2015.09.016>.

STRAATHOF, Gijsbert Bastiaan. *Neoproterozoic low latitude glaciations: an african perspective*. 2011. 251 f. University of Edinburgh, 2011.

SWETT, Keene; KNOLL, Andrew H. Stromatolitic bioherms and microphytolites from the late Proterozoic Draken Conglomerate Formation, Spitsbergen. *Precambrian Research*, v. 28, p. 327–347, 1985.

TERRA, José Gerson Salamoni *et al.*Classificações Clássicas De Rochas Carbonáticas. *Boletim de Geociências da Petrobras, Rio de Janeiro*, v. 18, n. 1, p. 9–29, 2010.

THIÉBLEMONT, D *et al.* Timing and characteristics of Neoproterozoic magmatism in SW-Gabon: first geochronogical and geochemical data on the West-Congolian orogen in Gabon. 2011, [S.l.]: University of Johannesburg, Republic of South Africa, Abstracts, 2011.

TONIETTO, Sandra Nélis. *Diagênese e hidrotermalismo em rochas carbonáticas proterozóicas: Grupos Bambuí e Vazante,* Bacia do São Francisco. 2011. 196 f. Universidade de Brasília, 2011.

TROFIMOV, V. A.; KHROMOV, V. T.; TROFIMOV, A. V. Tectonics and petroleum potential of the Kazan–Kazhim aulacogen, East European Platform. *Geotectonics*, v. 50, n. 5, p. 482–490, 11 set. 2016. Disponível em: <http://link.springer.com/10.1134/S0016852116050058>.

TUCKER, Maurice E.; WRIGHT, V. Paul. *Carbonate Sedimentology*. Oxford, UK: Blackwell

Publishing Ltd., 1990. v. 21. Disponível em: <http://jurassic.ru/%5Cnwww.blackwell-science.com%5Cnhttp://jurassic.ru/%5Cnwww.blackwell-science.com>.

UHLEIN, Alexandre *et al.* Glaciação neoproterozóica sobre o cráton do São Francisco e faixas dobradas adjacentes. In: MANTESSO-NETO, VIRGÍNIO *et al.* (Org.). . *Geologia do Continente Sul-Americano. Evolução da obra de Fernando Flávio Marques de Almeida*. [S.l.]: Editora Beca, 2004. p. 539–553.

UHLEIN, Gabriel J. *et al.* Ediacaran paleoenvironmental changes recorded in the mixed carbonate-siliciclastic Bambuí Basin, Brazil. *Palaeogeography, Palaeoclimatology, Palaeoecology*, v. 517, n. January, p. 39–51, mar. 2019. Disponível em: <https://doi.org/10.1016/j.palaeo.2018.12.022>.

UHLEIN, Gabriel J. *et al.* Early to late Ediacaran conglomeratic wedges from a complete foreland basin cycle in the southwest São Francisco Craton, Bambuí Group, Brazil. *Precambrian Research*, v. 299, p. 101–116, set. 2017. Disponível em: <http://dx.doi.org/10.1016/j.precamres.2017.07.020>.

UHLEIN, Gabriel J. *et al.* The Carrancas Formation, Bambuí Group: A record of pre-Marinoan sedimentation on the southern São Francisco craton, Brazil. *Journal of South American Earth Sciences*, v. 71, p. 1–16, nov. 2016. Disponível em: <http://dx.doi.org/10.1016/j.jsames.2016.06.009>.

VEIZER, Ján *et al.* Geochemistry of Precambrian carbonates: V. Late Paleoproterozoic seawater. *Geochimica et Cosmochimica Acta*, v. 56, n. 6, p. 2487–2501, jun. 1992. Disponível em: <https://linkinghub.elsevier.com/retrieve/pii/001670379290204V>.

VIEIRA, L. C. *et al.*Aragonite Crystal Fans In Neoproterozoic Cap Carbonates: A Case Study From Brazil and Implications For the Post-Snowball Earth Coastal Environment. *Journal of Sedimentary Research*, v. 85, n. 3, p. 285–300, 13 mar. 2015. Disponível em: <https://pubs.geoscienceworld.org/jsedres/article/85/3/285-300/145467>.

VIEIRA, Lucieth Cruz; ALMEIDA, Renato Paes; *et al.* A Formação Sete Lagoas em sua área-tipo: fácies, estratigrafia e sistemas deposicionais. *Revista Brasileira de Geociências*, v. 37, n. 4S, p. 1–14, 1 dez. 2007a. Disponível em: <http://ppegeo.igc.usp.br/index.php/rbg/article/view/9232/8711>.

VIEIRA, Lucieth Cruz; TRINDADE, Ricardo I.F.; *et al.*Identification of a Sturtian cap carbonate in the Neoproterozoic Sete Lagoas carbonate platform, Bambuí Group, Brazil. *Comptes Rendus Geoscience*, v. 339, n. 3–4, p. 240–258, mar. 2007b. Disponível em: <https://linkinghub.elsevier.com/retrieve/pii/S1631071307000302>.

WARREN, L. V. *et al.* The puzzle assembled: Ediacaran guide fossil Cloudina reveals an old proto-Gondwana seaway. *Geology*, v. 42, n. 5, p. 391–394, 2014.

WRIGHT, V.P. Calcrete. In: Nash, D.J., McLaren, S.J. (Eds.), Geoquemical Sediments and Landscapes. Blackwell, Oxford, pp. 10-45 , 2007.

WRIGHT, V.P. A micromorphological classification of fossil and recent calcic and petrocalcic microstructures, In: Douglas, L.A. (Ed.), Soil Micromorphology: a Basic and Applied Science. : Developments in Soil Science, vol. 19. Elsevier, Amsterdam, pp.401-407, 1990.

WRIGHT, V. Paul; TUCKER, Maurice E. Calcretes: an introduction. *The International Association of Sedimentologists*. [S.l: s.n.], 1991. p. 1–22.

Capítulo 2: Quimioestratigrafia

2.1. Introduction

This chapter presents detailed chemostratigraphic analysis (C, O, Sr) of the three 1st-order sequences preserved within the Pirapora aulacogen. The geochemical data includes Sr/Ca and Mg/Ca ratios, which were used to elucidate depositional and post-depositional processes recorded within each sequence. Our data reveals new elements to discuss the coupling of sequence stratigraphy and chemostratigraphy(e.g. CAETANO-FILHO et al., 2019) and their impact on understanding the chemical evolution of ancient sedimentary deposits.

2.2. Materials and methods

Thirty-one representative samples of carbonate rocks were selected for carbon and oxygen isotopic analyses (Table 2). For each sample, about 10 mg of carbonate powder was obtained by microdrilling, avoiding fractures, terrigenous components or post-depositional features. The powdered samples were put in reaction with orthophosphoric acid at 72 ºC and the released CO_2 was extracted in a Thermo Finnigan GasBench II under He atmosphere. C and O isotope compositions were determined in a Delta V Advantage IRMS at the Stable Isotope Laboratory of the Center of Geochronological Research, University of São Paulo (CPGeo/USP). Results were reported in conventional delta notation in per mil (‰) relative to the Vienna Pee-Dee Belemnite (V-PDB) standard. The analytical precision was ±0.07‰ for $\delta^{18}O$ and ±0.05‰ for $\delta^{13}C$.

Ten samples were selected for strontium isotopic analysis according to Sr content. The trace element analyses for 37 carbonate samples were conducted using a Portable X-Ray Fluorescence (pXRF), model Olympus Innov-X Delta, gently provided by the Geological Survey of Brazil (CPRM-SUREG BH). Each polished slab was analyzed in soil mode (180 seconds by 3 radiation beams) and mining mode (120 seconds by 2 radiation beams). The equipment was calibrated with reference material, analyzed every 5 measures: NIST 2711a (MACKEY et al., 2010) and blank (pure SiO_2). The blank standard displays not detected results for Sr (soil mode), Ca (mining mode) and Mg (mining mode) content. The average error of measurements in the reference material was ± 3 ppm for Sr, and ±0,06% for Ca and Mg.

Strontium isotopic compositions were obtained using a two-step leaching technique, which used HCl at 0.1M and 1.0M on both steps. The Sr was then separated from the second leachates and purified by ion exchange chromatography, and the $^{87}Sr/^{86}Sr$ ratios were measured in a Triton^{TM} thermal ionization mass spectrometer (TIMS). Corrections for mass fractionation were based on $^{87}Sr/^{86}Sr = 0.1194$. The average value of the NBS-987 standard measured during analyses was 0.710251 ±0.000018, and the measured blanks were not higher than 1933 pg.

2.3. Results: system tracts and chemostratigraphy

In order to favor a coupled analysis, geochemical data from the studied section are reported according to the above-mentioned stratigraphic array (Chapter 2, section 4.3). The obtained $\delta^{13}C$, $\delta^{18}O$, [Sr], $^{87}Sr/^{86}Sr$, [Mg] and [Ca] values of the analyzed samples are discriminated on Table 2 and displayed in Figure 12.

2.3.1. Upper-Espinhaço sequence

Six samples from the top of the sequence were analized, where mid- to outer-ramp carbonates prograde over siliciclastic mudstones (Fig.12, Table 2). $\delta^{13}C$ values vary from -4,42‰ and -3.65 ‰, in a discrete negative incursion, while $\delta^{18}O$ show a negative trend from -13,67 ‰ to -8.64 ‰ turning back to -8.55 ‰ in a positive excursion. Although this sequence has been clearly affected by post-depositional processes (diagenetic alteration, metamorphism, tectonics), the isotopic system seems not have been affected, since there is no correlation in $\delta^{13}C$ vs $\delta^{18}O$ plot (R^2=0.3599, Fig.13).

[Sr] in the samples range from 76 to 436 ppm, and the sample with the highest value (MGA-047-Table 2) was selected for Sr isotopic analysis. The sample yielded a very radiogenic $^{87}Sr/^{86}Sr$ ratio of 0.734.

Table 2: $\delta^{13}C$, $\delta^{18}O$, $^{87}Sr/^{86}Sr$, [Sr], [Ca], [Mg], Mg/Ca and Sr/Ca content from samples of the three 1st order sequences recorded in the Pirapora aulacogen. Values relative to V-PDB Standard. The analytical precision was ±0.07‰ for δ18O and ±0.05‰ for δ13C. "n.a" means not analyzed, and "Mac." refers to Macaúbas sequence and "*" mark [Sr] outline.

Seq.	Depht (m)	Sample	$\delta^{13}C$ ‰	$\delta^{18}O$ ‰	$^{87}Sr/^{86}Sr$	error (2s)	Sr (ppm)	Ca (%)	Mg (%)	Mg/Ca	Mg/Ca x 10^4	Sr/Ca	Sr/Ca x 10^4
Bambuí	1050.08	MGA-142	1.47	-13.95	n.a.	n.a.	294.0	376.885	13.171	0.03	34.946	0.00078	7.801
	1051.91	MGA-138	1.28	-13.65	n.a.	n.a.	285.0	376.606	13.253	0.04	35.191	0.00076	7.568
	1053.90	MGA-134	1.37	-13.53	0.719863	0.000017	310.0	354.383	0	0.00	0.000	0.00087	8.748
	1055.80	MGA-130	0.75	-14.58	n.a.	n.a.	228.0	377.135	0	0.00	0.000	0.00060	6.046
	1058.10	MGA-125	0.80	-13.75	n.a.	n.a.	285.0	358.537	28.457	0.08	79.369	0.00079	7.949
	1060.14	MGA-121	-0.32	-14.07	0.729968	0.000018	606.0	412.868	0	0.00	0.000	0.00147	14.678
	1062.91	MGA-115	-0.71	-14.25	0.718354	0.000020	388.0	388.619	0	0.00	0.000	0.00100	9.984
	1064.14	MGA-112	-0.42	-13.18	n.a.	n.a.	228.0	334.159	80.774	0.24	241.721	0.00068	6.823
	1066.67	MGA-106	-0.93	-12.15	0.724429	0.000018	206.0	274.842	155.474	0.57	565.685	0.00075	7.495
	1068.91	MGA-101	-0.34	-12.88	n.a.	n.a.	91.6	250.475	179.632	0.72	717.168	0.00037	3.657
	1071.41	MGA-96	-0.26	-12.39	0.721491	0.000016	78.5	258.364	189.230	0.73	732.417	0.00030	3.038
	1072.76	MGA-93	-0.44	-11.92	n.a.	n.a.	55.8	255.196	187.990	0.74	736.648	0.00022	2.187
	1074.68	MGA-89	-0.61	-12.12	n.a.	n.a.	59.0	256.651	201.849	0.79	786.473	0.00023	2.299
	1075.85	MGA-86	-1.05	-11.62	0.719872	0.000018	56.3	261.630	209.770	0.80	801.781	0.00022	2.152
	1077.38	MGA-83	-1.21	-11.29	n.a.	n.a.	60.4	259.508	191.669	0.74	738.587	0.00023	2.327
	1078,70	MGA-81	-2.08	-11.75	n.a.	n.a.	80.3	289.298	149.125	0.52	515.474	0.00028	2.776
	1079.50	MGA-79	-1.39	-12.03	n.a.	n.a.	70.6	252.478	170.368	0.67	674.782	0.00028	2.796
	1080.43	MGA-77	-1.53	-11.25	n.a.	n.a.	202.0	240.634	144.276	0.60	599.568	0.00084	8.394
	1081.16	MGA-75	-3.59	-14.76	0.711592	0.000017	217.0	384.444	0	0.00	0.000	0.00056	5.645
	1081.97	MGA-73	-4.74	-15.31	n.a.	n.a.	3934*	425980	0	0	0	0.00924	92.352
	1082.77	MGA-71B	-2.29	-13.65	0.710306	0.000020	n.a.	n.a.	n.a.	n.a.	n.a.	n.a.	n.a.

Seq.	Depht (m)	Sample	$\delta^{13}C$ ‰	$\delta^{18}O$ ‰	$^{87}Sr/^{86}Sr$	error (2s)	Sr (ppm)	Ca (%)	Mg (%)	Mg/Ca	Mg/Ca x 10^4	Sr/Ca	Sr/Ca x 10^4
	1082.90	MGA-71	-3.31	-9.94	n.a.	n.a.	146.0	228.659	173.930	0.76	760.651	0.00064	6.385
	1083.45	MGA-70	-3.47	-12.31	0.744215	0.000021	190.0	242.575	170.954	0.70	704.749	0.00078	7.833
Mac.	1089.57	MGA-65	-4.23	-7.42	n.a.	n.a.	76.9	246.124	177.928	0.72	722.923	0.00031	3.124
	1091.27	MGA-61	-3.48	-7.72	n.a.	n.a.	94.7	223.949	170.033	0.76	759.250	0.00042	4.229
Upper-Espinhaço	1091.87	MGA-60	-4.42	-8.55	n.a.	n.a.	75,9	207.316	146.749	0.71	707.852	0.00037	3.661
	1093.98	MGA-56	-3.96	-8.85	n.a.	n.a.	97,8	228.661	158.034	0.69	691.128	0.00043	4.277
	1095.79	MGA-52	-3.55	-9.28	n.a.	n.a.	75,7	243.824	187.913	0.77	770.690	0.00031	3.105
	1098.12	MGA-47	-4.80	-13.67	0.734936	0.000019	416.0	345.140	86.192	0.25	249.732	0.00121	12.053
	1099.43	MGA-44	-3.50	-10.11	n.a.	n.a.	118.6	248.571	173.218	0.70	696.852	0.00048	4.771
	1104.44	MGA-32	-3.65	-8.64	n.a.	n.a.	342.0	239.252	182.237	0.76	761.695	0.00143	14.295

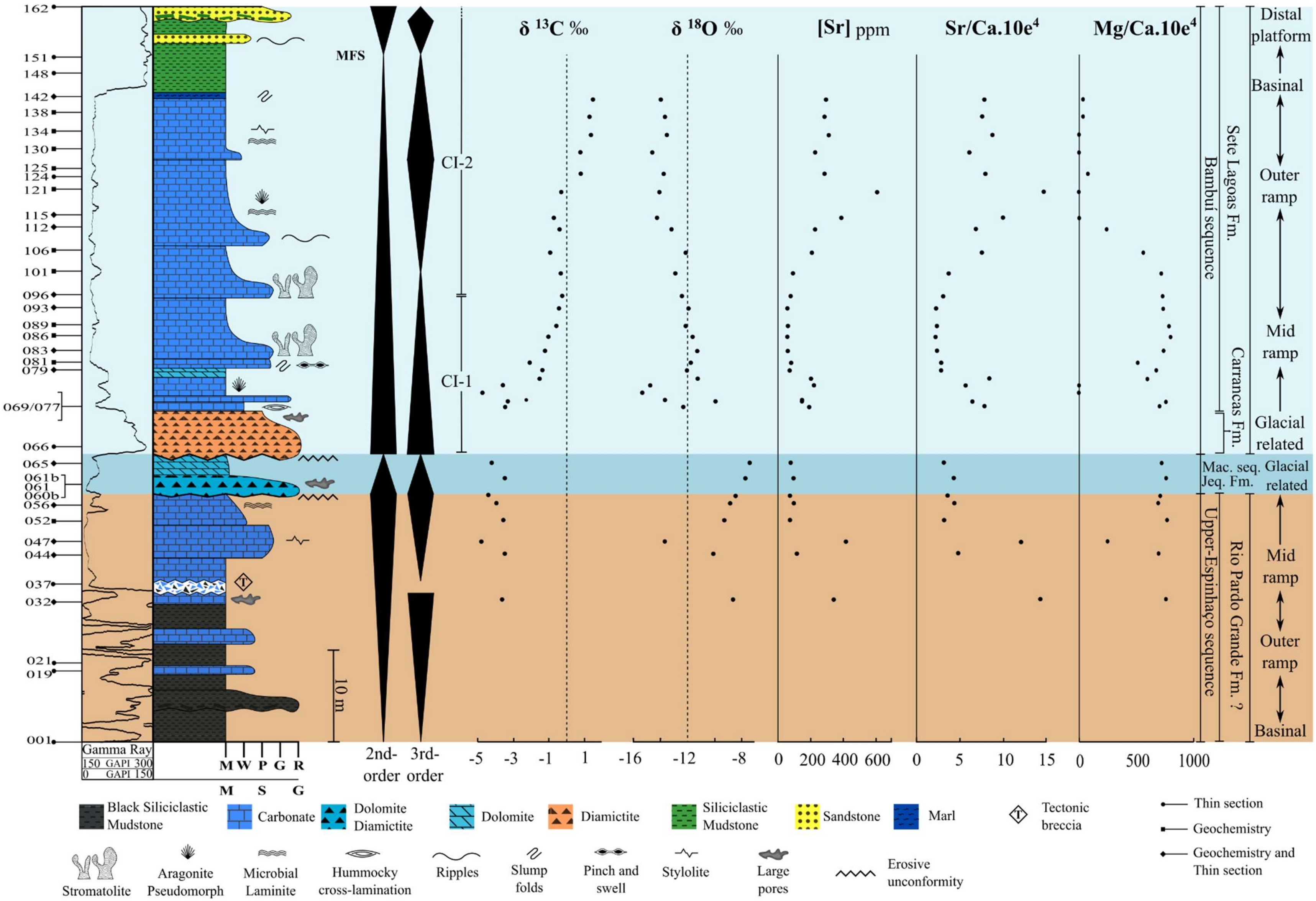

δ 13C ‰
δ 18O ‰
[Sr] ppm
Sr/Ca.10e4
Mg/Ca.10e4
MFS
CI-2
CI-1
2nd-order
3rd-order
Gamma Ray
150 GAPI 300
0 GAPI 150
M W P G R
M S G
10 m
Sete Lagoas Fm.
Bambuí sequence
Carrancas Fm.
Mac. seq.
Jeq. Fm.
Upper-Espinhaço sequence
Rio Pardo Grande Fm. ?
Distal platform
Basinal
Outer ramp
Mid ramp
Glacial related
Mid ramp
Outer ramp
Basinal
Black Siliciclastic Mudstone
Carbonate
Dolomite Diamictite
Dolomite
Diamictite
Siliciclastic Mudstone
Sandstone
Marl
Tectonic breccia
Thin section
Geochemistry
Geochemistry and Thin section
Stromatolite
Aragonite Pseudomorph
Microbial Laminite
Hummocky cross-lamination
Ripples
Slump folds
Pinch and swell
Stylolite
Large pores
Erosive unconformity

Figure 12: Well log: gamma-ray profile, stratigraphic column, sequence stratigraphy, chemostatrigraphic profiles, lithostratigraphic correlation and facies associations. Samples and their respective analysis are plotted on left side. The normal/inverted black triangles represent deepening/shallowing-upward trends and fining/coarsening-upward trends, respectively. MFS – Maximum flooding surface. CI-1/CI-2: Chemostratigraphic Intervals (CI) according to Paula-Santos et al. (2017). Carbonate depositional texture scale: M – mudstone, W – wackestone, P – packstone, G – grainstone and R – rudstone. Siliciclastic granulometry scale: M – mud, S – sand and G – gravel.

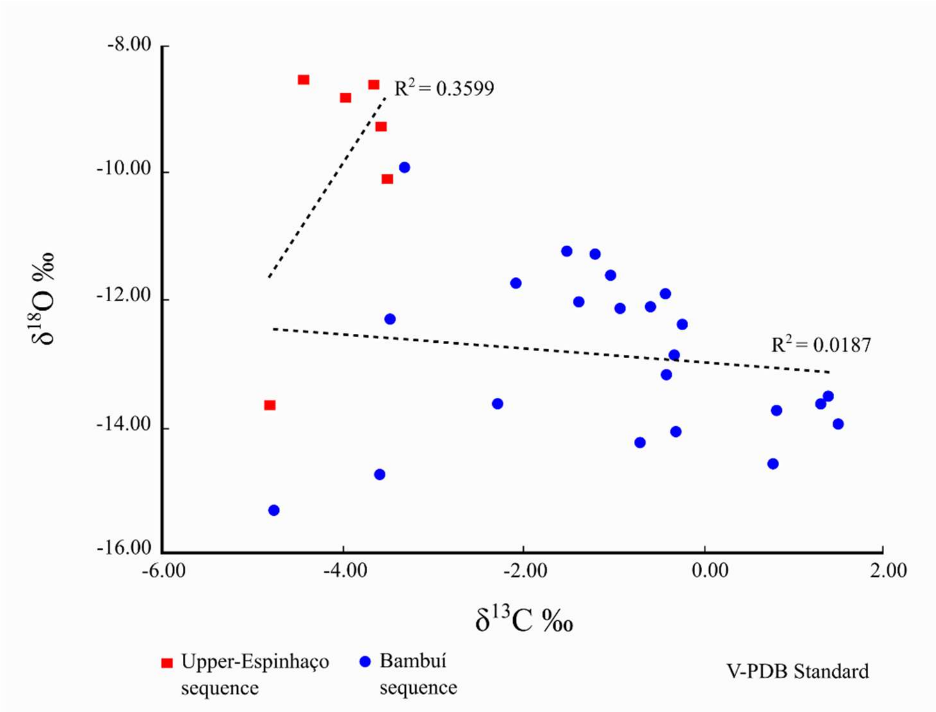

Figure 13: $\delta^{13}C$ versus $\delta^{18}O$ plot of the samples from Upper-Espinhaço and Bambuí sequences. Note the R^2 values denoting low correlations in both sequences.

2.3.2. Macaúbas sequence

The two samples chosen for isotopic analysis correspond to Facies D1 and D2. Since the carbonate content in these facies comes exclusively from diagenetic dolomitization, the analysis aimed to help in understanding the nature of the fluids involved in the alteration process. The basal sample was collected in the dolomitized matrix of the diamictite and showed $\delta^{13}C$ and $\delta^{18}O$ values of -3.48 ‰ and -7.72 ‰, respectively. The upper sample was collected in the dolomitized mudstone and yielded -4.23 ‰ for $\delta^{13}C$ and -7.42 ‰ for $\delta^{18}O$.

2.3.3. Bambuí sequence

All the carbonate samples collected for isotopic analysis in the Bambuí sequence are from the basal portion of Sete Lagoas Formation and are comprised in its basal 2nd-order Transgressive System Tract.

The samples were collected with a stratigraphic resolution of ~ 1m for the basal portion, and ~ 2m in the rest of the section. Regarding a post-depositional alteration assessment, $\delta^{13}C$ and $\delta^{18}O$ values show low correlations between them (R^2=0.0187), indicating that the results probably express depositional conditions (Fig. 13).

The $\delta^{13}C$ chemostratigraphic profile starts with an expressive negative excursion reaching -4.74 ‰. Topward, there is a gradual increase in the values, from -1 to +1 ‰ (Fig. 12). The profile for oxygen displays the same negative trend at base (down to -15‰) followed by a short positive excursion (-15.31 for -11.25 ‰). Topward, there is a gradual decrease to values around -14 ‰.

The [Sr] values in the samples range from 55.8 to 606 ppm, presenting 197.02 ppm of average and 202 ppm of median. It is worth mentioning that Sr contents higher than 200 ppm are associated to aragonite pseudomorphs (Facies C8 and C14), including the highest value achieved (3934 ppm - outline). The eight samples selected for $^{87}Sr/^{86}Sr$ analysis (Table 2) exhibited highly radiogenic values, ranging from 0.7103 to 0.7442, which in general increases toward the top.

2.3.4. Sr/Ca and Mg/Ca

The Mg/Ca and Sr/Ca ratios of carbonate successions has been used to investigate many paleoenvironmental parameters, such as the nature of aqueous solutions, climatic sazonal conditions, original carbonate mineralogy, salinity, alkalinity, among others. (e.g. Baker et al, 1982; Elderfield et al., 1982; Gieskes et al., 1982; Morse and Mackenzie, 1990). In addition, the relative content of these ions are also used to discriminate diagenetic fluids and burial conditions, especially concerning the dolomitizing fluids (Moore and Wade, 2013; Veizer et al., 1992).

The Sr/Ca x $10e^4$ ratios along the Upper-Espinhaço sequence varies from 14.3 to 3.1, with average and median of 7.0 and 4.5 (n=6), respectively. The Mg/Ca x $10e^4$ ratios occurs between 770.7 to 249.7, and present 646.3 for average and 702.3 for median (n=6). In the Macaúbas sequence, Facies D1 present values of 4.2 for Sr/Ca and

759.2 for Mg/Ca, while facies D2 yielded 3.1 and 722.9 for Sr/Ca and Mg/Ca, respectively. The Mg/Ca ratios of both Upper-Espinhaço and Macaúbas sequences might have been influenced by the dolomitization processes, since they present a relatively homogeneous behavior. On the other hand, along the Bambuí sequence, the Mg/Ca and Sr/Ca ratios show inverse correlation (Fig. 12). Mg/Ca ratios from Bambuí sequence occur in two main groups: (i) values lower than 241.7 (average=39.1, median=0.0, n = 10), related to aragonite pseudomorphs layers, laminites, carbonate mudstones and wackestone; (ii) values varying from 515.5 to 801.7 (average= 694.5, median=724.8, n = 12), related to stromatolite layers and the carbonates right above the diamictite. The Sr/Ca ratios, in contrast, has an inverse relationship, mirroring the Mg/Ca ratio in almost all the sequence. The group with higher Mg/Ca ratios present Sr/Ca ≤ 5, while the lower Mg/Ca ratios yielded higher ratios for Sr/Ca (average=8,5). The only exception is the basal interval (Fig.12, Table 2), which displays high ratios for both Mg/Ca and Sr/Ca.

2.4. Discussions

The isotopic results of the described section bring interesting discussions when compared to previously published data from the Upper-Espinhaço, Macaúbas and Bambuí sequences.

Firstly, the data from the Upper-Espinhaço 1st order sequence in the Pirapora aulacogen are slightly different from those available from this sequence within the Araçuaí orogen, where the Rio Pardo Grande Formation, the topmost unit of the Conselheiro Mata Group hosts stromatolitic dolostones. Santos et al., (2004) report a flat isotopic pattern in a section of the unit, with $\delta^{13}C$ ranging from -0.3 to +1.9‰ and $\delta^{18}O$ between -4.7 and -2.6‰, while Fraga (2013) reported $\delta^{13}C$ values from +1.5 to +2.2‰ and $^{87}Sr/^{86}Sr$ ratios ranging between 0.7074 and 0.7079 in dolostones. The Upper-Espinhaço sequence have been also considered as coeval to the passive margin deposits of the Paranoá Group, developed at the western margin of the São Francisco-Congo paleocontinent in late Mesoproterozoic (e.g. CAMPOS et al. 2013, REIS et al. 2017). The Paranoá Group hosts carbonate platform deposits with $\delta^{13}C$ varying in a narrow interval between +0.6 and +3.6‰, and $^{87}Sr/^{86}Sr$ between 0.7056 and 0.7068 (e.g. ALVARENGA et al., 2014). $\delta^{13}C$ and $\delta^{18}O$ values from the carbonates from the Upper-Espinhaço sequence in the described section are significantly lower than those reported for both Conselheiro Mata and Paranoá groups, and the $^{87}Sr/^{86}Sr$ ratios are much more radiogenic. This difference could indicate that the carbonate platform within the aulacogen was not connected to those developed in the pericratonicbasins, and were controlled by local factors. Nevertheless, this discrepancy could also indicate that the carbonate platform in the section is not chrono-correlated to those in the Paranoá and Conselheiro Mata groups, and record a different stage of the basin evolution.

Moore and Wade (2013) reports average isotopic compositions relative to the diagenetic processes associated to meteoric, marine and subsurface fluids. (Fig. 14). The meteoric cements will generally display isotope compositions with low oxygen values, whereas shallow marine settings will have cements with oxygen isotopic ratios near 0‰. Oxygen isotopes are also highly temperature dependent (FRIEDMAN and O'NEIL, 1977), and $\delta^{18}O$ becomes progressively lower with increasing temperature. Although carbon and oxygen isotopic compositions are used to infer paleoenvironmental parameters, calcretes/dolocretes have a complex range of influencing factors, due to their secondary genesis (e.g. ANDREWS et al., 1998; ROYER et al., 2001; DEUTZ et al., 2002). The formation of calcretes/dolocretes involve prolonged residence time in specific physicochemical conditions, during which diverse recrystallization processes take place. Thus, the more developed sections will present more heterogeneous chemical signatures (eg. DEUTZ et al., 2002; KELLY et al., 2000). As well as calcite, dolomite is susceptible to recrystallization, thus, isotopic composition will reach equilibrium during burial diagenesis, and may not reflect the original dolomitizing solution (MOORE and WADE, 2013).

The carbonate content in the Macaúbas sequence (Jequitaí Formation) is not primary, but product of intense dolomitization. Thereat, the isotopic signature from facies D1 and D2 can be used to discuss the characteristics of the fluids involved in such post-depositional processes. Carbonates will generally reflect the oxygen isotopic composition and temperature of the precipitating fluid. The oxygen isotope composition of Macaúbas samples (Fig. 14) is plotted near to the boundary of meteoric field. However, some influence of hydrothermalism is not ruled out, taking account that saddle/baroque dolomite is associated to high temperatures and could have isotopic patterns similar to those of meteoric waters. (MOORE, 1985).

It is also noteworthy that soil weathering and associated precipitation of calcite cements in the vadose and shallow phreatic zones will generally result in moderately negative $\delta^{13}C$ compositions (Fig. 14) (ALLAN and MATTHEWS, 1982; JAMES and CHOQUETTE, 1984). Thus, $\delta^{13}C$ signal of Macaúbas sample is in good agreement for meteoric domain for carbon isotope values, and also corroborate the hypothesis of pedogenesis, as indicated by the petrographic features.

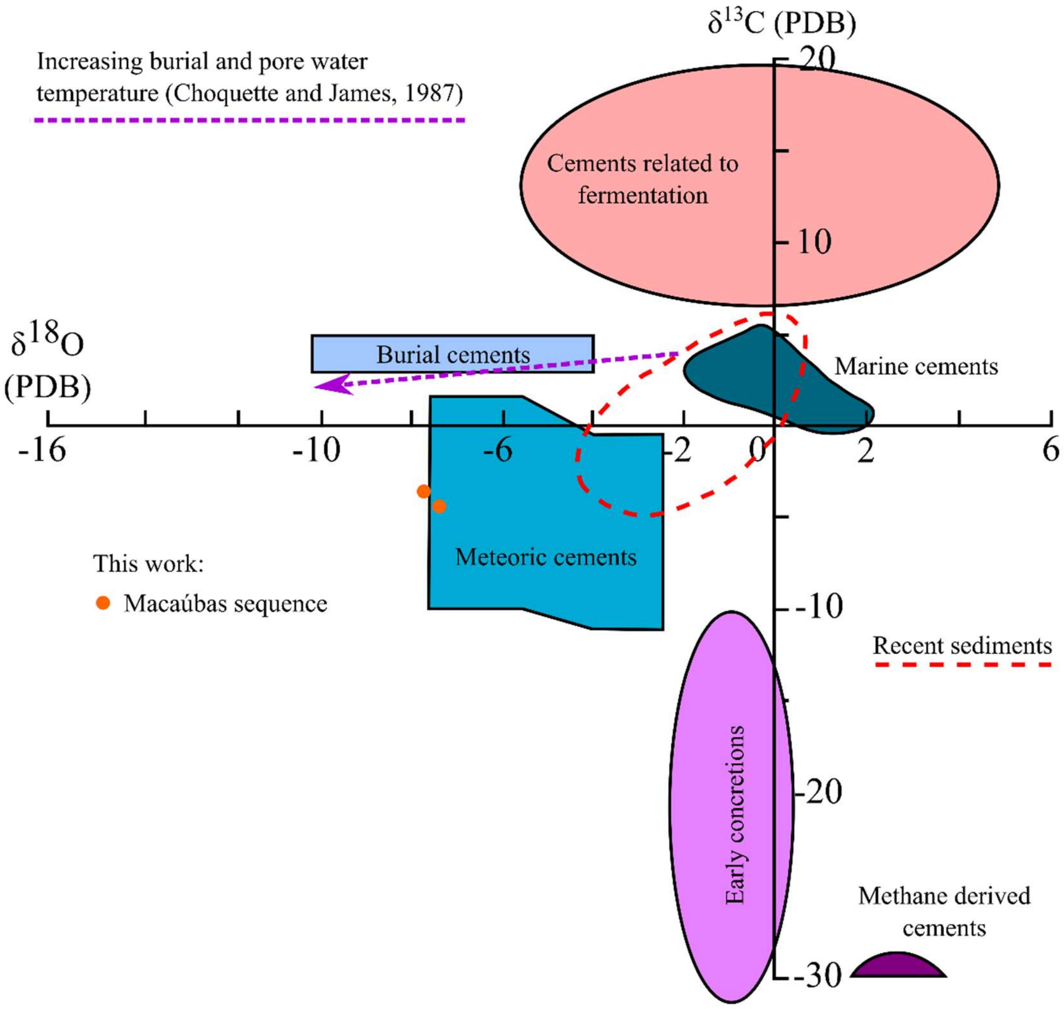

Figure 14: Crossplot of carbon and oxygen isotopic compositions of Macaúbas sequence, compared to fields of carbonates, sediments and cements, in diferent depositional and diagenetic environments, acording to Hudson (1977). Meteóric cements: Saller, 1984a,b and Matthews, 1974. Burial cements by Moore (1985). Modified from Hudson (1977) and Moore and Wade (2013).

Regarding the Bambuí 1st order sequence, the obtained $\delta^{13}C$ profile replicates important chemostratigraphic features recognized basinwide (Fig. 15). First, right above the diamictite, negative $\delta^{13}C$ followed by a recovery to values around 0‰ mark the cap-carbonate interval, which corresponds to the Chemostratigraphic Interval 1 (CI-1) described by Paula-Santos et al. (2017) in the lowermost Sete Lagoas Formation. This pattern has been interpreted as the decrease and progressive recovery of biological activity in the glacial aftermath, following the initial marine transgression over the craton (e.g. VIEIRA et al., 2007; SANCHEZ, 2014; SANTOS et al., 2000; ALVARENGA et al., 2014; KUCHENBECKER et al., 2016; GUACANEME et al., 2017; PAULA-SANTOS et al., 2017; PERRELLA JÚNIOR et al., 2017; CAETANO-FILHO et al., 2019). To the top, $\delta^{13}C$ values between -1 and +1 are compatible with the CI-2, which is envisaged as a stage of connection between the basin and the ocean, allowing isotopic homogenization and biological interchange (Paula-Santos et al. 2017). However, unlike in other sections on the basin (e.g. Arcos, Kuchenbecker et al. 2016, Santa Maria da Vitória, Caetano-Filho et al. 2019) where $\delta^{13}C$ values are consistently similar through the entire CI-2, in the studied section there is a progressive and gradual increase to the top, from values close to -1 to values close to +1. This trend engages the transgressive stratigraphic trend, indicating an inverse relation between the paleobathymetry and $\delta^{13}C$. Considering that the aulacogen represented a secondary depocenter in the basin, this pattern would likely be related to local conditions favoring a progressive increase in organic carbon preservation and burial, which would lead to progressively heavier carbonate carbon isotope compositions. Such variations driven by local controls have previously been reported in sections located within forebulge grabens (e.g. REIS et al., 2017; CAETANO-FILHO et al., 2019).

Most stromatolite deposits reported from Sete Lagoas Formation throughout the basin (see chapter 1 – discussions) are associated to shallower marine environments in the basal TST, and present $\delta^{13}C$ values compatible with the CI-2 (e.g. PAULA-SANTOS et al., 2017; VIEIRA et al., 2007; ALVARENGA et al., 2014; SANCHEZ, 2014; KUCHENBECKER et al., 2016; PERRELLA JÚNIOR et al., 2017; CAETANO-FILHO et al., 2019). In the described section, however, we present negative $\delta^{13}C$ values for columnar stromatolites (Fig. 12), which reinforces their interpretation as a very early biological record in the basin. Perrella et al. (2017) and Sanchez (2014) also reported stromatolites with negative $\delta^{13}C$ values around -4 ‰ in the Januária High domain, which could be chrono-correlated to those described in the Pirapora aulacogen.

In contrast with the good regional correlation of the carbon isotopes, the values of $^{87}Sr/^{86}Sr$ needs to be carefully analyzed. The only one data coming from Upper-Espinhaço sequence (Table 2) is probably masked by diagenetic alteration (see chapter 1, section 5), which would explain the highly radiogenic values. In the same way, the

$^{87}Sr/^{86}Sr$ obtained for the Bambuí sequence were all higher than 0.7100, which is abnormally radiogenic and probably do not reflect the seawater composition. Nevertheless, is a growing consensus that the Bambuí basin represented, at least during a time interval, a restricted marine basin, disconnected from the global ocean (e.g. PAULA-SANTOS et al. 2015, 2017; KUCHENBECKER et al. 2016; HIPPERT et al. 2019; CAETANO-FILHO et al. 2019; BEDOYA-RUEDA, 2019). These studies have demonstrated that such restriction influenced the isotopic record, preventing an efficient thermohaline circulation and, in consequence, the isotopic homogenization, thus allowing local or regional controls to predominate over global ones. In this sense, more studies are needed to evaluate if these abnormally radiogenic $^{87}Sr/^{86}Sr$ ratios could not have been caused by local conditions prevailing in the Pirapora aulacogen depocenter.

Finally, the [Sr], [Ca] and [Mg] results also show some points that worth mentioning. The Sr/Ca and Mg/Ca ratios from the Upper-Espinhaço, Macaúbas and part of Bambuí sequences show similar behavior throughout the sedimentary succession (Fig. 12), independent of facies or sedimentary trends. This pattern suggest homogenization by post depositional processes, such as the dolomitization recorded in the three sequences. The similarity between the three sequences would indicate that the main event associated to this process was the late hydrothermalism that affected the entire section.

Within the Bambuí sequence, an interesting pattern occurs in the aragonite-bearing layers and in deep water facies, in which, despite the pervasive dolomitization, the Mg/Ca and Sr/Ca present an inverse relation, behavior remarkably different from that observed in the rest of the sequence. The aragonite-bearing layers record periods of carbonate oversaturation in seawater (see discussion in chapter 1, section 6.5) during which the precipitated carbonate minerals could be different from those from the unsaturated periods. Based on that, the observed pattern in Mg/Ca and Sr/Ca might be related to differential chemical behavior of the original carbonate mineralogy during the dolomitization process.

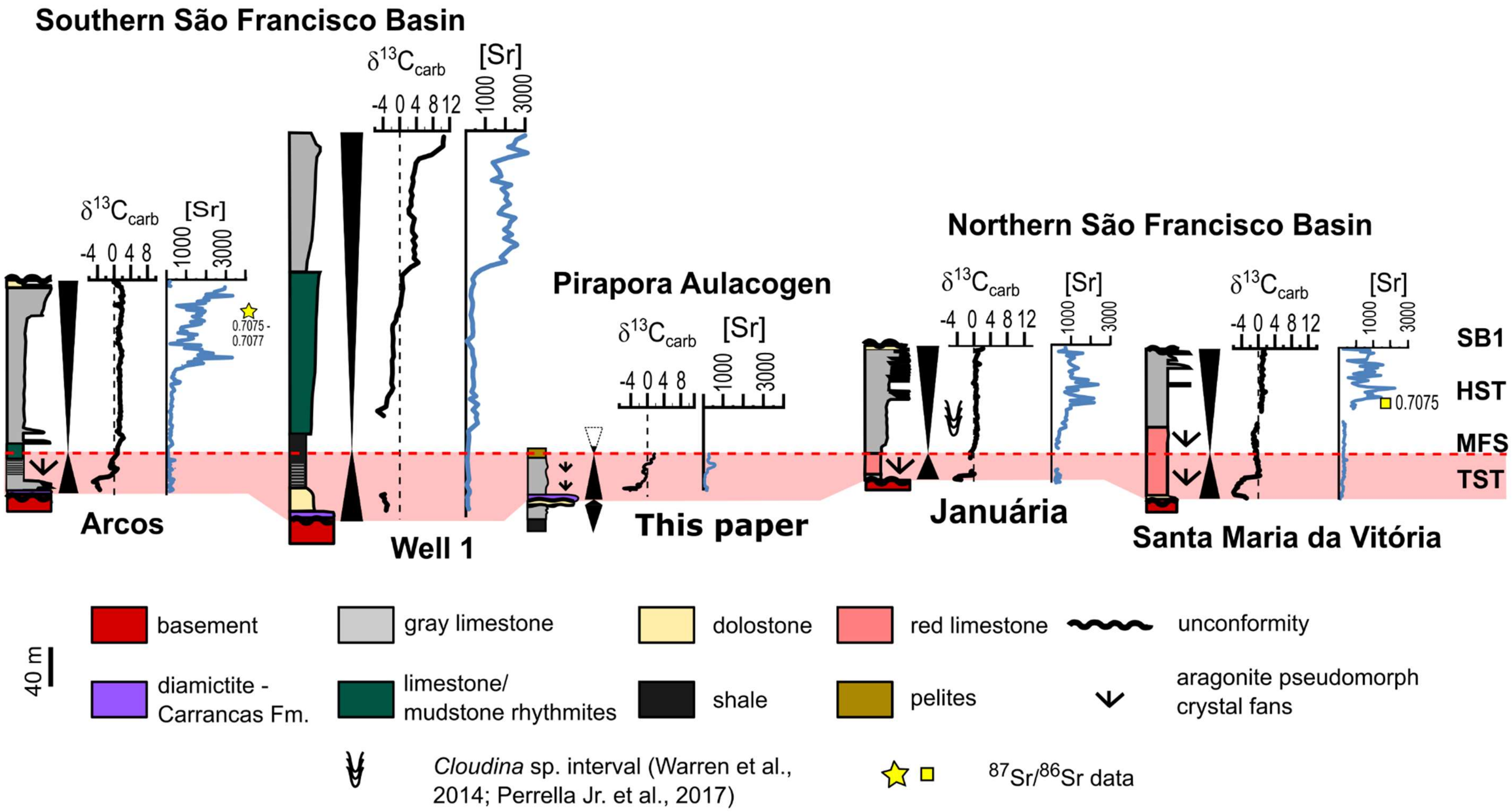

Southern São Francisco Basin
Pirapora Aulacogen
Northern São Francisco Basin
$\delta^{13}C_{carb}$
[Sr]
-4 0 4 8 12
1000 3000
0.7075 - 0.7077
0.7075
SB1
HST
MFS
TST
Arcos
Well 1
This paper
Januária
Santa Maria da Vitória
40 m
basement
gray limestone
dolostone
red limestone
unconformity
diamictite - Carrancas Fm.
limestone/ mudstone rhythmites
shale
pelites
aragonite pseudomorph crystal fans
Cloudina sp. interval (Warren et al., 2014; Perrella Jr. et al., 2017)
$^{87}Sr/^{86}Sr$ data

Figure 15: Schematic chemostratigraphic correlation for Transgressive System Tract (TST) of basal Bambuí sequence (light pink area), according to Caetano-Filho et al. (2019). Maximum flooding surface (MSF) establish the datum between sections located at Sete Lagoas High, Pirapora aulacogen and Januária High. δ13C data are in ‰ V-PDB, [Sr] in ppm, (HST) Highstand System Tract and (SB1) Sequence Boundary. Modified from Caetano-Filho et al. (2019).

During supersaturation events, Sr content is generally high and preferably incorporated on aragonite lattices, rather than in micritic sediments (PERYT et al., 1990; HALVERSON et al., 2004). According to the environmental conditions, such as alkalinity and temperature, the Low-Mg calcite (LMC) precipitates linked to aragonite (Fabre et al., 2013; VIEIRA et al., 2015). It is a consensus that LMC presents more stability than high magnesium calcite (HMC) and aragonite (e.g. TUCKER and WRIGHT, 1990; MORSE and MACKENZIE, 1990; SCHOLLE and ULMER SCHOLLE; 2003; FLÜGEL, 2004). In Facies C8 (Chapter 1, Table 1), the early aragonite recrystallization to calcite or LMC have provided mineralogic stability, that may have reduced its potential for dolomitization. Another favorable scenario to LMC formation is the deep marine settings. Bottom sea conditions, with reduced current influence, creates local chemical environments that decreases the Mg concentration, so, stable LMC precipitates directly from sea water (TUCKER and WRIGHT, 1990). In this scenario, outer-ramp laminites, wackestones and carbonate mudstones, deposited on the end of TST, could be less dolomitized in response to original stable mineralogy.

Thus, our data indicates that, in the Bambuí sequence, the early diagenetic processes are, somehow, conditioned by the parameters prevailing in the depositional environment. The early stabilized carbonates from the supersaturation events were poorly replaced by dolomite, as well as the LMC from the deeper environments. On the other hand, the completely dolomitized intervals are correlated to unstable precursor minerals, which could be directly replaced (higher [Sr]), or recrystallized and dolomitized afterward (lower [Sr]).

Capítulo 3: Conclusões

Este trabalho descreve, pela primeira vez, o arcabouço estratigráfico de uma seção sedimentar contínua na borda sul do Aulacógeno de Pirapora, composta por três ciclos sedimentares de primeira ordem.

O ciclo Espinhaço-Superior registra a reativação Steniana do aulacógeno, e sua porção basal compreende depósitos lamosos siliciclásticos ricos em matéria orgânica. O estágio diagenético dolomítico tardio (dolomita em sela/barroca) indica passagem pela janela óleo-gás, e a presença de betume residual reforçam o potencial gerador desse intervalo no sistema petrolífero da Bacia do São Francisco.

Pela primeira vez foi descrida uma seção contendo duas unidades de diamictitos sobrepostos na Bacia do São Francisco. A Formação Jequitaí provavelmente representa um registro da glaciação Sturtiana Criogeniana, correlata ao ciclo bacinal Macaúbas. (e.g. BABINSKI et al., 2012; KUCHENBECKER et al., 2016, 2015; REIS et al., 2017a; CAETANO-FILHO et al., 2019). Ocorre delimitada por discordância e apresenta intensa alteração pós-deposicional, anterior a deposição do diamictito sobrejacente, possivelmente dolomitização em ambiente meteórico, pedogênica ou freática. Os valores de $\delta^{13}C$ e $\delta^{18}O$ também apontam para alterações meteóricas, porém, a possibilidade da sobreposição do sinal isotópico do oxigênio por fluidos hidrotermais não está descartada. A Formação Carrancas, por sua vez, registra a glaciação tardia do Ediacarano, correspondendo ao ciclo bacinal Bambuí. (e.g. KUCHENBECKER et al., 2016a; PAULA-SANTOS and BABINSKI, 2018; CAETANO-FILHO et al., 2019).

Na margem sul do aulacógeno de Pirapora, a quimioestratigrafia do ciclo Bambuí compreende um Trato de Sistema Transgressivo (TST), correlato ao CI-1, seguido pelo Trato de Sistema de Mar Alto (TSMA). Estes correspondem ao ciclo de segunda-ordem basal da bacia, com arranjo estratigráfico e perfil isotópico de $\delta^{13}C$ concordante à correlação intrabacinal envolvendo seções dos altos de Januária e Sete Lagoas (CAETANO-FILHO et al., 2019). Isso indica que a evolução quimioestratigráfica da bacia também é válida para o domínio do aulacógeno. Todavia, os dados na literatura sugerem que a reativação ediacarana das falhas da margem norte do aulacógeno ocorreu anterior a reativação da margem sul.

O TST basal da Formação Sete Lagoas no aulacógeno de Pirapora pode apresentar os registros mais antigos de atividade biológica na bacia. Os estromatólitos colunares se formaram poucos metros acima do diamictito Carrancas, e apresentam valores de $\delta^{13}C$ negativos, compatíveis com o CI-1 (PAULA-SANTOS et al., 2017).

Os intervalos aragoníticos nos carbonatos basais da Formação Sete Lagoas parecem registrar diferentes eventos de supersaturação marinha, condicionados principalmente pela evolução climática e biológica da bacia. As razões Sr/Ca nesses intervalos mostram-se relativamente mais altas em comparação as seções adjacentes. O mesmo comportamento ocorre para as razões Mg/Ca, geralmente superiores nos intervalos dolomitizados, associados a baixas taxas de Sr/Ca, implica que os processos deposicionais provavelmente condicionaram a susceptibilidade e intensidade da dolomitização, em resultado da mineralogia precursora, estabilização mineralógica e parâmetros paleoambientais restritos.

O evento hidrotermal afetou as três sequências principais inseridas no aulacógeno. Esse estágio tardio foi influenciado por evento tectônico, provavelmente relacionado ao último ciclo de reativação, no Ediacarano superior. Betume e sulfetos grossos preenchem poros e fraturas nos carbonatos da Formação Sete Lagoas, portanto, o fraturamento tectônico promoveu a migração da matéria orgânica e percolação de fluidos enriquecidos em ferro, apontando para potencial petrolífero e metalogenético dessa formação na bacia do São Francisco.

Esse trabalho demonstra a importância do aulacógeno de Pirapora frente aos processos evolutivos da Bacia do São Francisco, podendo apresentar registros chaves para os processos tectônicos do Precambriano ao Fanerozóico, na América do Sul.

Referências

ALLAN, J. R.; MATTHEWS, R. K. Isotope Signatures Associated with Early Meteoric Diagenesis. *Sedimentology*. Oxford, UK: Blackwell Publishing Ltd., 1982. p. 197–217. Disponível em: <http://doi.wiley.com/10.1002/9781444304510.ch16>.

ALVARENGA, Carlos J.S. *et al.* Meso-Neoproterozoic isotope stratigraphy on carbonates platforms in the Brasilia Belt of Brazil. *Precambrian Research*, v. 251, p. 164–180, set. 2014. Disponível em: <http://dx.doi.org/10.1016/j.precamres.2014.06.011>.

ANDREWS, Julian E. *et al.* Do Stable Isotope Data from Calcrete Record Late Pleistocene Monsoonal Climate Variation in the Thar Desert of India? *Quaternary Research*, v. 50, n. 3, p. 240–251, 20 nov. 1998. Disponível em: <https://www.cambridge.org/core/product/identifier/S0033589400025485/type/journal_article>.

BABINSKI, M. *et al.* Neoproterozoic glacial deposits from the Araçuaí orogen, Brazil: Age, provenance and correlations with the São Francisco craton and West Congo belt. *Gondwana Research*, v. 21, n. 2–3, p. 451–465, 2012. Disponível em: <http://dx.doi.org/10.1016/j.gr.2011.04.008>.

BAKER, P. A.; GIESKES, J. M.; ELDERFIELD, H. Diagenesis of carbonates in deep-sea sediments - evidence from Sr/Ca ratios and interstitial dissolved Sr data. *Journal of Sedimentary Petrology*, v. 52, n. 1, p. 71–82, 1982.

BEDOYA-RUEDA, C. Quimioestratigrafia isotópica (C, O, Sr) de alta resolução dos carbonatos da Formação Sete Lagoas, Grupo Bambuí, na região sudoeste da Bacia do São Francisco. Dissertação de mestrado, USP, 111p., 2019.

BURKE, Kevin. Aulacogens and Continental Breakup. *Annual Review of Earth and Planetary Sciences*, v. 5, n. 1, p. 371–396, maio 1977. Disponível em: <http://www.annualreviews.org/doi/10.1146/annurev.ea.05.050177.002103>.

CAETANO-FILHO, Sergio *et al.* Sequence stratigraphy and chemostratigraphy of an Ediacaran-Cambrian foreland-related carbonate ramp (Bambuí Group, Brazil). *Precambrian Research*, v. 331, n. June, p. 105365, set. 2019. Disponível em: <https://doi.org/10.1016/j.precamres.2019.105365>.

CAMPOS J.E.G. *et al*. Geologia do Grupo Paranoá na porção externa da Faixa Brasília. Brazilian Journal of Geology, 43(3):461-476, 2013

CHOQUETTE, P.W. and JAMES, N.P. Diagenesis #12. Diagenesis in limestones: 3. The deep burial environment. Geosci. Can. 14, 3–35, 1987.

CRUZ, Simone Cerqueira Pereira; ALKMIM, Fernando F. The Paramirim Aulacogen. In: HEILBRON, MONICA; ALKMIM, FERNANDO F; CORDANI, UMBERTO G (Org.). . *São Francisco Craton,Eastern Brazil. Tectonic Genealogy of a Miniature Continent.* [S.l.]: Regional Geology Reviews, Springer International Publishing, 2017. p. 97–115. Disponível em: <http://link.springer.com/10.1007/978-3-319-01715-0_6>.

CRUZ, Simone Cerqueira Pereira; ALKMIM, Fernando F. The tectonic interaction between the Paramirim aulacogen and the Araçuaí belt, São Francisco craton region, Eastern Brazil. *Anais da Academia Brasileira de Ciências*, v. 78, n. 1, p. 151–173, 2006.

DEUTZ, P.; MONTANEZ, I. P.; MONGER, H. C. Morphology and Stable and Radiogenic Isotope Composition of Pedogenic Carbonates in Late Quaternary Relict Soils, New Mexico, U.S.A.: An Integrated Record of Pedogenic Overprinting. *Journal of Sedimentary Research*, v. 72, n. 6, p. 809–822, 1 nov. 2002. Disponível em: <https://pubs.geoscienceworld.org/jsedres/article/72/6/809-822/114128>.

ELDERFIELD, Henry *et al.* 87Sr/86Sr and 180/160 ratios, interstitial water chemistry and diagenesis in deep-sea carbonate sediments of the Ontong Java Plateau. *Geochimica et Cosmochimica Acta*, v. 46, p. 2259–2268, 1982.

FABRE, Sébastien *et al.* Origin of cap carbonates: An experimental approach. *Palaeogeography, Palaeoclimatology, Palaeoecology*, v. 392, p. 524–533, dez. 2013a. Disponível em: <https://linkinghub.elsevier.com/retrieve/pii/S0031018213004628>.

FABRE, Sébastien *et al.* Origin of cap carbonates: An experimental approach. *Palaeogeography, Palaeoclimatology, Palaeoecology*, v. 392, p. 524–533, 15 dez. 2013b.

FLÜGEL, Erik. *Microfacies of Carbonate Rocks*. Berlin, Heidelberg: Springer Berlin Heidelberg, 2004. Disponível em: <http://link.springer.com/10.1007/978-3-662-08726-8>.

FRAGA, L. M. S. *Análise estratigráfica do grupo Macaúbas no domínio meridional da serra do Espinhaço, Minas Gerais* (Universidade Federal de Minas Gerais), 2013. https://doi.org/10.22533/at.ed.8591910066

FRIEDMAN, Irving; O'NEIL, James R. Compilation of stable isotope fractionation factors of geochemical interest. In: FLEISCHER, MICHAEL (Org.). . *Geological Survey Professional Paper*. Sixth ed. Washington: Data of Geochemistry, 1977. v. 440. p. 1–12.

GIESKES, J. M.; JOHNSTON, Kirk; BOEHM, Marcus. Interstitial waters studies, central north Atlantic. p. 539–542, 1982.

GUACANEME, Cristian *et al.* C, O, and Sr isotopic variations in Neoproterozoic-Cambrian carbonate rocks from Sete Lagoas Formation (Bambuí Group), in the Southern São Francisco Basin, Brazil. *Brazilian Journal of Geology*, v. 47, n. 3, p. 521–543, 2017. Disponível em: <https://www.ars.usda.gov/ARSUserFiles/80400525/Articles/JN_FoodNutrDB.pdf%0Ahttp://www.sjmms.net/text.asp?2015/3/2/141/156425%0Ahttp://web.b.ebscohost.com.ezproxy.lib.utexas.edu/ehost/resultsadvanced?sid=7f6126c9-b053-47c1-89f6-49a395934040@sessionmgr113and>.

HALVERSON, G. P., MALOOF, A. C., and HOFFMAN, P. F. The Marinoan glaciation (Neoproterozoic) in northeast Svalbard. Basin Research, 16(3), 297–324., 2004. https://doi.org/10.1111/j.1365-2117.2004.00234.x

HIPPERTT, J.P.T.M. The Fate of a Neoproterozoic Intracratonic Marine Basin: Trace

Elements, TOC and Iron Speciation Geochemistry of the Bambuí Basin, Brazil. (MSc dissertation). Univ. Federal de Minas Gerais (74pp, unpublished), 2018.

HUDSON, J. D. Stable isotopes and limestones lithification. Geol. Soc. Lond., 133, 637–660, 1977.

JAMES, N.P. and CHOQUETTE, P.W. Diagenesis 9. Limestones: the meteoric diagenetic environment. Geosci. Can. 11, 161–194, 1984.

KELLY et al. Early Cretaceous giant bivalves from seep-related limestone mounds, Wollaston Forland, Northeast Greenland E.M. Harper, J.D. Taylor, J. Crame (Eds.), *The Evolutionary Biology of the Bivalvia*, Geological Society, London, Special Publications, 177 (2000), pp. 227-246

KUCHENBECKER, Matheus *et al.* Chemostratigraphy of the lower Bambuí Group, southwestern São Francisco Craton, Brazil: insights on Gondwana paleoenvironments. *Brazilian Journal of Geology*, v. 46, n. June, p. 145–162, 2016a. Disponível em: <http://www.scielo.br/scielo.php?script=sci_arttextandpid=S2317-48892016000700145andlng=enandnrm=isoandtlng=en>.

KUCHENBECKER, Matheus; PEDROSA-SOARES, Antônio Carlos; *et al.* Detrital zircon age patterns and provenance assessment for pre-glacial to post-glacial successions of the Neoproterozoic Macaúbas Group, Araçuaí orogen, Brazil. *Precambrian Research*, v. 266, p. 12–26, set. 2015. Disponível em: <http://dx.doi.org/10.1016/j.precamres.2015.04.016>.

MACKEY, E A; LINDSTROM, R M; MURPHY, K E. Certification of Three NIST Renewal Soil Standard Reference Materials for Element Content. *National Institute of Standards and Technology Special Publication 260-172*, p. 39, 2010. Disponível em: <http://www.nist.gov/srm/upload/SP260-172.pdf>.

MATTHEWS, R.K. A process approach to diagenesis of reefs and reefassociated limestones. In: Laporte, L.F. (Ed.), Reefs in Time and Space. SEPM Sp. Publ. 18, pp. 234–256, 1974.

MILANOVSKY, E.E. Aulacogens and aulacogeosynclines: Regularities in setting and evolution. *Tectonophysics*, v. 215, n. 1–2, p. 55–68, dez. 1992. Disponível em: <https://linkinghub.elsevier.com/retrieve/pii/004019519290074G>.

MOORE, C.H. Upper Jurassic subsurface cements: a case history. In: Schneidermann, N., Harris, P.M. (Eds.), Carbonate Cements. SEPM Sp. Publ. 36, pp. 291–308, 1985.

MOORE, Clyde H; WADE, William J. *Carbonate Reservoirs: porosity and diagenesis in a sequence stratigraphic framework*. second edi ed. [S.l.]: Elsevier B.V., 2013.

MORSE, J.W. and MACKENZIE, F.T. Geochemistry of Sedimentary Carbonates. Elsevier Scientific, New York, 696 pp., 1990.

PAULA-SANTOS, Gustavo Macedo De; BABINSKI, Marly. Sedimentary provenance in the southern sector of the São Francisco Basin, SE Brazil. *Brazilian Journal of Geology*, v. 48, n. 1, p. 51–74, jan. 2018. Disponível em: <http://www.scielo.br/scielo.php?script=sci_arttextandpid=S2317-

48892018000100051andlng=enandtlng=en>.

PAULA-SANTOS, Gustavo M. *et al.* Tracking connection and restriction of West Gondwana São Francisco Basin through isotope chemostratigraphy. *Gondwana Research*, v. 42, p. 280–305, fev. 2017. Disponível em: <http://dx.doi.org/10.1016/j.gr.2016.10.012>.

PERRELLA JÚNIOR, Pascoal *et al.* Facies analysis, sequence stratigraphy and chemostratigraphy of the Sete Lagoas Formation (Bambui Group), northern Minas Gerais State, Brazil: evidence of a cap carbonate deposited on the Januária basement high. *Brazilian Journal of Geology*, v. 47, n. 1, p. 59–77, jan. 2017. Disponível em: <https://www.ars.usda.gov/ARSUserFiles/80400525/Articles/JN_FoodNutrDB.pdf%0Ahttp://www.sjmms.net/text.asp?2015/3/2/141/156425%0Ahttp://web.b.ebscohost.com.ezproxy.lib.utexas.edu/ehost/resultsadvanced?sid=7f6126c9-b053-47c1-89f6-49a395934040@sessionmgr113and>.

PERYT, A. et al. Late Proterozoic aragonitic cement crusts, Bambuı´ Group, Minas Gerais, Brazil, *Sedimentology* 37 279–286, 1990.

REIS, Humberto L.S. *et al.* Ediacaran forebulge grabens of the southern São Francisco basin, SE Brazil: Craton interior dynamics during West Gondwana assembly. *Precambrian Research*, v. 302, n. September, p. 150–170, nov. 2017a. Disponível em: <https://linkinghub.elsevier.com/retrieve/pii/S0301926817301687>.

REIS, Humberto L S *et al.The São Francisco Basin*. Cham: Springer International Publishing, 2017b. Disponível em: <http://link.springer.com/10.1007/978-3-319-01715-0>. (Regional Geology Reviews).

ROYER, Dana L.; BERNER, Robert A.; BEERLING, David J. Phanerozoic atmospheric CO2 change: evaluating geochemical and paleobiological approaches. *Earth-Science Reviews*, v. 54, n. 4, p. 349–392, ago. 2001. Disponível em: <https://linkinghub.elsevier.com/retrieve/pii/S0012825200000428>.

SALLER, Arthur H. Petrologic and geochemical constraints on the origin of subsurface dolomite, Enewetak Atoll: An example of dolomitization by normal seawater. *Geology*, v. 12, n. 4, p. 217, 1984. Disponível em: <https://pubs.geoscienceworld.org/geology/article/12/4/217-220/203655>.

SALLER, Arthur Henry. Diagenesis of Cenozoic limestones on Enewetak atoll (dolomite, neomorphism,radiaxial). 1984.

SANCHEZ, Evelyn Aparecida Mecenero. Microbialitos e microfósseis da Formação Sete Lagoas, Neoproterozoico, Brasil: implicações geomicrobiológicas em um contexto de mudanças climáticas e evolutivas. p. 298, 2014.

SANTOS, R.V. *et al.* Carbon and oxygen isotope profiles across Meso-Neoproterozoic limestones from central Brazil: Bambuí and Paranoá groups. *Precambrian Research*, v. 104, n. 3–4, p. 107–122, nov. 2000. Disponível em: <https://linkinghub.elsevier.com/retrieve/pii/S0301926800000826>.

SANTOS, Roberto Ventura *et al.* Carbon isotopes of Mesoproterozoic–Neoproterozoic sequences from Southern São Francisco craton and Araçuaí Belt, Brazil: Paleographic implications. *Journal of South American Earth Sciences*, v. 18, n. 1, p. 27–39, dez. 2004. Disponível em: <https://linkinghub.elsevier.com/retrieve/pii/S0895981104000744>.

SCHOLLE, Peter A.; ULMER-SCHOLLE, Dana S. *A color guide to the petrography of carbonate rocks: grains,textures,porosity,diagenesis. AAPG Memoir 77*. [S.l.]: The American Association of Petroleum Geologists, 2003.

TUCKER, Maurice E.; WRIGHT, V. Paul. *Carbonate Sedimentology*. Oxford, UK: Blackwell Publishing Ltd., 1990. v. 21. Disponível em: <http://jurassic.ru/%5Cnwww.blackwell-science.com%5Cnhttp://jurassic.ru/%5Cnwww.blackwell-science.com>.

VEIZER, Ján *et al.* Geochemistry of Precambrian carbonates: V. Late Paleoproterozoic seawater. *Geochimica et Cosmochimica Acta*, v. 56, n. 6, p. 2487–2501, jun. 1992. Disponível em: <https://linkinghub.elsevier.com/retrieve/pii/001670379290204V>.

VIEIRA, L. C. *et al.* Aragonite Crystal Fans In Neoproterozoic Cap Carbonates: A Case Study From Brazil and Implications For the Post-Snowball Earth Coastal Environment. *Journal of Sedimentary Research*, v. 85, n. 3, p. 285–300, 13 mar. 2015. Disponível em: <https://pubs.geoscienceworld.org/jsedres/article/85/3/285-300/145467>.

VIEIRA, Lucieth Cruz; ALMEIDA, Renato Paes; *et al.* A Formação Sete Lagoas em sua área-tipo: fácies, estratigrafia e sistemas deposicionais. *Revista Brasileira de Geociências*, v. 37, n. 4S, p. 1–14, 1 dez. 2007a. Disponível em: <http://ppegeo.igc.usp.br/index.php/rbg/article/view/9232/8711>.

VIEIRA, Lucieth Cruz; TRINDADE, Ricardo I.F.; *et al.* Identification of a Sturtian cap carbonate in the Neoproterozoic Sete Lagoas carbonate platform, Bambuí Group, Brazil. *Comptes Rendus Geoscience*, v. 339, n. 3–4, p. 240–258, mar. 2007b. Disponível em: <https://linkinghub.elsevier.com/retrieve/pii/S1631071307000302>.

WARREN, L. V. *et al.* The puzzle assembled: Ediacaran guide fossil Cloudina reveals an old proto-Gondwana seaway. *Geology*, v. 42, n. 5, p. 391–394, 2014.